SAIMM
THE SOUTHERN AFRICAN INSTITUTE OF MINING AND METALLURGY
VOLUME 121 NO. 1 JANUARY 2021

Leaders in Slurry Systems Engineering

www.PatersonCooke.com

- Long Distance Slurry Pipelines
- Thickened, Paste and Filtered Tailings
- Mine Backfill Systems
- Hydraulic Hoisting Systems
- Process Engineering
- Specialist Engineering
- Slurry and Process Laboratories
- Process Technologies
- Site Services
- Courses and Training

Slurry Pipeline Systems: Paterson & Cooke has extensive experience in designing long distance slurry pipelines and mine residue disposal systems. Our capability includes filtration, thickening, cycloning, pump and pipeline transport, choke stations, gravity launder transport, deposition arrangements and water recovery from the residue storage facility.

Mine Backfill and Pastefill Systems: The design of deep level mine backfill distribution systems for hydraulic and paste backfill was revolutionized by Paterson & Cooke's full flow design methodology. We continue to set the standard for backfill service by performing our own in-house test work at our various specialised backfill laboratories around the world.

Process Expertise: Our process engineering expertise covers a wide range of mineral processing technologies including comminution, classification, beneficiation and solid/ liquid separation. Many projects require novel process solutions. Our resources allow us to conduct fundamental and practical research and develop new process flow sheet options and solutions specific to our clients' needs.

- AUSTRALIA (Perth)
- CANADA (Sudbury, Calgary, Vancouver)
- CHILE (Santiago)
- SOUTH AFRICA (Cape Town, Johannesburg)
- UNITED KINGDOM (Cornwall)
- USA (Denver)

PATERSON & COOKE

ESTABLISHED 1991

Our key strength is the intellect, commitment and creativity of the people who work for Paterson & Cooke

OFFICE BEARERS AND COUNCIL FOR THE 2020/2021 SESSION

Honorary President

Mxolisi Mgojo
President, Minerals Council South Africa

Honorary Vice Presidents

Gwede Mantashe
Minister of Mineral Resources, South Africa

Ebrahim Patel
Minister of Trade, Industry and Competition, South Africa

Blade Nzimande
Minister of Higher Education, Science and Technology, South Africa

President

V.G. Duke

President Elect

I.J. Geldenhuys

Senior Vice President

Z. Botha

Junior Vice President

W.C. Joughin

Incoming Junior Vice President

E Matinde

Immediate Past President

M.I. Mthenjane

Co-opted to Office Bearers

S. Ndlovu
G.R. Lane

Honorary Treasurer

W.C. Joughin

Ordinary Members on Council

B. Genc
G.R. Lane
K.M. Letsoalo
T.M. Mmola
G. Njowa
S.J. Ntsoelengoe
S.M Rupprecht
N. Singh
A.G. Smith
M.H. Solomon
A.J.S. Spearing
S.J. Tose
M.I. van der Bank
A.T. van Zyl
E.J. Walls

Co-opted Members

Z. Fakhraei

Past Presidents Serving on Council

N.A. Barcza
R.D. Beck
J.R. Dixon
H.E. James
R.T. Jones
A.S. Macfarlane
C. Musingwini
S. Ndlovu
J.L. Porter
S.J. Ramokgopa
M.H. Rogers
D.A.J. Ross-Watt
G.L. Smith
W.H. van Niekerk

G.R. Lane–TPC Mining Chairperson
Z. Botha–TPC Metallurgy Chairperson

S.F. Manjengwa–YPC Chairperson
A.T. Chinhava–YPC Vice Chairperson

Branch Chairpersons

Johannesburg	D.F. Jensen
Namibia	N.M. Namate
Northern Cape	I. Lute
Pretoria	S. Uludag
Western Cape	A.B. Nesbitt
Zambia	D. Muma
Zimbabwe	C.P. Sadomba
Zululand	C.W. Mienie

PAST PRESIDENTS

*Deceased

* W. Bettel (1894–1895)
* A.F. Crosse (1895–1896)
* W.R. Feldtmann (1896–1897)
* C. Butters (1897–1898)
* J. Loevy (1898–1899)
* J.R. Williams (1899–1903)
* S.H. Pearce (1903–1904)
* W.A. Caldecott (1904–1905)
* W. Cullen (1905–1906)
* E.H. Johnson (1906–1907)
* J. Yates (1907–1908)
* R.G. Bevington (1908–1909)
* A. McA. Johnston (1909–1910)
* J. Moir (1910–1911)
* C.B. Saner (1911–1912)
* W.R. Dowling (1912–1913)
* A. Richardson (1913–1914)
* G.H. Stanley (1914–1915)
* J.E. Thomas (1915–1916)
* J.A. Wilkinson (1916–1917)
* G. Hildick-Smith (1917–1918)
* H.S. Meyer (1918–1919)
* J. Gray (1919–1920)
* J. Chilton (1920–1921)
* F. Wartenweiler (1921–1922)
* G.A. Watermeyer (1922–1923)
* F.W. Watson (1923–1924)
* C.J. Gray (1924–1925)
* H.A. White (1925–1926)
* H.R. Adam (1926–1927)
* Sir Robert Kotze (1927–1928)
* J.A. Woodburn (1928–1929)
* H. Pirow (1929–1930)
* J. Henderson (1930–1931)
* A. King (1931–1932)
* V. Nimmo-Dewar (1932–1933)
* P.N. Lategan (1933–1934)
* E.C. Ranson (1934–1935)
* R.A. Flugge-De-Smidt (1935–1936)
* T.K. Prentice (1936–1937)
* R.S.G. Stokes (1937–1938)
* P.E. Hall (1938–1939)
* E.H.A. Joseph (1939–1940)
* J.H. Dobson (1940–1941)
* Theo Meyer (1941–1942)
* John V. Muller (1942–1943)
* C. Biccard Jeppe (1943–1944)
* P.J. Louis Bok (1944–1945)
* J.T. McIntyre (1945–1946)
* M. Falcon (1946–1947)
* A. Clemens (1947–1948)
* F.G. Hill (1948–1949)
* O.A.E. Jackson (1949–1950)
* W.E. Gooday (1950–1951)
* C.J. Irving (1951–1952)
* D.D. Stitt (1952–1953)
* M.C.G. Meyer (1953–1954)
* L.A. Bushell (1954–1955)
* H. Britten (1955–1956)
* Wm. Bleloch (1956–1957)
* H. Simon (1957–1958)
* M. Barcza (1958–1959)
* R.J. Adamson (1959–1960)
* W.S. Findlay (1960–1961)
* D.G. Maxwell (1961–1962)
* J. de V. Lambrechts (1962–1963)
* J.F. Reid (1963–1964)
* D.M. Jamieson (1964–1965)
* H.E. Cross (1965–1966)
* D. Gordon Jones (1966–1967)
* P. Lambooy (1967–1968)
* R.C.J. Goode (1968–1969)
* J.K.E. Douglas (1969–1970)
* V.C. Robinson (1970–1971)
* D.D. Howat (1971–1972)
* J.P. Hugo (1972–1973)
* P.W.J. van Rensburg (1973–1974)
* R.P. Plewman (1974–1975)
* R.E. Robinson (1975–1976)
* M.D.G. Salamon (1976–1977)
* P.A. Von Wielligh (1977–1978)
* M.G. Atmore (1978–1979)
* D.A. Viljoen (1979–1980)
* P.R. Jochens (1980–1981)
G.Y. Nisbet (1981–1982)
A.N. Brown (1982–1983)
* R.P. King (1983–1984)
J.D. Austin (1984–1985)
H.E. James (1985–1986)
H. Wagner (1986–1987)
* B.C. Alberts (1987–1988)
* C.E. Fivaz (1988–1989)
* O.K.H. Steffen (1989–1990)
* H.G. Mosenthal (1990–1991)
R.D. Beck (1991–1992)
* J.P. Hoffman (1992–1993)
* H. Scott-Russell (1993–1994)
J.A. Cruise (1994–1995)
D.A.J. Ross-Watt (1995–1996)
N.A. Barcza (1996–1997)
* R.P. Mohring (1997–1998)
J.R. Dixon (1998–1999)
M.H. Rogers (1999–2000)
L.A. Cramer (2000–2001)
* A.A.B. Douglas (2001–2002)
S.J. Ramokgopa (2002-2003)
T.R. Stacey (2003–2004)
F.M.G. Egerton (2004–2005)
W.H. van Niekerk (2005–2006)
R.P.H. Willis (2006–2007)
R.G.B. Pickering (2007–2008)
A.M. Garbers-Craig (2008–2009)
J.C. Ngoma (2009–2010)
G.V.R. Landman (2010–2011)
J.N. van der Merwe (2011–2012)
G.L. Smith (2012–2013)
M. Dworzanowski (2013–2014)
J.L. Porter (2014–2015)
R.T. Jones (2015–2016)
C. Musingwini (2016–2017)
S. Ndlovu (2017–2018)
A.S. Macfarlane (2018–2019)
M.I. Mthenjane (2019–2020)

Honorary Legal Advisers
MH Attorneys

Auditors
Genesis Chartered Accountants

Secretaries
The Southern African Institute of Mining and Metallurgy
Fifth Floor, Minerals Council South Africa
5 Hollard Street, Johannesburg 2001 • P.O. Box 61127, Marshalltown 2107
Telephone (011) 834-1273/7 • Fax (011) 838-5923 or (011) 833-8156
E-mail: journal@saimm.co.za

Typeset and Published by

The Southern African Institute of Mining and Metallurgy
P.O. Box 61127
Marshalltown 2107
Telephone (011) 834-1273/7
Fax (011) 838-5923
E-mail: journal@saimm.co.za

Printed by

Camera Press, Johannesburg

Advertising Representative

Barbara Spence
Avenue Advertising
Telephone (011) 463-7940
E-mail: barbara@avenue.co.za

ISSN 2225-6253 (print)
ISSN 2411-9717 (online)

Directory of Open Access Journals

SAIMM
JOURNAL OF THE SOUTHERN AFRICAN INSTITUTE OF MINING AND METALLURGY
VOLUME 121 NO. 1 JANUARY 2021

Contents

News of General Interest

PROFESSIONAL TECHNICAL AND SCIENTIFIC PAPERS

Stemming practices at a South African opencast coal mine were assessed and the influence of stemming practices on ground vibration and air blast investigated, using both quantitative and qualitative methods. Some level of non-compliance of actual stemming parameters with design was found. There was no direct correlation between stemming length and excessive air blast and ground vibration. Since stemming parameters are interrelated, it is crucial that all blasting procedures are executed in accordance with best practices and recorded accurately. There is a need for digital systems for capturing on-bench blasting parameters, as current manual data recording and reporting systems are inefficient and prone to errors.

The effect of flotation operational parameters on froth stability and froth recovery was studied. Froth stability was measured using a special column. It was found that the exponential model is more suitable than the froth height change method for determining froth recovery. The results showed that superficial air velocity and collector dosage have respectively the highest and lowest effect on the froth recovery, and that froth recovery decreases sharply with increasing froth height.

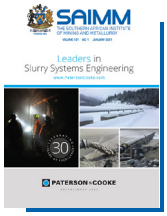

New Year, New Horizons

The beginning of a New Year brings with it the hope that new and better opportunities will arise, and this hope is no more acute than in this New Year. The difficulties encountered in all walks of life during 2020 will be long remembered. It remains to be seen how the world fares in 2021.

However, despite all the disruptions of the past year it is gratifying to note growth and continued interest in the SAIMM, its *Journal* and its published papers. Statistics show that over the year 2020, more than 300 new papers were submitted from 44 countries, with contributions from South Africa (42%), China (12%), Turkey (7%), Iran (6%), India and Indonesia (both 3%), an increasing number from north, central, and other southern African countries, the EU and USA, and from as far afield as Australia to Argentina and Chile to Russia. In terms of website statistics, data indicate that up to 17 000 visitors seek the SAIMM website per month, with the largest overview of pages on publications and Journal papers. As reported by the ASSAf and SciELO SA, over a period of 12 months to July 2020, the *Journal* recorded 10 349 resolutions for the 1 409 papers, giving and average of 7.4 resolutions per paper.

In the interests of increasing the standard of published scientific papers, new guidelines for authors are currently being drawn up and are due to be published shortly, with new schedules for reviewers to reduce the time for reviewing. The Editorial Board has recently expanded to include the panel of International Editorial Advisors as well as increased representation from industry and academia. As the *Journal* is now produced exclusively online, this has led to the elimination of printing costs and expanded the potential for circulation to a wider community.

With respect to content, it is worthy to note that the *Journal* continues to serve the interests of academia and industry, and in so doing it publishes fundamental research and applied industrial papers of interest to both. In addition, the Publication Committee has sought to re-define the *Journal's* focus areas, dividing the minerals, mining, and metallurgical (MMM) sectors into further defined disciplines and sub-disciplines, with experienced Editorial Board members dedicated to each sector. In so doing, the disciplines may be seen to cross the entire MMM value chain, *i.e.*, from geological exploration and mineral resources/reserves through mining and metallurgy, to digitalization, the environment, energy, and economics. Some editions provide papers on a dedicated theme, while others present a mix of general papers from a wide range of sources in this multidisciplinary industry.

This current edition of the *Journal* presents papers that illustrate the multidisciplinary nature of the publication. One paper is on mining (examining the influence of stemming practices on ground vibration on an opencast coal mine), two on extractive metallurgy (one on adapting a crusher design and a second on the effect of froth flotation operational parameters on froth stability and recovery), and a further paper is on energy efficiency (designing a framework to improve current efficiency in electrowinning).

The final contribution illustrates the interdisciplinary aspect of certain papers. For example, the overlap between the mining and geological disciplines. In this case, a pothole stress investigation is reported in the Merensky and UG2 reefs of the Bushveld Complex. The stress measurement in one porthole was found to be unique, indicating a very high stress level in the pothole rock which could have significance from a mining safety point of view. Questions regarding the nature, structure, and mechanical features of the pothole rocks and the geological process responsible for their formation were raised, which require collaboration between the mining and geological communities. It is to be hoped that further such collaboration between these disciplines will ensue. For the present, however, these issues remain unanswered. This paper was published in the interests of safety and not scientific prowess.

With the new steps being taken regarding the operation and content of the *Journal* and the clearer definitions of its fields of focus, it is to be hoped that such approaches will be of benefit to the entire MMM community and that collaboration, integration, and expansion of technical horizons across the MMM board will increasingly ensue.

R.M.S. Falcon

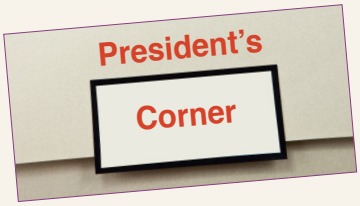

Disruption

'An interruption in the usual way that a system, process, or event works' (the Cambridge Business English Dictionary (© Cambridge University Press)

Covid-19 has done exactly this. We all had to innovate, creatively adapt, and behave differently as the pandemic disrupted our lives and our livelihoods. Our usual routines and mindsets changed as we witnessed the various ups and downs of 2020 unfolding.

- It was good that families were able to spend more time at home with one another. However, it is unfortunate that at the same time, South Africans witnessed an increase in domestic abuse and violence.
- A clampdown on the sale of alcohol saw a dramatic drop in trauma-related hospital admissions, and this freed up beds for Covid-19 patients. There were sadly many consequent job losses, which highlighted how urgently our social services need to be improved. To compound matters SAB Miller recently announced that the company was withdrawing an investment of some R2.5 billion into the sector.
- Restricted travel has meant less congestion on roads and pollution levels around the globe have reduced. There have been many reports of increased sightings of animals in areas previously void of wildlife.
- Social isolation has, unfortunately been emotionally unhealthy for many, especially for older folk confined to retirement homes. We have also seen increased levels of depression in younger people living on their own, and among our youth, who should be spending more time socializing with peers.

Our businesses were all affected in some form or another by the pandemic. Employers generally responded quickly at the onset of the lockdown by changing their processes to allow people to work from home. Many have actually benefitted from this disruption and it is now unlikely that they will return to their pre-pandemic ways of operating.

These extraordinary times required careful thought on changing strategies and methods. Our mindsets and paradigms will probably never be the same again, but this has enabled us to adjust for enhanced performance in ways that we may not have previously considered. Entrepreneurs and leaders found creative and innovative ways to deal with the many levels of disruption brought about by the pandemic. It was interesting to see how one restaurateur converted his premises to a drive-in facility, which allowed him to not only survive 2020, but also to prosper as his market share began to improve.

Last year was difficult. It was filled with, at times, unwanted changes that are set to continue into 2021. Although businesses responded remarkably well to the disruption, the profit margins of many were severely impacted, and government revenue from taxes was substantially lower at a time when significantly more expenditure was incurred on managing the pandemic. This has affected our already poorly performing economy, to the extent that an immediate re-adjustment towards economic reform is urgently required. This may, hopefully, have already started, with refreshing signs of improved collaboration between unions, government, and civil society.

The SAIMM is aware that the post Covid-19 world is going to be very different to that of pre-2020, but a big challenge has been the difficulty in predicting just how different the future is going to be. Therefore, despite some radical changes in our collective mindset, our approach to dealing with this uncertainty has been an exercise in agility, while also ensuring meaningful and steady progress on implementing the changes required of the Institute.

The global trend to moving online is now well established, and the SAIMM is following suit. A full online membership interface system is now in place and our website is becoming increasingly user-friendly. It is rich with information and allows members easy access to the many benefits that the SAIMM has to offer. Our staff are now also placing greater emphasis on communicating and marketing our activities through digital and social media platforms

V.G. Duke
President, SAIMM

SAMCODES

THE SOUTH AFRICAN MINERAL REPORTING CODES

SAMREC

THE SOUTH AFRICAN CODE FOR THE REPORTING OF EXPLORATION RESULTS, MINERAL RESOURCES AND MINERAL RESERVES

SAMVAL

THE SOUTH AFRICAN CODE FOR THE REPORTING OF MINERAL ASSET VALUATIONS

SAMCODES NEWS (January 2021)

Please go to www.samcode.co.za to read these and other items of interest to the CP/CV/QRE communities

CRIRSCO Annual Meeting 2020

The first virtual meeting of CRIRSCO took place from 14-19 September, chaired by Ken Lomberg, Chairperson of CRIRSCO. The virtual platform allowed the meeting to include additional delegates from the National Reporting Organisations (NROs). As well as discussing the strategy of CRIRSCO, a review of the 15 Standard Definitions contained in the International Reporting Template commenced. A total of seven countries – China, Philippines, Argentina, Peru, Kyrgyzstan, Ecuador, and Mexico – presented to the meeting on the status of their applications to become members of CRIRSCO. The level of interest, enthusiasm, and professionalism bodes well for the future health of the CRIRSCO organization.

Dr Ferdi Camisani passed away on 23 November 2020. Ferdi will best be remembered for his pioneering work with the establishment of CRIRSCO and the SAMREC Code. He represented South Africa and the SAMREC Code on the CRIRSCO Committee from its inception in 2002 until 2012.

SAMCODES have launched an app that allows one to access and search the SAMREC, SAMVAL, and SAMOG codes, the JSE Section 12 Listing Rules, as well as SAMESG and the Diamond/Precious Stones Reporting Guidelines. Click here to download the User Guide.

The SAMCODES 2021 Conference will take place on 26-27 October 2021. The precise format (face-to-face or hybrid meeting) will depend on prevailing circumstances and will be announced in due time.

➢ Your contributions in terms of photographs, articles, and content are welcome – please send to sam@saimm.co.za

T.R. Marshall

The influence of stemming practice on ground vibration and air blast

M. Mpofu[1], S. Ngobese[1], B. Maphalala[1], D. Roberts[1], and S. Khan[1]

Affiliation:
[1] Council for Scientific and Industrial Research (CSIR), Pretoria, South Africa.

Correspondence to:
S. Khan

Email:
skhan2@csir.co.za

Dates:
Received: 30 Apr. 2020
Revised: 9 Oct. 2020
Accepted: 18 Nov. 2020
Published: January 2021

How to cite:
Mpofu, M., Ngobese, S., Maphalala, B., Roberts, D., and Khan, S. 2021
The influence of stemming practice on ground vibration and air blast.
Journal of the Southern African Institute of Mining and Metallurgy, vol. 121, no. 1, pp. 1–10.

DOI ID:
http://dx.doi.org/10.17159/2411-9717/1204/2021

ORCID
M. Mpofu
https://orcid.org/0000-0003-2010-7596

S. Khan
https://orcid.org/0000-0002-6362-5361

Synopsis

This paper details an assessment of stemming practices at a South African opencast coal mine and their influence on ground vibration and air blast. Quantitative and qualitative analysis methods were used for the study. The parameters assessed for the quantitative analyses included stemming length, stemming material type, blast-hole depth, burden, and spacing. Pre-blast data from the mine was analysed to determine the deviation between actual and mine design stemming parameters. Mine design stemming length was also compared to the rule-of-thumb stemming lengths. Peak particle velocity (ground vibration) and air blast data from seismograph stations around the mine was analysed to determine the correlation between stemming length and excessive ground vibration and air blast. The qualitative analysis involved observations of blasting procedures at the mine to determine compliance with mine procedures. Some level of non-compliance of actual stemming parameters to design stemming parameters was found, which initially suggested that non-compliance may have contributed to excessive air blast. However, further analysis of the seismograph results indicated no direct correlation between stemming length and excessive air blast and ground vibration. Since stemming parameters are interrelated, it is crucial that all blasting procedures, including stemming, are executed in accordance with best practice, and recorded accurately. There is a need for digital systems for capturing on-bench blasting parameters, as the currently used manual data recording and reporting systems are inefficient and prone to error. Improvements to blast designs are possible through efficient and accurate data recording and reporting systems.

Keywords

opencast mining, blasting, stemming, ground vibration, air blast.

Introduction

Rock blasting using explosive energy is an integral part of the mining process. However, poor blasting from inefficient blast designs and practices may result in adverse impacts on the environment, infrastructure, and the health and safety of people and wildlife in surrounding communities. Some of the negative impacts of inefficient blasting include excessive ground vibrations, air blast, flyrock, noise, and blasting fumes. Potential causes of these effects include, but are not limited to (Bajpayee, Verakis, and Lobb, 2004; Mohamed, Armaghani, and Motaghedi, 2013):

i. Undercharging or overcharging blast-holes
ii. Overly confined or inadequately confined blast-holes
iii. Inappropriate timing sequence
iv. Unfavourable geological and geotechnical conditions.

A team of researchers at the Council for Scientific and Industrial Research (CSIR) undertook a project for Coaltech on 'Monitoring of Blasting and Determination of Optimal Stemming' in 2018. This paper forms part of the research work that was done to assess stemming practices at a South African opencast coal mine and the influence of stemming practices on ground vibration and air blast at the mine. The hypothesis was that excessive ground vibration and air blast are a result of incorrect stemming design and practice. 'Incorrect stemming design and practice' in this context refers to non-compliance of actual stemming parameters with mine design parameters.

The paper highlights the design guidelines for stemming parameters (length and material type), compares the actual stemming parameters to mine design stemming parameters (stemming length, burden, spacing, and hole depth) at the mine; qualitatively assesses the compliance with standard operating blasting procedures; and discusses the relationship between stemming practices, air blast, and ground vibration at the mine.

The influence of stemming practice on ground vibration and air blast

Background

Study site

The study was conducted at an opencast mine located in the Mpumalanga Province of South Africa, in the Witbank Coalfield. The Witbank Coalfield has five mineable bituminous coal seams numbered consecutively from the oldest (No.1 Seam) to the youngest (No. 5 Seam) (Banks *et al.*, 2011). The Witbank Coalfield contains a large and important resource of high-yield, export quality coal (especially in the No. 4 Seam), and an estimated 50% of South Africa's recoverable coal reserves (Banks *et al.*, 2011).

The mine geology consists of alternating layers of sandstone, shale, and coal seams. The No. 2, 3, 4, and 5 seams are mined by opencast methods.

The importance of stemming in relation to ground vibration and air blast

Stemming involves placing an inert material on top of explosives in a blast-hole (NPS, 1999; de Graaf, 2013). The stemming material may include drill chippings, gravel, or sand. Stemming enables the efficient use of energy for rock breakage and prevents the escape of gases when explosives are detonated (Boshoff and Webber-Youngman, 2011). Appropriate stemming material also protects the loaded explosives from accidental detonation and aids in the generation of a loose muckpile that is easy to load (NPS, 1999). The premature ejection of stemming material results in the loss of explosive energy and the rapid venting of gases to the atmosphere. This leads to air blast, a shock wave that results from the detonation of explosives, which is usually accompanied by violently ejected flyrock (de Graaf, 2013). Poor stemming practices also contribute to poor fragmentation, surface overbreak, bad heave or rock displacement, and excessive noise and ground vibration that affect the surrounding environment (Sereme *et al.*, 2019). Overconfinement can result in excessive ground vibration, especially when excessive subdrilling is practiced or larger than recommended burdens are used. Unconfined or inadequately confined blast-holes cause air blast, suggesting that the appropriate stemming length and material type is an important factor to consider in blasting practices (de Graaf, 2013).

Aspects to consider in stemming design are stemming length, material type, and stemming-related parameters such as burden, spacing, and hole depth. The stemming length is dependent on various factors that include the power of the explosives, blast-hole diameter, burden, spacing, stemming material, and the surrounding rock properties (Neale, 2010; de Graaf, 2013).

Stemming length

Generally, stemming parameters are designed for each mine based on the unique geology and varying conditions such as material thickness (Neale, 2010). The stemming length adopted by the mine investigated, as shown in Equation [1] (NPS, 1999; de Graaf, 2013; Lusk and Worsey, 2013), is based on best practice guidelines.

$$T = 20 \times D \quad [1]$$

where: T = stemming length (m) and D = blast-hole diameter (m).

A different rule-of-thumb recommends that the stemming length should fall within the range shown in Equation [2] (NPS, 1999; de Graaf, 2013; Lusk and Worsey, 2013).

$$T = 0.7\text{b to } 1.2\text{b} \quad [2]$$

where: T = stemming length (m) and b = burden (m).

Generally, stemming lengths shorter than 0.7b result in air blast, flyrock, noise, and overbreak (Lusk and Worsey, 2013).

Stemming material

A stemming material should have high shear strength and high density to improve the effectiveness of a blast (BME, 2018). Furthermore, stemming material should be of such a size and shape that the fragments achieve good interlocking.

According to Lusk and Worsey (2013), the following basic guideline is applied to stemming material (Equation [3]):

$$\text{Stemming material size} = \frac{1}{8} \times D \quad [3]$$

Generally, the stemming material type is selected based on availability at the mine. According to Patidar (2017), sand, fly ash, and clay are commonly found at surface coal mines and may be used separately or mixed to improve stemming efficiency. Drill chippings, the fine material generated by drilling of blast-holes, are a readily available type of stemming material. Drill chippings may be used wet or dry, with the wet chippings being less effective than dry chippings due to reduced interlocking ability (BME, 2018). Crushed stone or aggregate is another cost-effective type of stemming material that can be produced at the site to a desirable size (de Graaf, 2013). An alternative to aggregate is chrome slag, which is the waste material from the production of ferrochrome. Its physical and mechanical qualities make it a suitable replacement for natural aggregate as stemming material (Moodie, 2016). One of the benefits of using chrome slag is that it is otherwise considered as waste material, therefore its use eliminates the cost and issues associated with discarding it. The choice between natural aggregate and chrome slag depends on stemming material size, availability, and associated costs.

Stemming accessories used in conjunction with stemming materials and which are commercially available include concrete plugs, stemming plugs, Rocklock plugs, tulip plugs, and foam plugs (Karakus *et al.*, 2003; Cevizci, 2012).

Stemming-related parameters (burden, spacing, blast-hole depth)

An assessment of stemming practice could not have been done in isolation. Other parameters that affect blast results are closely linked to stemming practice. Burden, spacing, and blast-hole length (depth) are some of the interrelated parameters, critical during drilling, which were assessed for this study (de Graaf, 2013). The other interrelated parameters are hole diameter, bench height, subdrill, and drilling patterns (NPS, 1999; Lusk & Worsey, 2013). Due to the complex nature of blast design, it was not possible to evaluate all the parameters mentioned. This may constitute a limitation of the study. The parameters assessed were those for which data was readily available and which were critical for the research project.

Sereme *et al.* (2019) defined spacing as the distance between adjacent blast-holes, measured perpendicular to the burden. Spacing is generally measured between holes positioned parallel to the cut face of the bench. The relationship for burden and spacing is a ratio of 1.0 to 1.5. Burdens that are too large produce inadequate fragmentation, toe problems, and excessive ground vibrations (NPS, 1999; Lusk & Worsey, 2013; de Graaf, 2013).

The hole length is a function of the bench height and the subdrill combined. The subdrill is the distance drilled below the floor level to ensure that the full face of the rock is removed. Hole depths that are less than 1.5 times the burden cause excessive air blast and flyrock (NPS, 1999; Lusk & Worsey, 2013; de Graaf, 2013).

Methodology

The stemming practices at the mine were assessed using quantitative and qualitative methods. The tasks included the collation of stemming parameters; analyses and comparisons of the stemming parameter (mine design *vs*. actual *vs*. rule-of-thumb) values; collation and analyses of data indicating the performance of the blasts (ground vibration and air blast); and finally a monitoring exercise to determine compliance of the mine blasting practices with their standard operating procedures.

Quantitative analysis

The quantitative analysis included the collation and scrutiny of pre-blast and post-blast data. Pre-blast reports, blast-hole data sheets, and the stemming design guidelines were obtained from the mine to conduct the pre-blast quantitative analysis. The stemming parameters assessed were stemming length, stemming material, and stemming-related parameters that included burden, spacing, and hole depth.

Data on coal (No. 2 and No.4 seams), shale, sandstone, and interburden (mixture of sandstone and torbanite) blasts was assessed. The majority of the available data was from blasts prior to the researchers' presence at the study area.

Some of the challenges encountered during the collation of data from the pre-blast reports included the need for re-organization of reports in chronological order; illegibility and data capturing errors; incomplete fields of data; and the need to scan the hardcopy reports. These challenges necessitated re-capturing of the data on a spreadsheet to facilitate ease of interpretation and analysis of the data.

The actual stemming lengths recorded in the pre-blast reports were compared against the recommended mine design stemming lengths to determine their level of compliance. A total of 70 blasts (25 coal, 17 interburden, 16 shale, and 12 sandstone) were analysed. Thereafter, the stemming length variations for actual, mine design, and rule-of-thumb (Equation [1]) stemming lengths were analysed for coal, interburden, shale, and sandstone. Based on the results, the researchers deemed it necessary to further analyse how the design stemming length varied with the rule-of-thumb (Equation [2]).

The post-blast analysis was conducted by assessing fourteen months of data from eight seismograph stations around the mine that record peak particle velocity (PPV ground vibration) and air blast. The seismographs measure data continuously and trigger only when a pre-set threshold value is exceeded. The threshold values set by the mine for ground vibration and air blast were guided by the international US Bureau of Mines (USBM) standards. According to Sereme *et al.*, (2019) these values were below the threshold of 134 dB typically set for South African coal mines. The ground vibration threshold limits set by the mine were such that 95% of all blasts should be below 130 dB and 85% below 125 dB. The air blast threshold limits set by the mine were such that 95% of all blasts should be below 2 mm/s and 85% below 1 mm/s.

The pre-blast data and post-blast results were examined and plotted graphically to determine if there was a correlation between stemming length compliancy and air blast or ground vibration.

Qualitative analysis

The qualitative analysis was aimed at monitoring stemming practice and compliance with mine standards and procedures (Sereme *et al.*, 2019). The researchers observed the drilling, charging, and blasting procedures at three mining blocks for three consecutive weeks. Data gathered during the observations included the blast location, bench material, hole condition, detonator type, stemming parameters, and comments on the observations. Measurements of newly drilled holes, while the researchers were at the mine, were done by the drill-and-blast team, closely observed by the researchers.

Results and discussion

Quantitative analysis

Stemming length

Figure 1 illustrates the general relationship between the actual stemming lengths and the mine design stemming lengths for all the blasts.

The sandstone blasts show the greatest variation in stemming length compared to coal, interburden, and shale. Deviations of the actual stemming length from the design for coal, interburden, shale, and sandstone are quantified in Figures 2–5.

As shown in Figure 2 the actual stemming length used on the mining block differed from the design stemming length for all the 25 coal blasts investigated. Blasts 1 to 12 were No. 2 Seam coal, while blast 13 to 25 were on No. 4 Seam coal. There was also a variation between the rule-of-thumb stemming length (20*D*) and the design stemming length.

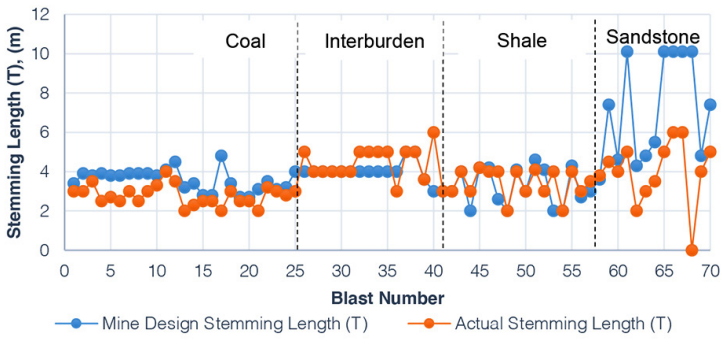

Figure 1—A comparison of mine design and actual stemming lengths for all blasts

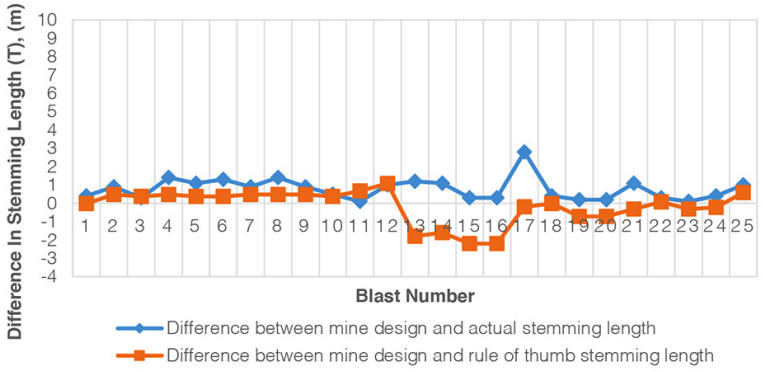

Figure 2—Stemming length variations for coal blasts

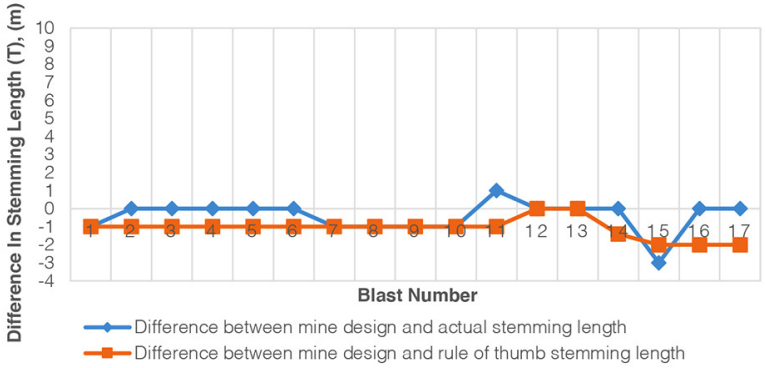

Figure 3—Stemming length variations for interburden

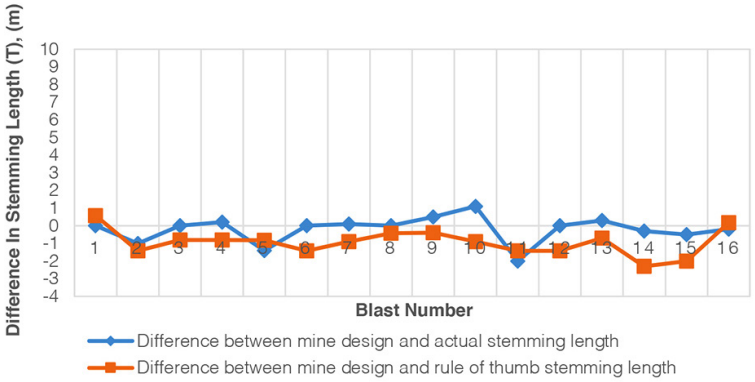

Figure 4—Stemming length variations for shale blasts

The mine design stemming length was greater than the actual stemming length for all the analysed coal blasts, as shown by the positive differences in Figure 2. The average and maximum differences were 0.78 m and 2.8 m (blast 17), respectively. Hole diameters for blasts 1 to 12 and blasts 18 to 25 were 171 mm, while those for blasts 13 to 17 were 250 mm. This equated to rule-of-thumb stemming lengths of 3.42 m and 5.0 m for 171 mm and 250 mm diameter holes, respectively. The variation between mine design and rule-of-thumb stemming lengths was less than 0.5 m for the first eleven blasts. The mine design stemming length was less than the rule-of-thumb values in thirteen blasts. The average difference between mine design and rule-of-thumb stemming length was 0.67 m, with a maximum difference of 2.20 m (blast 16).

More than half (10 out of 17) of the interburden blasts showed compliance between the design stemming length and the actual stemming length. The design stemming length exceeded the actual stemming length by 1.0 m for blast 11 and was 3.0 m less than the actual stemming length for blast 15 (Figure 3).

The design stemming length was less than or equal to the rule-of-thumb stemming length for all the interburden blasts, with an average difference of 1.0 m. Hole diameters were designed at 250 mm, which corresponds to a rule-of-thumb stemming length of 5.0 m. The maximum difference between the mine design and rule-of-thumb stemming length was 2.0 m.

An analysis of shale blasts (Figure 4) showed that the mine design stemming length corresponded with the actual stemming length for five of the sixteen blasts. The average and maximum differences between the design and actual stemming lengths were 0.5 m and 2.0 m, respectively.

The mine design stemming length was less than the rule-of-thumb stemming length in all blasts except blasts 1 and 16. The average and maximum deviation from the rule-of-thumb stemming length values was 1.0 m and 2.3 m respectively.

The actual stemming lengths used on the mining block for sandstone blasts were found to be less than the design stemming length for all 12 blasts investigated, as shown in Figure 5.

The actual stemming length values deviated from the design stemming length by an average of 3.4 m. Blast number 10 was anomalous, with 10.0 m difference between the design and the actual stemming length. The design stemming length was greater than the rule-of-thumb stemming length for eight of the 12 blasts, with an average difference of 2.7 m and a maximum difference of 5.1 m. In the sandstone blasts, hole diameters were designed at 250 mm.

Sereme *et al.* (2019) provided the following possible reasons for the variation of actual stemming length from that recommended in the mine design:

i. The blasting team was given some flexibility to alter the blast design according to the block conditions after drilling
ii. Inaccurate drilling resulted in shorter or longer holes, and therefore in shorter or longer stemming lengths respectively
iii. Inaccuracy in charging of holes, with undercharging and overcharging resulting in longer and shorter stemming lengths respectively
iv. The presence of cracks may have affected the amount of explosives charged
v. The inaccuracy of the air-gap length
vi. Manual data entry of stemming lengths was inaccurate and prone to error
vii. Unverified data before filing
viii. Distortion of the correct measurement of holes due to uncleaned hole collars
ix. Collapsed holes may have resulted in inaccurate stemming length when measured.

Non-technical reasons for the variation of actual stemming length from design stemming length may be attributed to non-compliance, hence poor stemming practice.

Due to the variance between the design stemming length and the rule-of-thumb (20*D*) stemming length, the researchers decided to perform further analyses by comparing how the design stemming length varied with the rule-of-thumb: $T = 0.7b$ to $1.2b$ (Equation [2]). In Figure 6, upper and lower limit stemming length values were determined using Equation [2]. The majority of the coal blasts used a burden of 6.0 m, which translates to upper and lower limit stemming length values of 7.2 m and 4.2 m. The majority of the stemming length values were found to be less than the lower stemming length limit, as shown in Figure 6. Only one blast (blast 11) had a design stemming value that was within the rule-of-thumb bounds.

For interburden, the upper limit stemming length value of 9 m represents blasts with a burden of 7.5 m and the lowest limit value of 3.5 m corresponds to those blasts with a burden of 5.0 m. The design stemming length was closer to the lower limit. and less than half of the design stemming length values fell within the rule-of-thumb bounds (Figure 7).

Design stemming length values for sandstone (Figure 8) blasts differed slightly from the trends shown by the coal and interburden blasts. All the sandstone blasts used a burden of 6.0 m, which translates to an upper limit stemming length of 7.2 m and a lower bound of 4.2 m. Of the 12 blasts analysed, five design stemming length values fell above the upper limit, two values were equal to the upper limit, and the rest were within the two limits.

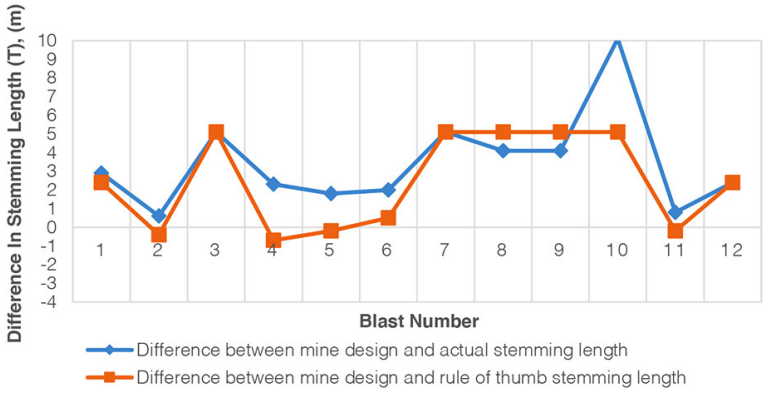

Figure 5—Stemming length variations for sandstone blasts

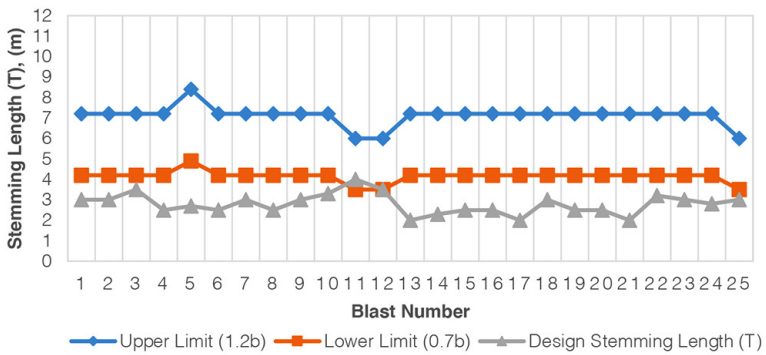

Figure 6—Design stemming length *vs.* the rule-of-thumb values for coal

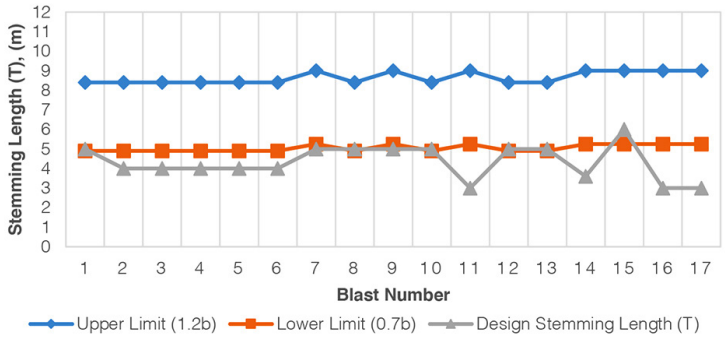

Figure 7—Stemming length *vs.* the rule-of-thumb values for interburden

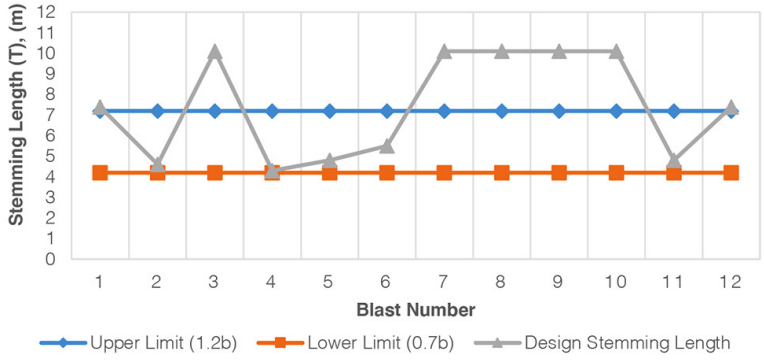

Figure 8—Stemming length *vs.* the rule-of-thumb values for sandstone

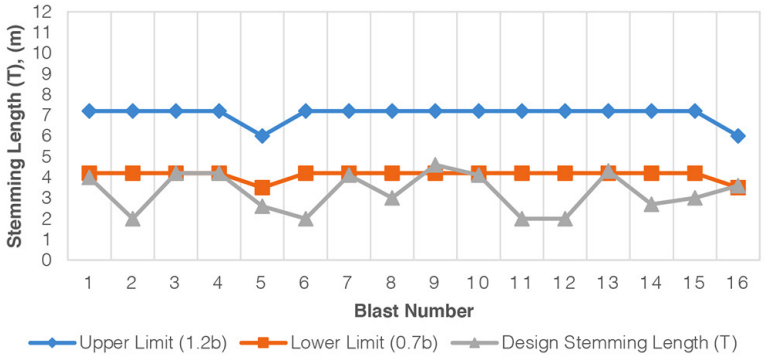

Figure 9—Stemming length *vs.* the rule-of-thumb values for shale

The majority of the values were below the lower limit of 4.2 m (which corresponds to a burden of 6 m), and only one value was within the rule-of-thumb limit for stemming. It is also noteworthy that the design stemming lengths varied for most of the blasts.

The mine design stemming lengths for coal varied from the rule-of-thumb for the majority of the blasts. The differences between the rule-of-thumb stemming length and the design stemming length may be attributed to the site conditions, which necessitated modifications to the design. Fragmentation size requirements or the need to limit air blast and ground vibration may have been factors considered when designing the stemming length, resulting in a deviation from the rule-of-thumb stemming length.

Stemming material

An analysis of stemming material used for all the blasts revealed that the designed stemming material was used in practice on the mining block. The stemming materials used for the different blasts were aggregate, chrome slag, and drill chippings (for coal blasts). Compliance between the design and actual stemming material size with the rule-of-thumb for material size (Equation [3]) could not be ascertained due to the relevant data not being available. However, it should be emphasised that the rule-of-thumb serves as a guide only. Experience and mine-specific environmental conditions inform the choice of stemming material. Different stemming materials and stemming accessories had either been trialled by the mine or were trialled or being used in other operations with similar geology.

Stemming-related parameters

Burden and spacing

A comparison between the mine design and actual burden on 122 data-points showed that 78% of the burden values complied with the design (Figure 10). Since most of the burden values for different rock types were equal, and thus superimposed on each

other, the number of data-points that are visible on the straight line of the graph is not a true reflection of compliance. Blasts with a design burden value of zero may have been one-row or pre-split blasts. However, actual burden values greater than zero were recorded for some of these blasts. This may have been because of incorrect data capture.

Similarly, for spacing it was found that 22% of the actual spacing values did not comply with the mine design spacing. This type of non-compliance may have resulted from inaccurate manual capturing of data and/or a change in the design based on environmental conditions on the block. The spacing variation results are shown in Figure 11.

Since burden and spacing are a function of hole diameter, it is possible that a change in diameter resulted in the deviations of the actual burden and spacing from the design values. Further discussion on burden and spacing is provided in the qualitative analysis section.

Hole depth analysis

An analysis of actual hole depths was conducted to determine any variations from mine design hole depths. Figure 12 shows that there was some variation from designed hole depths, as indicated by the points which lie below or above the x = y trendline. Of the 122 hole depth values, 78% did not correspond with the design hole depth. The average difference between the design and actual hole depth values was 1.6 m, with a maximum difference of 13 m.

Based on the graph, the general trend shows a close grouping of the points around the x = y trendline. There are outliers; the difference between the design and actual hole depths was 10 m and 13 m for two blasts, shown within the dotted circle in Figure 12.

Hole depth is a function of bench height and subgrade drilling. The deviation between mine design and actual blast-hole depths may possibly be attributed to the actual bench

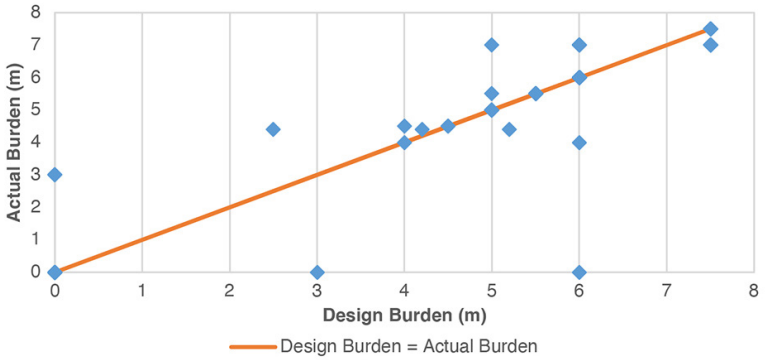

Figure 10—Variation between design and actual burden for all blasts

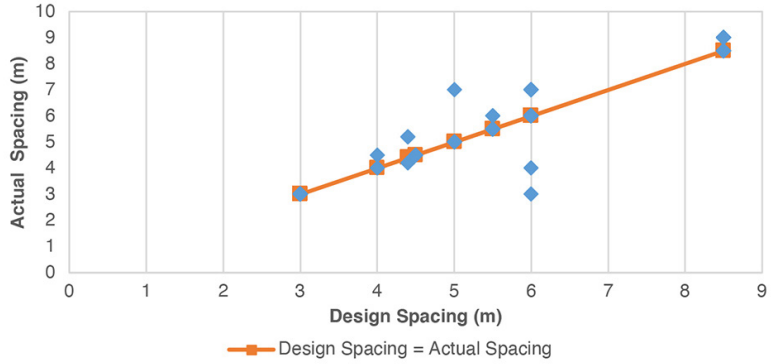

Figure 11—Variation between design and actual spacing for all blasts

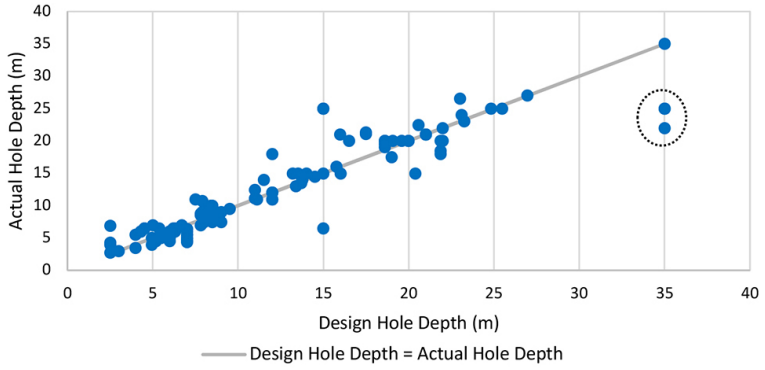

Figure 12—Variation between design and actual hole depths for all blasts

height being less than or greater than the design bench height. Alternatively, some holes may have partially collapsed and become filled with drill chippings from the crest of the hole.

There are currently no guidelines to show the relationship between deviations from the design and the corresponding impacts on blasting. Hence, it is unclear whether the 1.6 m average difference in hole depth had a significant impact on blasting conditions. This statement also applies to the other parameters assessed, such as stemming length, burden, and spacing.

Analysis of post-blast data in relation to stemming length

As presented in Figure 13, the actual and design stemming lengths were compared and assessed against the air blast and ground vibration (PPV) results to determine if there was a correlation. The data for ground vibration and air blast recordings less than and greater than the threshold values are shown. The distribution of the seismograph results indicates that there is no correlation between non-compliant stemming lengths and ground vibration and air blast.

This is evident from the fact that some PPV and air blast results that exceeded the threshold plot on the y = x line. Even though the actual stemming length for these blasts complied with the design stemming length, the ground vibration and air blast values exceeded the threshold values. Similarly, the two values at 7.4 m design stemming length (within the dotted circle), were below the PPV-air blast threshold, although the stemming length was less than designed.

There are, however, two exceptional cases for designed stemming lengths of 10.0 m in sandstone (within the dashed circle). Non-compliance of actual parameters with the design parameters such as stemming length and drill-hole depth may have resulted in inadequately confined or overconfined blast-holes, possibly contributing to excessive air blast. Based on the majority of the results, as discussed above, there is insufficient evidence to suggest that poor stemming practice was the only cause of high PPVs and air blast (Sereme *et al.*, 2019). However, poor stemming practices cannot be completely ruled out as a contributing factor to these adverse conditions. Further studies may be required to determine the actual causes of excessive ground vibration and air blast by timeously analysing data associated with blasts exceeding the thresholds. The results, however, will be highly dependent on the accuracy of data recorded by the drill-and-blast team.

Qualitative analysis

The following observations were made in relation to stemming practices, as reported by Sereme *et al.* (2019):

i. The block was not well prepared, *e.g.* blast-hole collars were not cleaned
ii. Short holes that required re-drilling were charged without being re-drilled
iii. Burden and spacing were mostly inconsistent
iv. Blast-hole depths were mostly incorrect and no corrective measures were implemented
v. Trucks used for charging and stemming had difficulty manoeuvering around the holes due to the uneven and muddy nature of the floor, potentially covering already drilled holes
vi. Twining procedures were not followed at all times
vii. The explosive mobile manufacturing unit (MMU) operator had an assistant that informed him when the hole was pumped with sufficient explosives. This information was communicated by a whistle blow from the assistant. This manual operation has a high potential for human error and inconsistency
viii. Tying up of shock tubes (initiation systems) was a challenge due to misaligned holes.

Twining is a conventional method of ensuring that sufficient space is left in the hole for gassing of explosives, using a string to mark where stemming should start. In some blast-holes twining was not done, which increases the likelihood of incorrect stemming length. The positioning of blast-holes (burden and spacing) was done using a geographical positioning system (GPS), which is dependent on the network connection. It was observed that the GPS would often get disconnected from the network and blast-holes would be incorrectly positioned. Additionally, the qualitative analysis reaffirmed the quantitative analysis results by revealing that short holes were not re-drilled, burden and spacing were inconsistent, and incorrect blast-hole depths were not corrected.

Poor stemming practices cannot be attributed to a single non-compliant parameter, but may be caused by the knock-on effect of inconsistencies in any part of the process. For example, if blast-holes were drilled shorter or longer than designed, the stemming length would be affected. This emphasises the importance of adhering to the design parameters and, in the example above, ensuring that incorrectly drilled holes are re-drilled to their correct depth if necessary. In cases where a blast-hole is longer than designed, drill chippings should be used to refill it to the designed depth.

Although all activities in the mining cycle are important and interrelated, drilling is the backbone of all processes (Abbaspour *et al.*, 2018; Messaoud, 2006). Non-compliant drilling

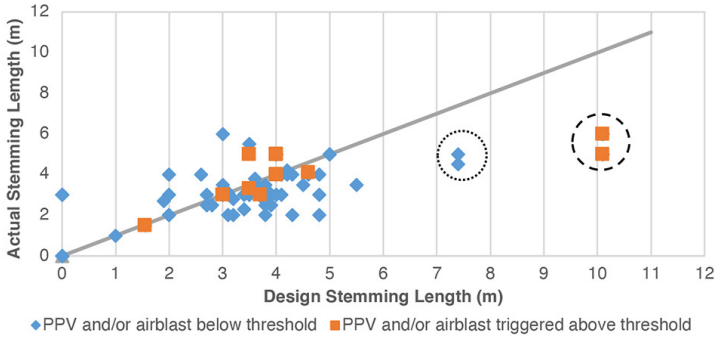

Figure 13—The relationship between stemming lengths and post-blast data

practices directly result in non-compliant stemming practices, inconsistencies in charging and timing and, consequently, a non-conformant blast.

Recommendations

Based on the results of the study, the following recommendations are provided to improve stemming practices, which may ultimately contribute to improving the blast conditions at the mine.

i. Ensure the correct capturing of data and full completion of fields with the correct data format before submitting to the last level of authority for final sign-off
ii. Blast reports and charging control sheets should be thoroughly checked and verified by the various levels of authority before final sign-off
iii. The mine standards for quality control and quality assurance should be strictly followed after drilling of holes, after charging, gassing, and stemming
iv. Any deviations from the blasting plan parameters should be reported to the person of authority, who will then make an informed decision on appropriate mitigation measures
v. The responsible person of authority should update the blasting plan based on the deviations and feed back the information to the personnel on the block
vi. Investigate the development of digital entry and recording systems for capturing on-bench blasting parameters to reduce inefficiency and errors. Digital methods to record data may improve processes and ultimately result in better blasting
vii. Recording of blasting outcomes (*e.g.*, fragmentation, loading times) could be correlated with (digitally recorded) blasting inputs and used as a tool to improve blast designs.

Improved information flow between personnel on the block and those at the mine offices may enhance the overall blast performance.

Conclusion

The stemming practices at a South African surface coal mine were investigated to determine if they had a significant influence on air blast and ground vibration. The investigation revealed that there is a need for digital entry and recording systems for capturing on-bench blasting parameters, as the current data recording and reporting systems are inefficient and prone to error. Improvements to blasting practices are possible through efficient and accurate data recording and reporting systems.

Non-compliance of actual parameters with the design parameters such as stemming lengths and drill-hole depths may have resulted in inadequately confined or overconfined blast-holes, possibly contributing to excessive ground vibration and air blast. However, the quantitative analysis indicated that there was no direct correlation between stemming length and excessive air blast and ground vibration. Since blasting parameters are interrelated, we may conclude that poor stemming practice was not the sole cause of excessive air blast and ground vibration, but may have been a contributing factor to these adverse outcomes. It is therefore important that all blasting procedures (including stemming) are executed correctly and recorded accurately.

Finally, all blasting parameters should be assessed when air blast and ground vibration values exceed the threshold. This should be done as soon as such measurements are recorded, so that the fundamental cause may be determined and appropriate mitigation measures implemented.

References

Abbaspour, H., Drebenstedt, C., Badroddin, M., and Maghaminik, A. 2018. Optimized design of drilling and blasting operations in open pit mines under technical and economic uncertainties by system dynamic modelling. *International Journal of Mining Science and Technology*, vol. 28. pp. 839–848.

Bajpayee, T., Verakis, H., and Lobb, T. 2004. An analysis and prevention of flyrock accidents in surface blasting operations. National Institute for Occupational Safety and Health, Washington, DC. https://www.cdc.gov/niosh/mining/userfiles/works/pdfs/apfasbo.pdf

Banks, V.J., Palumbo-Roe, B., van Tonder, D.B., Davies, J., Fleming, C., and Chevrel, S. 2011. Conceptual models of Witbank Coalfield, South Africa. Natural Environment Research Council, Swindon, UK.107 pp. http://nora.nerc.ac.uk/id/eprint/506746/1/EO-MINERS-D3.1-2%20CSM%20Witbank%20FINAL_signed_20120329.pdf

BME. 2018. Resources: Blasting Guide.: Bryanston, South Africa. http://demo.bme.co.za/downloads/send/2-brochures/2-blasting-guide [accessed 2 April 2018].

Boshoff, D. and Webber-Youngman, R. 2011. Testing stemming performance, possible or not?. *Journal of the Southern African Institute of Mining and Metallurgy*, vol. 111, no. 12. pp. 871–874.

Cevizci, H. 2012. A newly developed plaster stemming method for blasting. *Journal of the Southern African Institute of Mining and Metallurgy*, vol. 112, no. 12. pp. 1071–1078.

De Graaf, W. 2013. Surface mining explosives. *Explosives Engineering*: University of Pretoria. pp. 3.10–3.19.

Karakus, D., Onur, A.H., Konak, G., Köse, H., and Kizilcaağaçli, M. 2003. Application of stemming plugs and a case study in a limestone quarry. *Proceedings of the 18th International Mining Congress and Exhibition of Turkey (IMCET 2003)*. http://www.maden.org.tr/resimler/ekler/107931de60c5a7c_ek.pdf [accessed 6 May 2018].

Lusk, B. and Worsey, P. 2013. Explosives and blasting. *SME Mining Engineering Handbook*. Society for Mining, Metallurgy & Exploration, Littleton, CO, pp. 443–459.

Messaoud, L. 2006. Drilling technology in mining industry. *Acta Montanistica Slovaca*, vol. 11. pp. 113–118.

Mohamed, E., Armaghani, D., and Motaghedi, H. 2013. The effect of geological structure and powder factor in flyrock accident, Masai, Johor, Malaysia. *Electronic Journal of Geotechnical Engineering*, vol. 18. pp. 5561–5572.

Neale, A.M. 2010. Blast optimization at Kriel Colliery. *Journal of the Southern African Institute of Mining and Metallurgy*, vol. 110, no. 4. pp. 161–168.

NPS. 1999. Blast design. *Handbook for the Transportation, and Use of Explosives*. National Park Service, US Cepartment of the Interior, Washington, DC. https://www.nps.gov/parkhistory/online_books/npsg/explosives/Chapter8.pdf [accessed 10 May 2018].

Patidar, P. 2017. Role of stemming in open cast mine. https://www.slideshare.net/pankajpatidar15/role-of-stemming-in-open-cast-mine [accessed 17 May 2018].

Sereme, B., Mpofu, M., Roberts, D., Ngobese, S. and Lumbwe, T. 2019. Monitoring of blasting and determination of optimal stemming. Coaltech Research Association, Johannesburg. Unpublished report. ◆

21 South African mining and metallurgy researchers ranked in the world's top 2% scientists

A recently published database [1] from Stanford University lists the top 2% of science researchers in the world. Numerous South African scientists have found a place in the rankings for the sub-discipline of mining and metallurgy.

The research team, led by Dr John Ioannidis, created a database that includes the best scientists in the world, using standard citation indicators. The indicators took into account the number of citations, h-index, co-authorship adjusted hm-index, citations of papers in different authorship positions, and a composite indicator. The database categorized 160 000 scientists in 22 scientific fields and 176 sub-fields.

The 21 South African scientists who featured in the Mining and Metallurgy ranking according to career-long citation impact are as follows:

Name	Institution	No. of papers	Ranking
Frank Crundwell	CM Solutions	65	13
Sue Harrison	University of Cape Town	156	38
Herman Potgieter	University of the Witwatersrand	167	45
John Preston	Mintek	51	55
Dick Stacey	University of the Witwatersrand	98	108
Jochen Petersen	University of Cape Town	84	119
Leon Lorenzen	Stellenbosch University	87	123
Dee Bradshaw	University of Cape Town	156	128
Michael Moys	University of the Witwatersrand	89	135
Cyril O'Connor	University of Cape Town	185	151
Kathy Sole	University of Pretoria	42	159
Dave Deglon	University of Cape Town	50	221
Jan Svoboda	De Beers Group	32	225
Mariekie Gericke	Mintek	30	272
Geoff Hansford	University of Cape Town	54	274
Steven Bradshaw	Stellenbosch University	100	286
Sehliselo Ndlovu	University of the Witwatersrand	59	316
Salih Ramazan	AngloGold Ashanti Limited	16	369
Jean-Paul Franzidis	University of Cape Town	97	468
Victor Ross	Mintek	22	524
Rob van Hille	University of Cape Town	53	572

1. Baas, J., Boyack, K., and Ioannidis, J. 2020. Data for 'Updated science-wide author databases of standardized citation indicators'. Mendeley Data, vol. 2. doi: 10.17632/btchxktzyw.2. https://data.mendeley.com/datasets/btchxktzyw/2

Effects of flotation operational parameters on froth stability and froth recovery

M. Ostadrahimi[1,3], S. Farrokhpay[2], K. Gharibi[1], A. Dehghani[1], and M. Aghajanloo[3]

Affiliation:
[1] Faculty of Mining & Metallurgical Engineering, University of Yazd, Iran.
[2] GeoRessources, University of Lorraine, 54505 Nancy, France.
[3] Iranian Mines & Mining Industries Development & Renovation Organization (IMIDRO), Tehran, Iran.

Correspondence to:
S. Farrokhpay

Email:
farrokhpay@hotmail.com

Dates:
Received: 9 Jul. 2020
Revised: 6 Dec. 2020
Accepted: 11 Dec. 2020
Published: January 2021

How to cite:
Ostadrahimi, M., Farrokhpay, S., Gharibi, K., Dehghani, A., and Aghajanloo, M. 2021
Effects of flotation operational parameters on froth stability and froth recovery.
Journal of the Southern African Institute of Mining and Metallurgy, vol. 121, no. 1, pp. 11–20.

DOI ID:
http://dx.doi.org/10.17159/2411-9717/1272/2021

ORCID
S. Farrokhpay
https://orcid.org/0000-0001-8848-8490

Synopsis

The effect of flotation operational parameters on froth stability and froth recovery was studied. Froth stability was measured using a special column. To determine the froth recovery, the froth height change model and froth height exponential model were used. It was found that since the interactions between the pulp and froth zones affect the time of froth formation, the exponential model is more suitable than the froth height change method for determining the froth recovery. The results showed that superficial air velocity and collector dosage have, respectively, the highest and lowest effect on the froth recovery, while froth recovery decreases sharply with increasing froth height.

Keywords
froth stability, froth recovery, superficial air velocity, collector dosage, frother dosage.

Introduction

Froth stability plays an important role in determining selectivity and recovery in flotation (Farrokhpay, 2011). It should be noted that froth with very high stability is not desirable because in addition to recovering the particles attached to the bubbles, it creates favourable conditions for entrainment (Zheng, Franzidis, and Johnson, 2006). Froth stability can be defined as froth retention time, which depends on the structure of the froth and size distribution of the bubbles (Aktas, Cilliers, and Banford, 2008), or decay time of the froth (Tsatouhas, Grano, and Vera, 2006).

Froth stability can be determined by dynamic or static tests. The froth dynamic is determined by measuring the maximum froth height, and the froth static is determined by the time taken the froth to decay after the air is shut off (Farrokhpay, 2011).

The concept of dynamic froth stability was first introduced by Bickerman in 1973 and was later modified by Barbian, Ventura-Medina, and Cilliers (2003). Dynamic froth stability is the ratio of froth volume to the aeration value; if the cross-sectional area of the whole cell is assumed to be the same, the dynamic froth stability is equal to the froth retention time and is calculated using Equation [1]:

$$\sum = \frac{V_f}{Q} = \frac{H_{max}}{J_g} \quad [1]$$

where
V_f is froth volume
Q is air volume flow rate
H_{max} is maximum froth height
J_g is superficial gas velocity.

The effect of particle size has been investigated by several researchers (Achaye, 2018; Norori-McCormac *et al.*, 2017; Cilek and Uysal, 2018; Aveyard *et al.*, 1994; Long Liang *et al.*, 2015; Ata, Ahmed, and Jameson, 2004; Vera *et al.*, 2002). In general, fine particles affect froth stability and the role of hydrophobic particles is significant.

The type and amount of frother also affect the froth stability (Ata, 2009; Gupta *et al.*, 2007; Castro *et al.*, 2013; McFadzean, Marozva, and Wiese, 2015). Ata (2009) examined the separation of particles during bubble coalescence, and found that increasing the frother dosage sincreases the contact surface and decreases the particle separation, and thus reduces the bubble coalescence and increases the froth stability.

Another factor that affects the froth stability is pH. It can change the behaviour of the minerals in the pulp by affecting the charge level of the particles. Farrokhpay and Zanin (2012) examined the effect

of water quality on the froth stability for a zinc concentrate from Australia. They found that decreasing the pH increases the froth half-life due to the decrease in the zeta potential of the particle surfaces, and increases the pulp viscosity.

Other factors affecting the froth stability include dissolved oxygen (Do), reduction potential (Eh), and ionic strength (Is) (Farrokhpay and Zanin, 2012; Sheni, Corin, and Wiese, 2018; Manono, Corin, and Wiese, 2012). Increasing the Eh or Is and decreasing the Do results in increased froth stability (Sheni, Corin, and Wiese, 2018). Increasing the Eh increases the number of particles entering the froth phase, which can lead to a higher froth stability. However, due to the increase in the water recovery, the probability of entrainment of particles with poor hydrophobicity is also higher.

Froth recovery, which is the ratio of the mass of particles released into the concentrate through true flotation to the mass of the particles attached at the pulp-froth interface, is often used to measure the performance of the froth phase (Yianatos *et al.*, 2008). This approach focuses on the overall behaviour of the froth, which is used for modelling in flotation plants. The concept of froth recovery was first proposed by Finch and Dobby (1990). In general, froth recovery can be measured by direct or indirect methods. In the direct methods, by measuring the bubble loading, froth recovery can be calculated (Bhondayi and Moys, 2011). The direct methods have been introduced by various researchers, including Falutsu and Dobby (1992), Seaman, Franzidis, and Manlapig, (2004), Dyer (1995), and Rahman, Ata, and Jameson (2013).

One indirect method to measure the froth recovery is using froth height changes and the overall flotation recovery. In this method, the kinetic constant of flotation (k) is obtained according to the froth height (H) and then an H-k diagram is drawn (Figure 1). Due to the linearity of the constant kinetic-froth height graph, their relationship will be as follows:

$$k = a - b \times H \quad [2]$$

where
a is the width is from the origin and is equal to the kinetic constant at a froth height equal to zero (kinetic constant of the collection zone (k_c))
B is the length of the origin (the point where the kinetic constant is zero)s.

Equation [2] can be written as:

$$k = k_c \left(1 - \frac{H}{H_{(k=0)}}\right) \quad [3]$$

According to the froth recovery equation provided by Dobby and Finch (1991), froth recovery is defined as follows (Seaman, Manlapig, and Franzidis, 2006):

$$R_f = \left(1 - \frac{H}{H_{(k=0)}}\right) \quad [4]$$

This method has been used by various researchers, including Feteris, Frew, and Jowett (1987), Vera, Franzidis, and Manlapig (1999), and Seaman, Franzidis, and Manlapig (2004). Other methods of indirect froth recovery measurement have been discussed by Savassi *et al.* (1997), Alexander, Franzidis, and Manlapig (2003), Yianatos, Bergh, and Cortj (1998), Gorain *et al.* (1998), Wilson (1952), Neethling (2008), and Amelunxen *et al.* (2018).

Materials and methods

Froth stability measurement

Froth stability was measured using a column similar to that used by Zanin *et al.* (2009) and McFadzean, Marozva, and Wiese (2015) (Figure 2).

Froth recovery

Froth recovery was calculated using froth height changes (Equation [5]). Recall that at the maximum froth height, the froth recovery is zero.

$$R_f = \frac{k}{k_c} = 1 - \frac{H}{H_{max}} \quad [5]$$

Froth height can be related to the froth formation time according to Equation [6] (Technological Resources Pty Limited, 2004):

$$\frac{dH}{H_{max}} = \frac{1}{\tau} e^{-t/\tau}\, dt \quad [6]$$

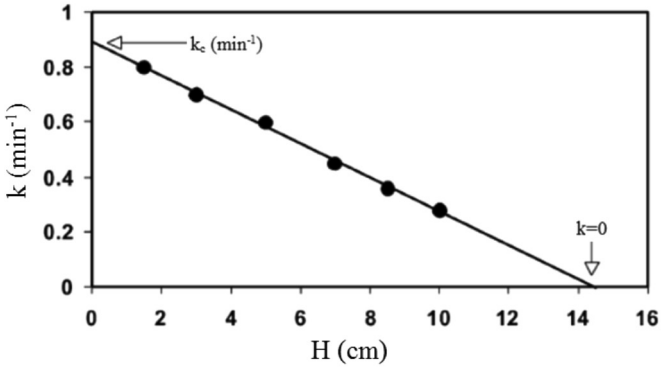

Figure 1—Relationship between the kinetic constant and froth height (Seaman, Manlapig, and Franzidis, 2006)

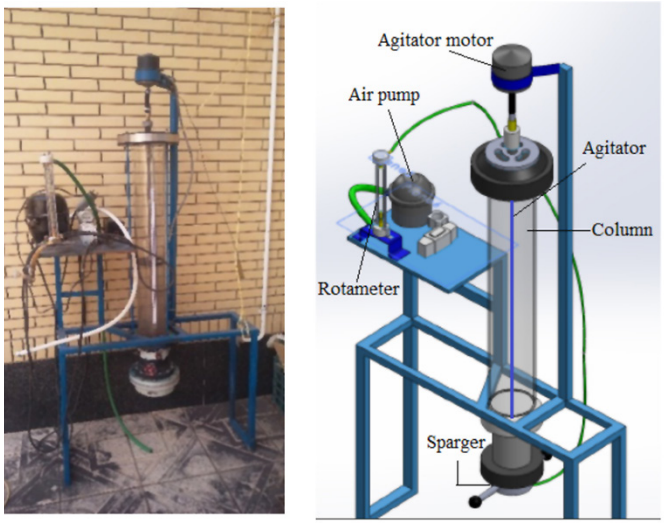

Figure 2—The froth stability column

Given that the maximum height occurs at infinite time, the integral of Equation [6] is shown as Equation [7]:

$$\int_{H}^{H_{max}} \frac{dH}{H_{max}} = \int_{t}^{\infty} \frac{1}{\tau} e^{-t/\tau} dt$$

$$1 - \frac{H}{H_{max}} = e^{-t/\tau} \quad [7]$$

According to Equations [5] and [7], froth recovery can be calculated using Equation [8]:

$$R_f = e^{-t/\tau} \quad [8]$$

Test method

One of the most suitable methods for designing experiments is central composite rotatable design (CCRD). This method is useful for examining independent variables that affect the dependent variables and provides a statistical and mathematical procedure for studying the relationship between responses and a number of influential factors (Napier-Munn, 2014).

The experiments were performed using Design Expert software version 10 (DX10). Independent variables or input parameters for this study were: collector and frother dosage, superficial air velocity, and particle size (d_{50}). The dependent variables or responses were froth half-life, maximum froth height, and froth recovery.

Sample specifications

A sample of iron ore concentrate containing sulphide minerals from Gole-Gohar Sirjan Company (Iran) was used. The prepared samples were stored in a dryer at 95°C for 24 hours to dry.

Sample characterization

Mineralogy studies (XRD and SEM) showed magnetite as the main mineral. The sample also contained haematite, pyrite, and talc. Pyrite was the most important sulphur-bearing mineral in the sample (Figures 3 and 4).

According to the Cyclosizer results, 50% and 80% of the sample were less than 36 and 100 µm, respectively (Figure 5).

Materials

Potassium amyl xanthate (PAX) and methyl isobutyl carbinol (MIBC) were used as collector and frother, respectively.

Results and discussion

Since one of the flotation parameters was the particle size, a screen analysis was performed and after homogenization (according to d_{50}) the sample was divided into 1 kg portions. Sample analysis is shown in Table I. It seems that sizing does not have a significant effect on the grade of the sample.

For each of the 30 experiments, samples were taken from the froth section and the concentration of solid particles (Pc) was obtained. Sampling was performed about 5 cm above the pulp-froth interface.

The results showed that the concentration of the solid particles had a significance level of 95%. Accordingly, decreasing the particle size, as well as increasing the superficial air velocity (J_g), collector dosage (Cc), and frother dosage (Fc), all result in an increased concentration of the solid particles in the froth phase (Figure 6).

Froth stability

Froth formation

According to the results of the variance analysis, the effect of the tested parameters on the froth stability and froth recovery are

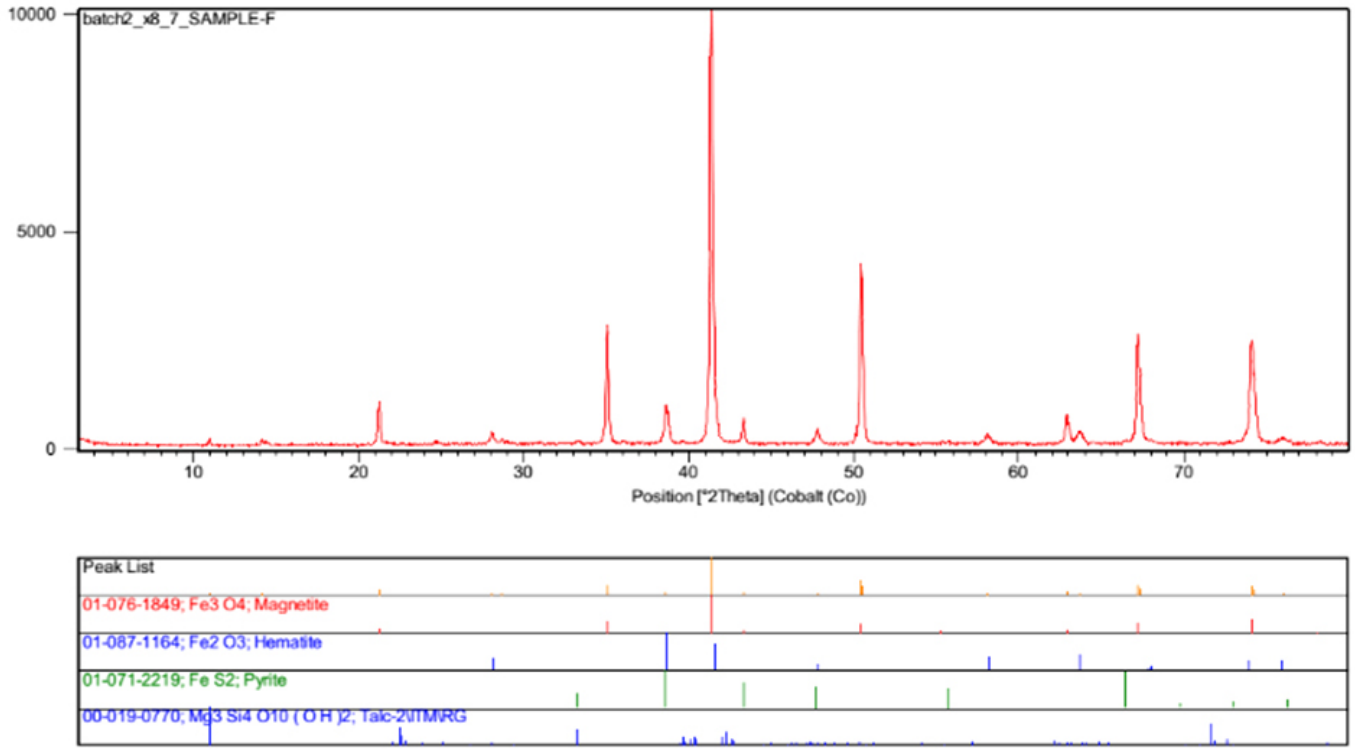

Figure 3—X-ray diffraction (XRD) results on the sample

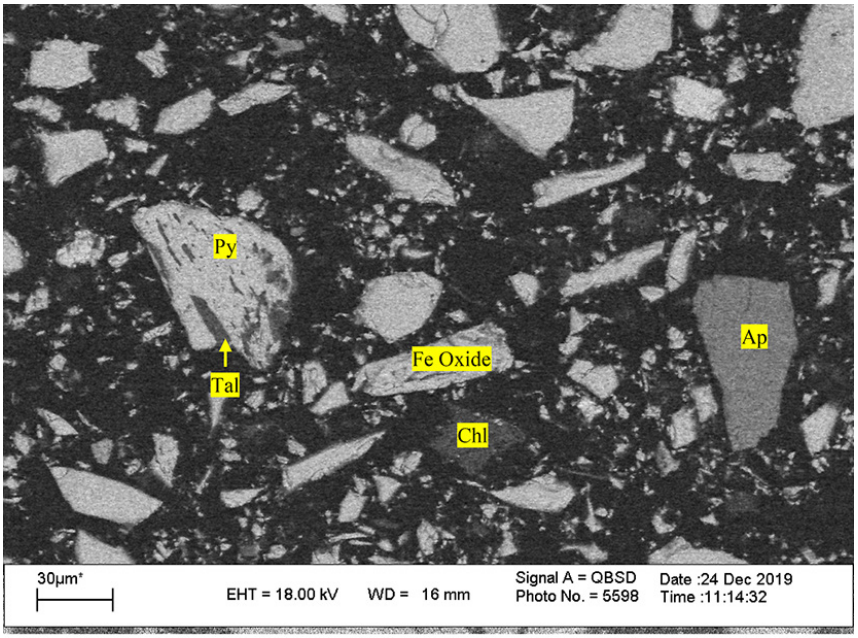

Figure 4—SEM micrograph of the sample, showing iron minerals, pyrite, talc, apatite, and chlorite

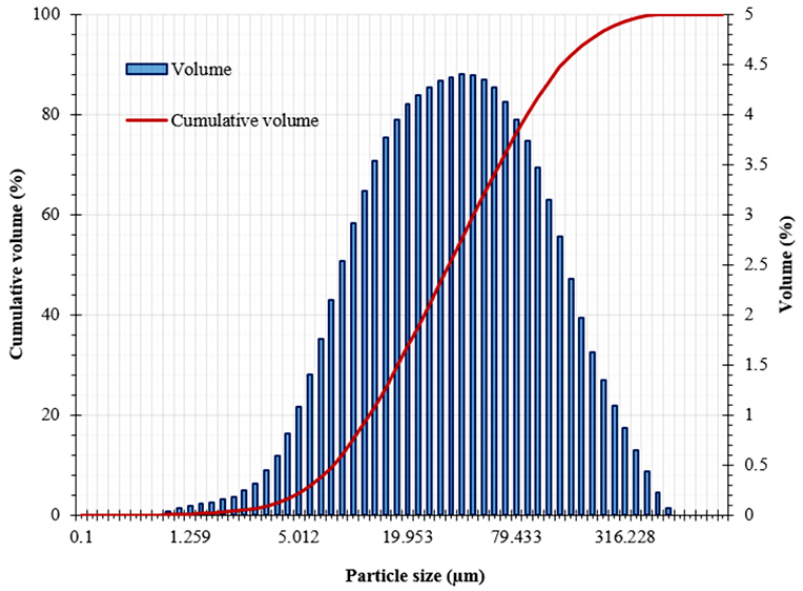

Figure 5—Size distribution of the sample

Table I

Chemical analysis of the samples at different d_{50} sizes

NO.	d_{50} (µm)	Fe (%)	FeO (%)	S (%)
1	15	67.25	23.34	1.26
2	20	67.63	23.46	1.23
3	36	68.04	23.59	1.22
4	60	68.67	23.84	1.18
5	84	68.78	23.53	1.15

statistically significant at a 95% confidence level. The interaction between the superficial air velocity and frother dosage, and frother dosage and particle size, is also significant, at a 95% confidence level.

Figure 7 shows the effect of various factors on the froth retention time (FRT). It can be observed that increasing the superficial air velocity, collector dosage, or frother dosage increases the FRT, while increasing the particle size reduces the FRT.

The superficial air velocity significantly changes the composition and structure of the froth phase; however, its exact effect is not clear (Li *et al*, 2016). Increasing the superficial air velocity increases the gas holdup (Pérez-Garibay *et al*., 2014), as well as the probability of particle-bubble collisions and attachment. This in turn increases the volume of solid particles in the froth phase (James Noel, Prokop, and Tanner, 2002; Al-Fariss, El-Aleem, and El-Nagdy, 2013). Therefore, the higher concentration of particles in the froth phase leads to an increase in the froth height (Figure 6). However, an excessive superficial

Effects of flotation operational parameters on froth stability and froth recovery

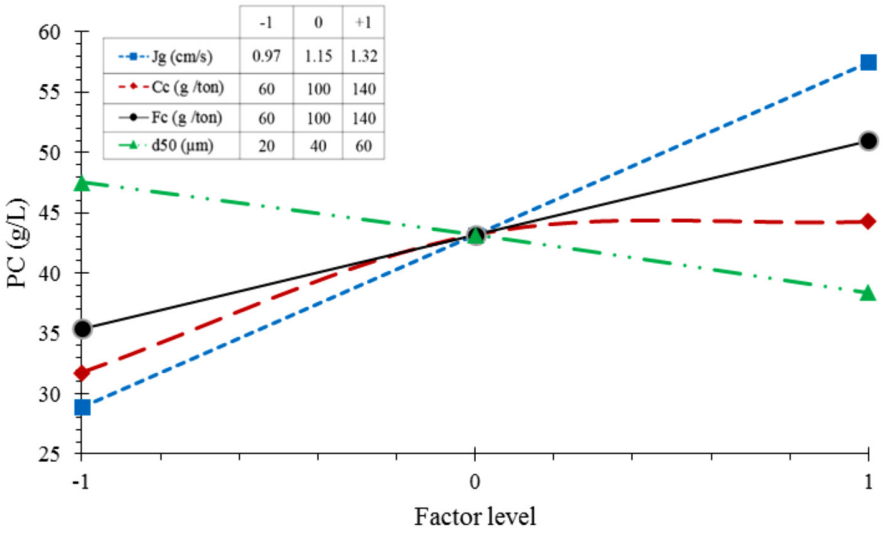

Figure 6—The effect of different variables on the concentration of solid particles in the froth phase

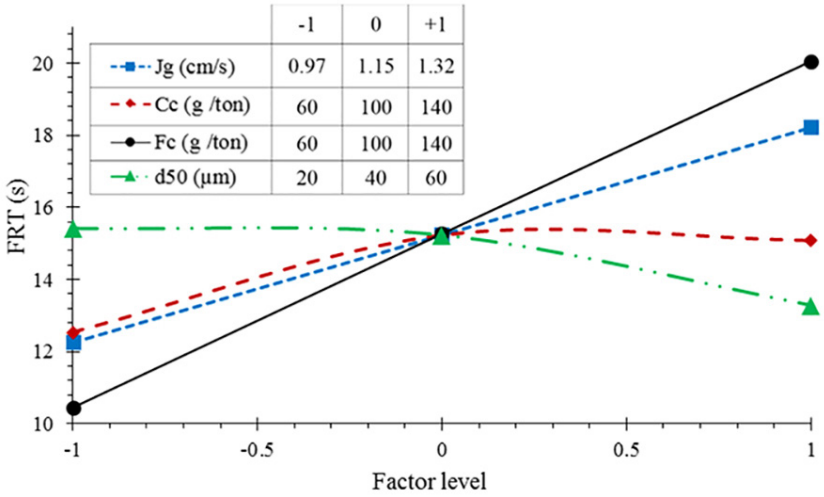

Figure 7—The effect of various factors on froth formation

air velocity can reduce the volume of the particles in the froth phase (Al-Fariss, El-Aleem, and El-Nagdy, 2013).

The enhancement in the bubble load depends on the collector dosage (Eskanlou *et al.*, 2018): at higher collector dosage, the concentration of particles in the froth phase increases due to increased bubble-particle attachment. However, an excessive amount of collector will cause bubble clustering and has a negative effect on the bubble loading (Eskanlou *et al.*, 2018; Ata and Jameson, 2005).

An increase in the frother dosage will reduce the bubbles size (Wei, and Finch, 2014; Zhu *et al.*, 2019) and increase bubble stability. The probability of collision of a particle with a bubble also increases (Reis *et al.*, 2019). Therefore the bubble loading, or in other words the amount of particles that enter the froth phase by attachment to the bubbles, increases, which will stabilize the froth (Ata, 2009). Although small bubbles are beneficial, as noted above, the absence of large bubbles may reduce the flotation recovery (Hassanzadeh *et al.*, 2017).

It seems that the superficial air velocity interacts with the frother dosage (Figure 8). For example, when the frother dosage was increased from 60 to 140 g/t, the maximum froth height at an air velocity of 0.97 and 1.32 cm/s increased by about 7.3 and 15.2 cm, respectively. The same trend was observed for froth retention time.

An increase in the superficial air velocity is accompanied by an increase in the volume of air inside the cell (Pérez-Garibay *et al.*, 2014), and an increase in the frother dosage reduces the bubble size (Wei, and Finch, 2014; Zhu *et al.*, 2019), so the interaction of these two factors results in increasing the number of bubbles, which has a positive effect on the froth formation. It will also increase the likelihood of particles-bubble collisions, which increases the presence of particles in the froth phase.

Increasing the particle size results in fewer particles, which may reduce the slurry viscosity (Cilek and Uysal, 2018; Long Liang *et al.*, 2015; Wei and Finch, 2014. Decreasing the particle size, on the other hand, can reduce the rate of bubble coalescence and consequently decreases the bubble size (Li *et al.*, 2016). This hinders the fluid drainage (Achaye, 2018) which leads to increased froth stability. When the particles are very small, there is a possibility of an increase in entrainment (Cilek and Umuka, 2001; Wang *et al.*, 2015), so it can affect the froth instability.

It is worth mentioning that a significant difference between the maximum initial and the fixed froth height was observed at the maximum value of d_{50} and frother dosage (Figure 9).

Effects of flotation operational parameters on froth stability and froth recovery

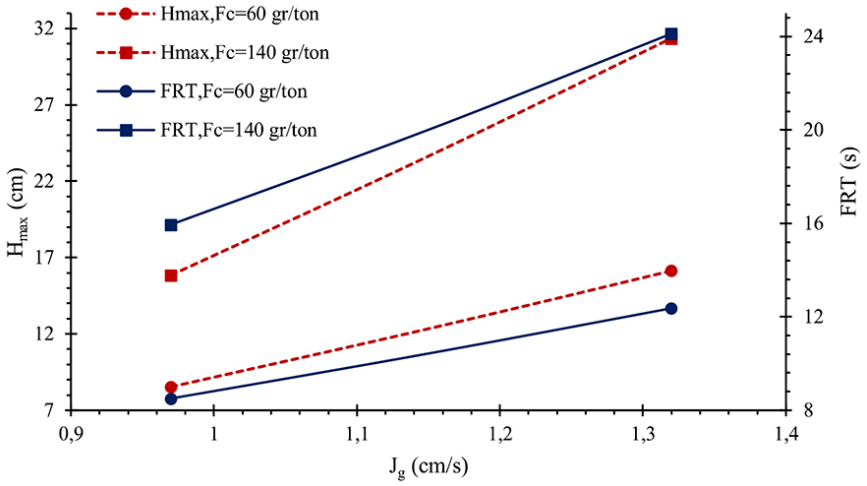

Figure 8—The interaction between superficial air velocity and frother dosage

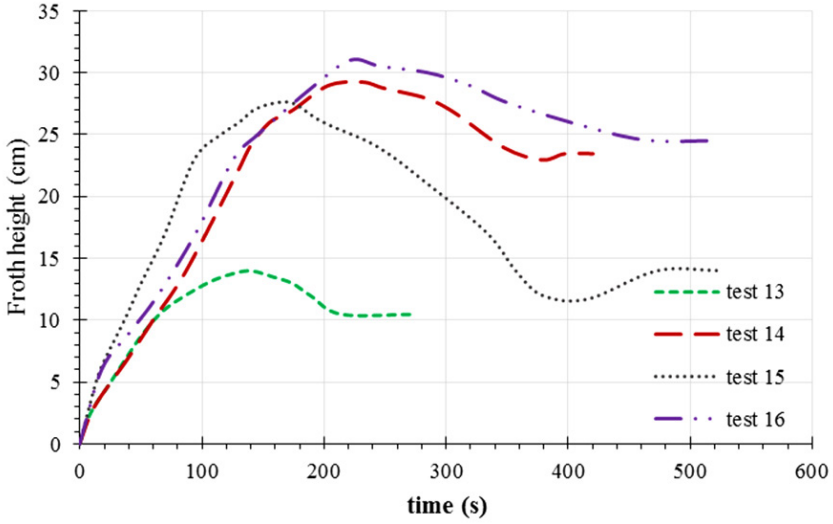

Figure 9—Froth height changes in experiments 13 to 16

Froth decay

The analysis of variance shows that the effect of independent variables is significant, with a 95% confidence level, while the confidence level for the frother dosage-d_{50} is 90%. It should be noted that the effect of the superficial air velocity (*Jg*), collector dosage (*Cc*) and frother dosage (*Fc*) is similar to that discussed for the froth formation.

Figure 10 shows that the froth half-life increases with increasing the superficial air velocity, collector dosage, frother dosage, and particle size (d_{50}).

An increase in fine particles accelerates the process of froth decay, perhaps due to the presence of more water along with the fine particles, which causes the froth to become more fluid (Eskanlou *et al.*, 2018). If the concentration of very small particles increases, the presence of these particles in the froth phase and increased viscosity will retard froth decay.

Froth recovery

Table II shows the froth recovery results at different froth heights.

Comparison of the two models

A comparison between the results obtained from two methods (using Equations [5] and [8]) shows that with increasing froth height, the difference between the two methods decreases. At average heights of 4, 8, 10, and 15 cm, the differences are 6.6, 4.8, 5.4, and 2.0%, respectively.

Figure 11 shows a comparison of the average recoveries for the two models at different froth heights. It can be seen that with increasing froth height, froth recovery obtained in the exponential model is less than that from the froth height change model.

The effect of various parameters

Experimental design results show that the froth recoveries obtained at froth heights of 4, 8 and 10 cm are at 95% confidence level, but for 15 cm froth height the collector dosage did not have the required level of confidence.

(i) Superficial air velocity (J_g)
Froth recovery increases with increasing J_g. Increasing the superficial air velocity enhances the froth height and thus results in increased froth stability and consequently froth recovery. Also, according to the froth recovery model, in the same experimental conditions, increasing

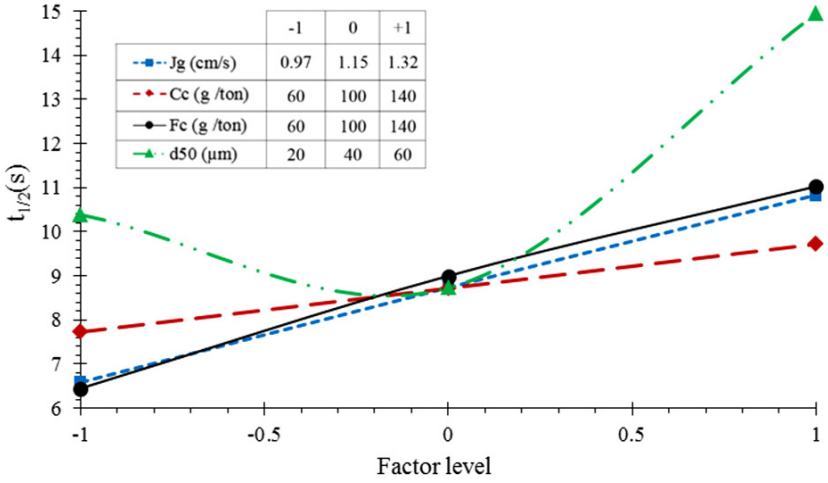

Figure 10—The effect of various factors on froth decay

Table II

Froth recovery % at different froth heights (cm)

No.	Froth height change model (Equation [5])				Exponential model (Equation [8])			
	H=4	*H*=8	*H* H=10	*H*=15	*H*=4	*H*=8	*H*=10	*H*=15
1	31.03	0.00*	0.00	0.00	34.63	0.00	0.00	0.00
2	70.80	41.61	27.01	0.00	79.66	44.31	19.87	0.00
3	50.00	0.00	0.00	0.00	63.62	2.12	0.00	0.00
4	71.43	42.86	28.57	0.00	90.58	52.42	10.34	0.00
5	69.23	38.46	23.08	0.00	69.78	34.13	21.67	0.00
6	86.67	73.33	66.67	50.00	91.95	83.97	74.74	46.43
7	70.37	40.74	25.93	0.00	81.08	37.52	31.69	0.00
8	88.41	76.81	71.01	56.52	86.00	71.67	65.03	50.12
9	0.00	0.00	0.00	0.00	4.54	0.00	0.00	0.00
10	66.67	33.33	16.67	0.00	68.43	25.78	15.59	0.00
11	46.67	0.00	0.00	0.00	50.64	0.00	0.00	0.00
12	73.33	46.67	33.33	0.00	84.41	42.54	28.79	0.00
13	61.90	23.81	4.76	0.00	51.29	18.84	10.13	0.00
14	82.98	65.96	57.45	36.17	70.51	46.48	37.43	24.40
15	71.43	42.86	28.57	0.00	53.21	29.12	18.00	0.00
16	83.67	67.35	59.18	38.78	81.56	57.18	47.49	29.72
17	40.30	0.00	0.00	0.00	41.44	0.00	0.00	0.00
18	86.89	73.77	67.21	50.82	84.76	72.11	50.64	45.01
19	42.86	0.00	0.00	0.00	40.85	0.00	0.00	0.00
20	73.33	46.67	33.33	0.00	82.90	41.69	26.91	1.83
21	20.00	0.00	0.00	0.00	10.00	0.00	0.00	0.00
22	86.89	73.77	67.21	50.82	91.05	79.45	67.57	49.72
23	87.69	75.38	69.23	53.85	91.65	80.94	75.14	57.63
24	60.00	20.00	0.00	0.00	50.82	14.97	7.96	0.00
25	78.14	56.28	45.36	18.03	83.62	48.35	39.54	19.22
26	76.47	52.94	41.18	11.76	81.07	52.56	42.23	14.65
27	77.78	55.56	44.44	16.67	76.83	53.57	42.91	18.93
28	80.00	60.00	50.00	25.00	82.05	64.28	55.23	19.22
29	74.19	48.39	35.48	3.23	66.29	43.94	38.01	1.64
30	77.01	54.02	42.53	13.79	71.88	49.11	32.72	11.85

J_g causes the maximum froth height and the froth formation rate (τ) to be increased, which consequently increases the froth recovery.

Figure 12A shows that the froth recovery at all froth heights increases with increasing J_g. For example, when the superficial air velocity increases from 0.97 to 1.32 cm/s, froth recovery at heights of 4, 8, 10, and 15 cm increased by 47%, 146%, 117%, and 260% respectively.

(ii) Collector dosage (*Cc*)

Figure 12B shows that increasing the collector dosage leads to an increase in the froth recovery, although the effect is less pronounced compared to the other studied factors. The maximum increase in froth recovery is about 29%, which is related to a froth height of 8 cm (*Cc* increases from 60 to 140 g/t).

The increase in froth recovery is possibly due to an increase in the amount of concentrate due to the increased number of particles entering the froth phase, as well as the positive effect on the froth stability. It was also observed that the effect of the collector dosage decreases with increasing froth height. Since increasing the *Cc* leads to the presence of low-hydrophobicity

Effects of flotation operational parameters on froth stability and froth recovery

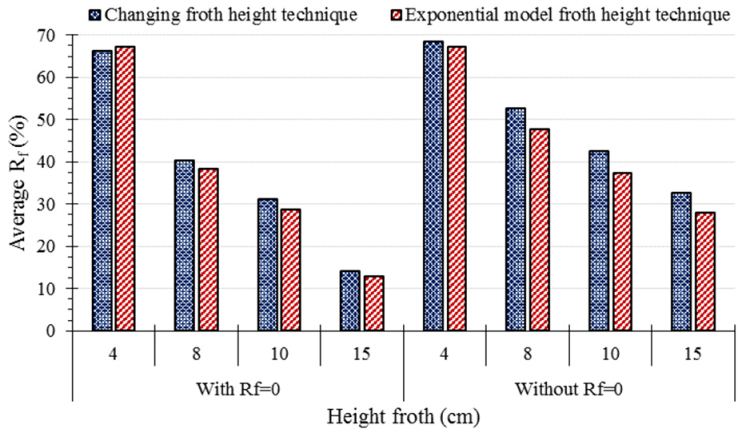

Figure 11—Comparison of two froth recovery models (R_f) at different heights according to the maximum froth height (H_{max})

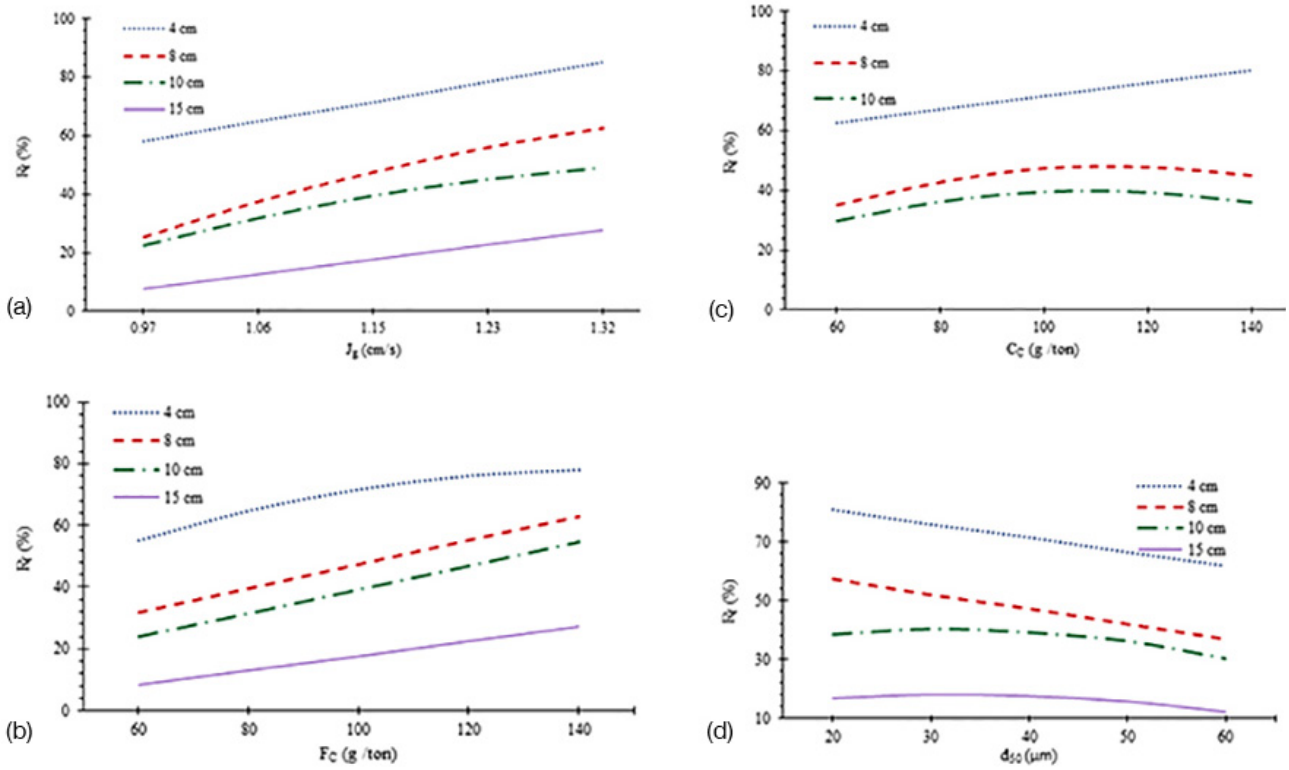

Figure 12—The effect of various factors on the froth recovery (R_f)

particles in the froth, as the froth height increases, these particles usually leave the froth zone and drop back into the pulp (Pita, 2017), so considering that these particles are not recovered, raising the collector dosage at a high froth height does not have a significant effect on the froth recovery.

(iii) Frother dosage (*Fc*)

Increasing the frother dosage increases the froth recovery, and the effect is similar at different froth heights. For example, in Figure 12C, when froth height is 10 cm, the froth recoveries at dosage of 60 and 140 g/t are 24 and 55%, respectively.

Based on the results, there is an interaction between *Jg* and *Fc*. However, the interaction varies with the froth height. As the froth height increases, the intensity of the effect of superficial air velocity for frother dosage decreases. Figure 13A shows that when the frother dosage increases from 60 to 140 g/t with *Jg* = 1.32 cm/s, froth recovery at a height of 4 cm increases by only 14%, while for heights of 10 and 15 cm, froth recoveries of 134% and 400% were observed, respectively. This can be related to the detachment of particles from the bubbles and increased aeration of the bubbles (Vinnett Contreras, and Yianatos, 2014), which also increases the froth height, leading to an increase in the bubble size (Bhondayi and Moys, 2014). This increases the likelihood of bubbles coalescence, resulting in reduced output concentrations. An increased frother dosage will prevent this phenomena and hence increase the effect on the froth recovery at greater froth heights compared with lower froth heights. Also, at low froth heights, particles have less opportunity to detach from the bubbles, and it seems that at these heights, the effect of the superficial air velocity is much greater than that of frother dosage.

(iv) Particle size (d_{50})

Figure 12D shows that as the particle size increases, the froth recovery decreases. For example, for froth heights of 4, 8, 10, and 15 cm at d_{50} = 20 µm, recoveries are about 81%, 58%, 39%, and 17% respectively. The corresponding values for d_{50} = 60 µm are 62%, 37%, 30%, and 12%. According to previous results, increasing the particle size leads to fewer particles in the froth phase, and hence to a reduction in the bubble loading, transfer of particles to the concentrate zone, froth instability, and particle drainage. Also, with increasing froth height the probability of small particles entering the froth zone through entrainment decreases (Figure 12D). The interaction between d_{50} and *Fc* at froth heights of 10 and 15 cm was found to be significant. The effect of increasing frother dosage on the froth recovery is far greater in the case of fine particles than for for coarse particles (Figure 13B). This is due to the fact that fine particles are more susceptible to entrainment. The number of bubbles increases with increasing frother dosage, which consequently increases the amount of fine particles in the concentrate zone.

Conclusions

Increasing the superficial air velocity, or dosage of collector or frother, increases the rate of froth formation and froth decay. However, the behaviour of the particles at different sizes was found to be different. This indicates that an increase in fine particles has a positive effect on the froth formation due to the increased viscosity of the pulp. However, when the froth decays, the greater loading of fine particles accelerates the process of froth destruction, probably due to the presence of more water along with the fine particles.

The froth recovery results obtained from the exponential model seems to be more accurate than those from the froth height change models. In addition to the effect of froth height, the time to reach the maximum froth height was also considered. It was found that the superficial air velocity has the greatest effect on the froth recovery, while the collector dosage has the least effect. Increasing the superficial air velocity, collector dosage, and frother dosage had a positive effect on froth recovery, but increasing the particle size led to a lower froth recovery.

References

Achaye, I. 2018. Effect of particle properties on froth stability. PhD thesis, University of Cape Town, South Africa.

Aktas, Z., Cilliers, J.J., and Banford, A.W. 2008. Dynamic froth stability: Particle size, airflow rate and conditioning time effects. *International Journal of Mineral Processing*, vol. 87. pp. 65–71.

Alexander, D.J., Franzidis, J.P., and Manlapig, E.V. 2003. Froth recovery measurement in plant scale flotation cells. *Minerals Engineering*, vol. 16, no. 11. pp. 1197–1203.

Al-Fariss, T.F., El-Aleem, F.A., and El-Nagdy, K.A. 2013. Beneficiation of Saudi phosphate ores by column flotation technology. *Journal of King Saud University Engineering Sciences*, vol. 25. pp. 113–117.

Amelunxen, P., LaDouceur, R., Amelunxen, R., and Young, C. 2018. A phenomenological model of entrainment and froth recovery for interpreting laboratory flotation kinetics tests. *Minerals Engineering*, vol. 125. pp. 60–65.

Ata, S. 2009. The detachment of particles from coalescing bubble pairs. *Journal of Colloid and Interface Science*, vol. 338. pp. 558–565.

Ata, S., Ahmed, N., and Jameson, G.J. 2004. The effect of hydrophobicity on the drainage of gangue minerals in flotation froths. *Minerals Engineering*. vol. 17. pp. 897–901.

Ata, S. and Jameson, G.J. 2005. The formation of bubble clusters in flotation cells. *International Journal of Mineral Processing*, vol. 76. pp. 123–139.

Aveyard, R., Binks, B.P., Fletcher, P.D.I., Peck, T.G., and Rutherford, C.E. 1994. Aspects of aqueous foam stability in the presence of hydrocarbon oils and solid particles. *Advances in Colloid and Internee Science*, vol. 48. pp. 93–120.

Barbian, N., Ventura-Medina, E., and Cilliers, J.J. 2003. Dynamic froth stability in froth flotation. *Minerals Engineering*, vol. 16. pp. 1111–1116.

Bhondayi, C. and Moys, M.H. 2014. Measurement of a proxy for froth phase bubble sizes as a function of froth depth in flotation machines Part 1. Theoretical development and testing of a new technique. *International Journal of Mineral Processing*, vol. 130. pp. 8–19.

Bhondayi, C. and Moys, M.H. 2011. Determination of sampling pipe (riser) diameter for a flotation bubble load measuring device. *Minerals Engineering*, vol. 24. pp. 1664–1676.

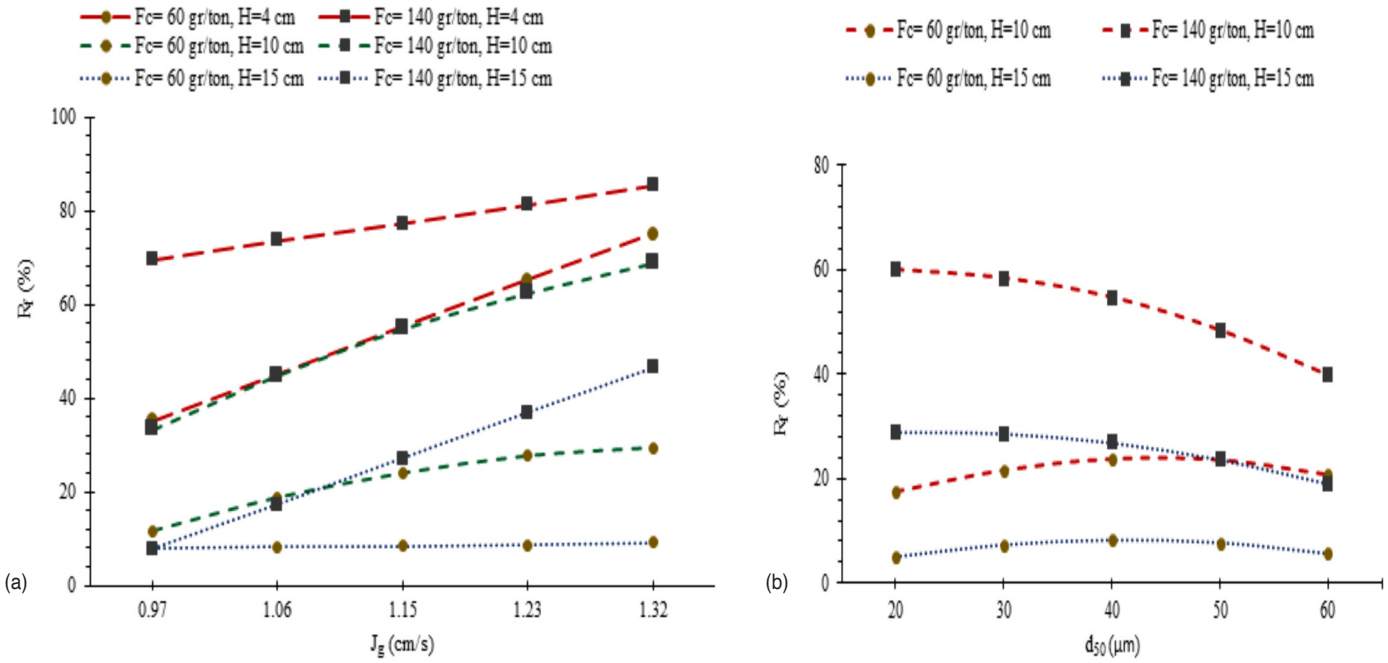

Figure 13—The interaction between various factors and their effect on froth recovery (R_f)

Castro, S., Miranda, C., Toledo, P., and Laskowski, J.S. 2013. Effect of frothers on bubble coalescence and foaming in electrolyte solutions and seawater. *International Journal of Mineral Processing*, vol. 124. pp. 8–14.

Cilek, E.C. and Uysal, K. 2018. Froth stabilization using nanoparticles in mineral flotation. *Physicochemical Problems in Mineral Processing*, vol. 54, no. 3. pp. 878–889.

Cilek, E.C. and Umuka, Y. 2001. A statistical model for gangue entrainment into froths flotation of supplied ores. *Minerals Engineering*, vol. 14, no. 9. pp. 1055–1066.

Dobby, G.S. and Finch, J.A. 1991. Column flotation: A selected review, part II. *Minerals Engineering*, vol. 4, no. 7–11. pp. 911–923.

Dyer, C. 1995. An investigation into the properties of the froth phase in the flotation process. MSc thesis, University of the Witwatersrand.

Eskanlou, A., Khalesi, M.R., Abdollahy, M., and Hemmati, C.M. 2018. Interactional effects of bubble size, particle size, and collector dosage on bubble loading in column flotation. *Journal of Mining and Environment*, vol. 9. pp. 107–116.

Falutsu, M. and Dobby, G.S. 1992. Froth performance in commercial sized flotation columns. *Minerals Engineering*, vol. 5, no. 10–12. pp. 1207–1223.

Farrokhpay, S. 2011. The significance of froth stability in mineral flotation - A review. *Advances in Colloid and Interface Science*, vol. 166. pp. 1–7.

Farrokhpay, S. and Zanin, M. 2012. An investigation into the effect of water quality on froth stability. *Advanced Powder Technology*, vol. 23. pp. 493–497.

Feteris, S.M., Frew, J.A., and Jowett, A. 1987. Modelling the effect of froth depth in flotation. *International Journal of Mineral Processing*, vol. 20, no. 1–2. pp. 121–135.

Gorain, B.K., Harris, M.C., Franzidis, J.P., and Manlapig, E.V. 1998. The effect of froth residence time on the kinetics of flotation. *Minerals Engineering,* vol. 11, no. 7. pp. 627–638.

Gupta, A.K., Banerjee, P.K., Mishra, A., and Satish, P. 2007. Effect of alcohol and polyglycol ether frothers on foam stability. *International Journal of Mineral Processing*, vol. 82. pp. 126–137.

Hassanzadeh, A., Kouachi, S., Hasanzadeh, M., and Çelik, M.S. 2017. A new insight to the role of bubble properties on inertial effect in particle-bubble interaction. *Journal of Dispersion Science and Technology*, vol. 38, no. 7. pp. 953–960.

James Noel, L., Prokop, A., and Tanner, R.D. 2002. Foam fractionation of a dilute solution of bovine lactoferrin. *Applied Biochemistry and Biotechnology*, vol. 98–100. pp. 395–402.

Li, C., Farrokhpay, S., Runge, K., and Shi, F. 2016. Determining the significance of flotation variables on froth rheology using a central composite rotatable design. *Powder Technology*, vol. 287. pp. 216–225.

Long Liang, L., Li, Z., Peng, Y., Tan, J., and Xie, G. 2015. Influence of coal particles on froth stability and flotation performance. *Minerals Engineering*, vol. 81. pp. 96–10.

Manono, M.S., Corin, K.C., and Wiese, J.G. 2012. An investigation into the effect of various ions and their ionic strength on the flotation performance of a platinum bearing ore from the Merensky reef. *Minerals Engineering*, vol. 36–38. pp. 231–236.

McFadzean, B., Marozva, T., and Wiese, J. 2015. Flotation frother mixtures: Decoupling the sub-processes of froth stability, froth recovery and entrainment. *Minerals Engineering*, vol. 85. pp. 72–79.

Napier-Munn, T.J. 2014. Statistical Methods for Mineral Engineers - How to Design Experiments and Analyse Data. Julius Kruttschnitt Mineral Research Centre, Brisbane.

Neethling, S.J. 2008. Simple approximations for estimating froth recovery. *International Journal of Mineral Processing*, vol. 89. pp. 44–52.

Norori-McCormac, A., Brito-Parada, P.R., Hadler., Cole, K., and Cilliers, J.J. 2017. The effect of particle size distribution on froth stability in flotation. *Separation and Purification Technology*, vol. 184. pp. 240–247

Pérez-Garibay, R., Ramirez-Aguilera, N., Bouchard, J., and Rubio, J. 2014. Froth flotation of sphalerite: Collector concentration, gas dispersion and particle size effects. *Minerals Engineering*, vol. 57. pp. 72–78.

Pita, F. 2017. Influence of froth height on column flotation of kaolin ore. *Minerals*, vol. 7. p. 235. https://doi.org/10.3390/min7120235

Rahman, R.M., Ata, S., and Jameson, G.J. 2013. Froth recovery measurements in an industrial flotation cell. *Minerals Engineering*, vol. 53. pp. 193–202.

Reis, A.S., Reis Filho, A.M., Demuner, L.R., and Barrozo, M.A.S. 2019. Effect of bubble size on the performance flotation of fine particles of a low-grade Brazilian apatite ore. *Powder Technology*, vol. 356. pp. 884–891.

Savassi, O.N., Alexander, D.J., Johson, N.W., Franzidis, J.P., and Manlapig, E.V. 1997. Measurement of froth recovery of attached particles in industrial flotation cells. *Proceedings of the Sixth Mill Operators Conference*, Madang, Papua New Guinea. Australasian Institute of Mining and Metallurgy, Melbourne. pp. 149–155.

Seaman, D.R., Manlapig, E.V., and Franzidis, J.P. 2006. Selective transport of attached particles across the pulp–froth interface. *Minerals Engineering*, vol. 19. pp. 841–851.

Seaman, D.R., Franzidis, J.P., and Manlapig, E.V. 2004. Bubble load measurement in the pulp zone of industrial flotation machines-a new device for determining the froth recovery of attached particles. *International Journal of Mineral Processing*, vol. 74, no. 1–4. pp. 1–13.

Sheni, N., Corin, K., and Wiese, J. 2018. Considering the effect of pulp chemistry during flotation on froth stability. *Minerals Engineering*, vol. 116. pp. 15–23.

Technological Resources Pty Limited, University of Manchester Institute of Science and Technology. 2004. Measuring froth stability. Pat. WO 2004/080600 A1. https://patents.google.com/patent/WO2004080600A1/en

Tsatouhas, G., Grano, S., and Vera, M. 2006. Case studies on the performance and characterisation of the froth phase in industrial flotation circuits. *Minerals Engineering*, vol. 19. pp. 774–783.

Vera, M.A., Franzidis, J.P., and Manlapig, E.V. 1999. Simultaneous determination of collection zone rate constant and froth zone recovery in a mechanical flotation environment. *Minerals Engineering*, vol. 12, no. 10. pp.1163–1176.

Vera, M.A., Mathe, Z.T, Franzidis, J.P., Harris, M.C., Manlapig, E.V., and O'Connor, C.T. 2002. The modelling of froth zone recovery in batch and continuously operated laboratory flotation cells. *International Journal of Mineral Processing*, vol. 64. pp. 135–151.

Vinnett, L., Contreras, F., and Yianatos, J. 2014. Gas dispersion pattern in mechanical flotation cells. *Minerals Engineering*, vol. 26. pp. 80–85.

Wang, L.Y., Peng, Y., Runge, K., and Bradshaw, D. 2015. A review of entrainment: Mechanisms, contributing factors and modelling in flotation. *Minerals Engineering*, vol. 70. pp. 77–91.

Wei, Z. and Finch, J.A. 2014. Effect of solids on pulp and froth properties in flotation. *Journal of Central South University*, vol. 21. pp. 1461–1469.

Wilson, A.J. 1952. Foams: Physics, Chemistry and Structure. Springer Series on Applied Biology.

Yianatos, J.B., Bergh, L.G., and Cortj, G.A. 1998. Froth zone modeling of an industrial flotation column. *Minerals Engineering*, vol. 11, no. 5. pp. 423–435.

Yianatos, J.B., Moys, M.H., Contreras, F., and Villanueva, A. 2008. Froth recovery of industrial flotation cells. *Minerals Engineering*, vol. 21. pp. 817–825

Zanin, M., Wightman, E., Grano. S.R., and Franzidis, J.-P. 2009. Quantifying contributions to froth stability in porphyry copper plants. *International Journal of Mineral Processing*, vol. 91. pp. 19–27.

Zheng, X., Franzidis. J.P., and Johnson, N.W. 2006. An evaluation of different models of water recovery in flotation. *Minerals Engineering*, vol. 19. pp. 871–882.

Zhu, H., Valdivieso. A.L., Zhu, J., Min. F., Song, S., and Corona Arroyo, M.A. 2019. Air dispersion and bubble characteristics in a downflow flotation column. *Mineral Processing and Extractive Metallurgy Review*, vol. 40, no. 3. pp. 224–229. ◆

A continuous quality improvement framework for electrowinning current efficiency

T.E. Moongo[1,2] and S. Michael[1]

Affiliation:
[1] Department of Mechanical and Marine Engineering, Namibia University of Science and Technology, Namibia.
[2] Department of Mining and Process Engineering, Namibia University of Science and Technology, Namibia.

Correspondence to:
T.E. Moongo

Email:
tmoongo@gmail.com

Dates:
Received: 8 Jun. 2020
Revised: 13 Nov. 2020
Accepted: 26 Nov. 2020
Published: January 2021

How to cite:
Moongo, T.E. and Michael, S. 2021
A continuous quality improvement framework for electrowinning current efficiency.
Journal of the Southern African Institute of Mining and Metallurgy, vol. 121, no. 1, pp. 21–28.

DOI ID:
http://dx.doi.org/10.17159/2411-9717/1243/2021

ORCID
T.E. Moongo
https://orcid.org/0000-0002-2465-0409

S. Michael
https://orcid.org/0000-0002-8003-5216

Synopsis

Electrowinning consumes a substantial amount of electrical energy, and owing to the ever-increasing unit cost of electrical power there is a need to improve current efficiency in the process. This research was carried out to design a continuous quality improvement framework for improving electrowinning current efficiency by applying statistical process control (SPC) on an online industrial copper electrowinning operation. A sequential mixed research methodology was applied and a statistical software package utilized for analysing data. It was concluded that metallurgical short-circuits (hotspots) had the most significant effect on current efficiency. Bringing hotspots under statistical control resulted in a 5.40% improvement in current efficiency, which is equivalent to approximately 74 t of 99.999% pure grade A copper cathode production over a period of 1.5 months.

Keywords

quality, continuous improvement, continuous quality improvement, statistical process control, and current efficiency.

Introduction

The mining industry is a significant contributor to the Namibian economy, accounting for 9.3% of the GDP in 2019 (Chamber of Mines, 2019). The Namibian mining sector is the world leader in deep-sea mining/marine mining, and is currently the fourth-largest producer of uranium oxide worldwide (World Nuclear Association, 2020; Debmarine Namibia, 2020). In Namibia, the mining industry produces a wide range of commodities such as special high-grade zinc, gold bullion, blister copper, grade A copper cathodes, uranium oxide, gem-quality diamonds, cement, dimension stone, semi-precious stones, salt, chemicals, tin concentrate, zinc, and lead concentrates.

One of the state-of-the-art technologies used in the Namibian mining industry is the electrowinning (EW) process. This power-intensive electrical process is utilized for the production of refined copper cathodes (Parada and Asselin, 2009). Regrettably, the unit cost of electrical energy is ever-increasing (Nampower, 2019; Eskom, 2019). In Namibia, the EW process is applied in mine-to-metal operations which are producing gold bullions, special high-grade zinc, and grade A copper cathodes. This research was conducted in Namibia's only copper solvent extraction and electrowinning (SX-EW) plant that applies electrowinning technology to produce copper cathodes of 99.999% purity.

The use of quality control techniques such as statistical process control (SPC) has become essential for any business to thrive in modern industry. Statistical quality control is one of the reasons why the Japanese had a significant advantage over their competitors in the manufacturing industry. This experience may be transferred to the EW process by applying SPC to control current efficiency variables, and hence maintaining an improved current efficiency. However, many organizations are still not applying this powerful quality control technique (Ben and Jiju, 2000; Helm, 2018).

The electrical energy utilized in the electrowinning process can be applied more efficiently and cost-effectively by improving current efficiency (Wang *et al.*, 2016). A typical electrowinning process consumes approximately 60% to 80% of the total electrical energy for a metallurgical plant applying heap leaching (Gonzalez-Dominguez and Dreisinger, 1997). Consequently, there is an opportunity for substantial electrical energy saving and for increasing copper cathode production if electrowinning current efficiency is improved.

Statistical process control

Continuous quality improvement via the application of statistical process control (SPC) has long been

recognized in the metallurgical industry. SPC assists with monitoring process variability and maintaining process stability, thereby ensuring that the plant is under operational control (Godina *et al.*, 2018). The process can get out of statistical control due to process variations, such as controlled process variation and uncontrolled process variation (SCME, 2017).

Occasionally, there are special or assignable causes of process variability that are temporary or not inherently in the process, unlike common (also called random or chance) causes of process variability (Pavol, 2015; Montgomery, 2009). Normally, all the special causes of process variability should be addressed by developing and implementing an Out of Control Action Plan (OCAP) (Amitava, 2016; Helm, 2018; SCME, 2017).

According to the literature, the following tools are utilized in SPC: histograms, scatter diagrams, check sheets, defect-concentration diagrams, cause-and-effect diagrams, process control charts, and Pareto charts (Helm, 2018). In this research, process control charts, Pareto charts, and the Ishikawa diagram were applied.

Process control charts

Process control charts are used to maintain the production process under statistical control. They are frequently employed as diagnostic tools because they can indicate when adjustments should be made in the process. Process control charts monitor process variability and provide information about the stability of the process (Helm, 2018; Montgomery, 2009; SCME, 2017; Wild and Seber, 2017; Leavengood and Reeb, 2015).

Process control charts are constructed by assuming that the quality characteristic data follows a normal/Gaussian distribution. The bell-shaped curve should be reflected on the histogram. This is because the central limit theorem holds if the population distribution of the sample is unimodal and close to symmetric. In general, a process control chart contains three horizontal lines: the upper control limit (UCL), lower control limit (LCL), and the centre line (process average) (Montgomery, 2009; Baradaran and Dashtbani, 2014, Amitava, 2016; SCME, 2017).

It is worth noting that process control charts work with rules for deciding when the process is within or out of SPC. Walter Shewhart developed the eight Shewhart Rules for process control charts. The first four rules are also referred to as the Western Electric Rules. The first rule states that if a point is plotted outside the control limits it is deemed to be out of control. Due to the complexity of the electrowinning process, this is the only Shewhart Rule applied. Typical SPC charts include Xbar (mean) and range ($\bar{X}$ – R) control charts, Individual moving range (I-MR) control charts, proportion control charts (p-charts), Xbar (mean) and standard deviation ($\bar{X}$ – S), and many others (SCME, 2017).

Current efficiency

Current efficiency may be defined as the ratio of direct current utilized for electroplating the metal of interest to the total direct current that is applied to the electrolytic cells (Kafumbila, 2017). From the practical viewpoint, current efficiency refers to the actual quantity of the electroplated metal divided by the theoretical quantity calculated by applying Faraday's equation (Beukes and Badenhorst, 2009; Anderson, 2017).

In industrial copper electrowinning the current efficiency can range from 90% to 95% (Robinson, 2011). Other authors have reported that current efficiency in copper electrowinning should be greater than 92%. Nevertheless, lower current efficiencies may also be experienced depending on the influencing factors. The inefficiently used direct current or low current efficiency represents the direct current that was utilized for any unintentional purpose other than electroplating the metal of interest onto the cathode blank sheet (Moats and Free, 2007; Ntengwe, Mazana, and Samadi, 2010).

Methodology

A sequential mixed research methodology was applied. A total of 1629 L of electrolyte solution samples comprised of 6516 samples of 250 mL each was analysed by an independent laboratory. The instrument data from the electrowinning process was retrieved every 2 hours during the study period. The data studied was for 6 months from January 2019 to the end of June 2019. Questionnaires were completed by operators, process engineers, academics, and consultants who understand the EW process. The data was analysed using the Minitab statistical software package by applying the Anderson Darlington normality test, Pearson correlation analysis, Box-Cox transformation, Johnson transformation, Shewhart control charts, and process capability analysis (Moongo, 2020). A detailed roadmap of the research strategy is depicted in Figure 1.

Results and discussion

Creating process control charts for current efficiency factors

Before control charts were created, an Anderson Darlington normality test was carried out using Minitab (Minitab, 2019). Thereafter, non-normal data was transformed using Box-Cox transformation and/or Johnson transformation (Minitab, 2020). An Anderson Darlington normality test was repeated by using the transformed data. A statistical summary report was generated for all the factors to confirm that the data indeed followed a normal distribution and formed a bell-shaped curve. The transformed data and/or normally distributed data was then used to create control charts similar to that shown in Figure 2 (Moongo, 2020).

Analysis of process control charts for continuous data

The process control charts were analysed for continuous data by undertaking an out-of-control points alignment analysis and

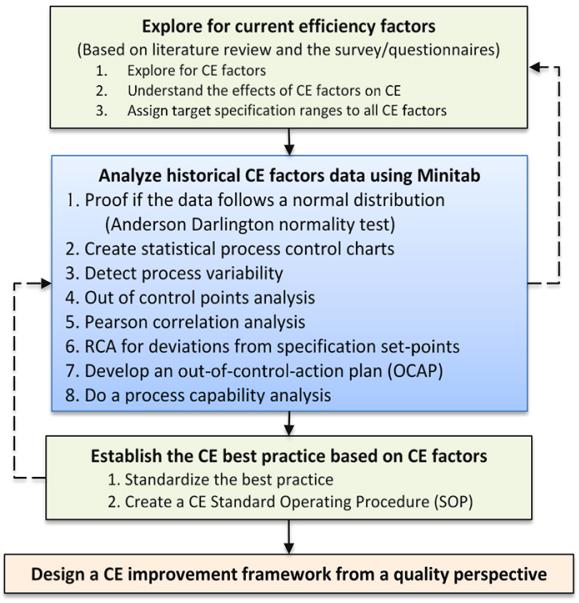

Figure 1—The designed research strategy

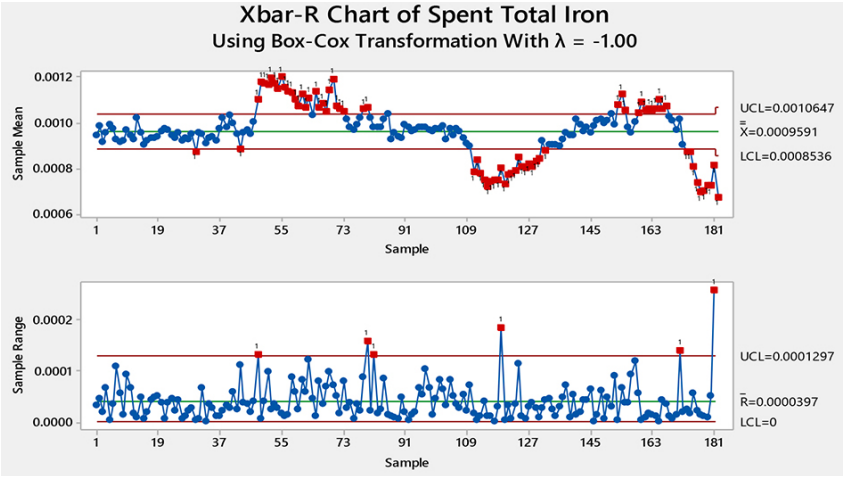

Figure 2—Mean and range (Xbar-R) control chart

Pearson correlation analysis. The out-of-control points alignment in Figure 3 shows that for rectifier current and current density, 87.5% of the out-of-control points were aligned to current efficiency. However, the correlation coefficients for these factors are only 0.053 and 0.179, indicating that they do not have the most significant effect on current efficiency compared to other factors. The difference in the correlation coefficient is most likely to be due to unstable EW operation (Moongo, 2020).

This indicates that the factor that has the most significant effect on current efficiency cannot be found by only using one method of analysis. All the points should be considered in the analysis. From Figure 4, it can be seen that the exit temperatures from the commercial cells and polishing cells, and the advance electrolyte exit temperature from the polishing cells to the commercial cells, have the highest Pearson correlation coefficients with respect to current efficiency, at 0.295, 0.301, and 0.321 respectively. These factors will have the most significant effect on current efficiency provided no other factor has a higher correlation coefficient. This is because of the large number of factors affecting current efficiency, and the process may not have been stable during the study (Moongo, 2020).

Analysis of process control charts for attribute data

Attribute data for some current efficiency factors was collected manually in the plant, as opposed to data collected by analysing samples in the laboratory and retrieved from the supervisory control and data acquisition (SCADA) server database. The main attribute for which data was collected manually was metallurgical short-circuits (hotspots). The hotspots were detected by using an infrared (IR) camera (Figure 5). The temperature of the electrode contacts is normally maintained ≤ 55°C. However, a lot hotspots with temperatures as high as > 150°C were detected, as shown in Figure 6 (Moongo, 2020).

Implementing an out-of-control action plan

The presence of hotspots was addressed by understanding the root causes shown in Figure 7, followed by developing and implementing an OCAP. The procedure involved (Moongo, 2020):

- An exhaustive hotspot detection and rectification, troubleshooting exercise
- Knocking off cathode nodules
- Reviewing current efficiency calculations
- Monitoring and controlling electrolyte impurities such as manganese and iron

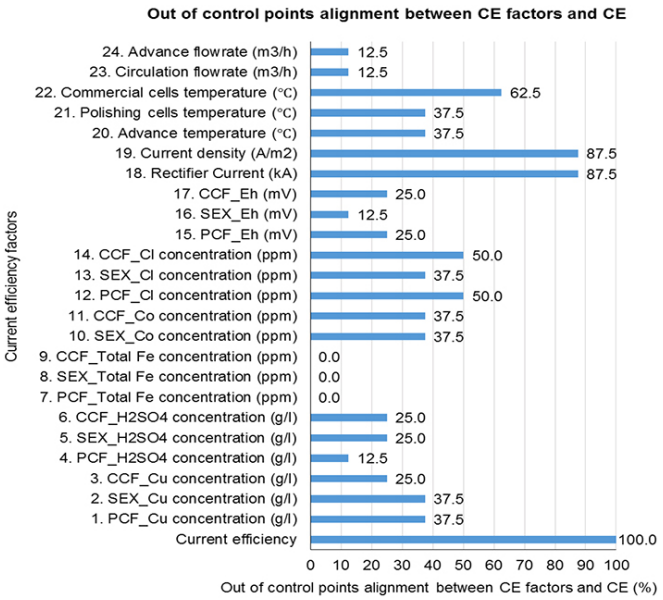

Figure 3—Out-of-control points alignment analysis

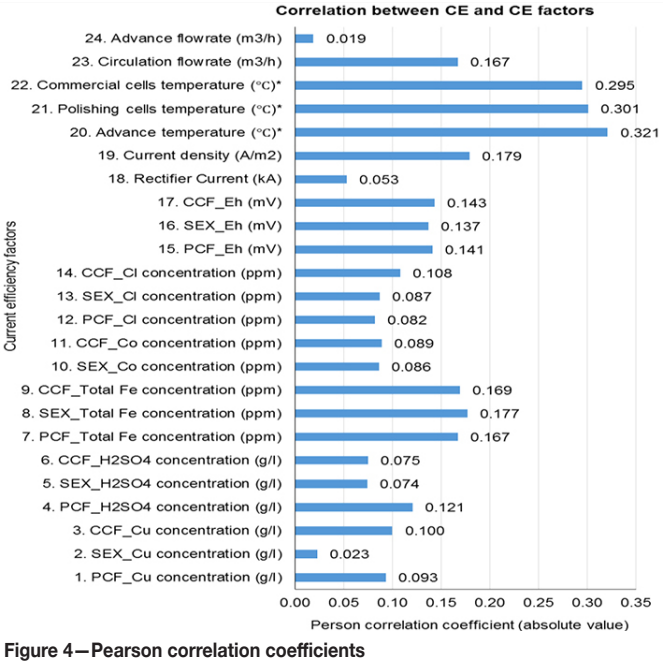

Figure 4—Pearson correlation coefficients

Figure 5—Detecting hotspots using an infrared (IR) camera

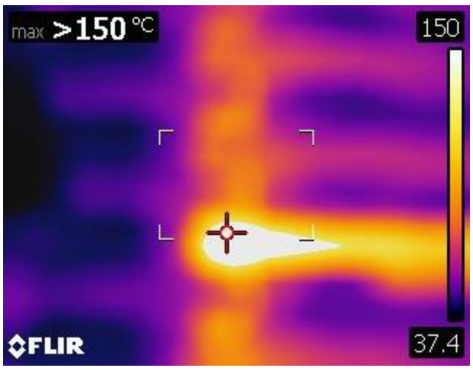

Figure 6—An infrared (IR) camera image of a hotspot

- Monitoring and controlling the addition of cathode smoothing agent, which prevents the formation of nodules (see Figure 8)
- Improving electrode maintenance, including anode cleaning and cell cleaning
- Carrying out proper electrode alignment ('rat patrol') as shown in Figure 9
- Straightening bent electrodes (Figure 10)
- Replacement of damaged electrodes without side insulators (Figure 11)
- Replacing insulators
- Cleaning anode contacts (Figure 12).

Figure 8—Excessive cathode nodules

Figure 9—Electrode alignment ('rat patrol')

Figure 10—Straightening a bent anode manually

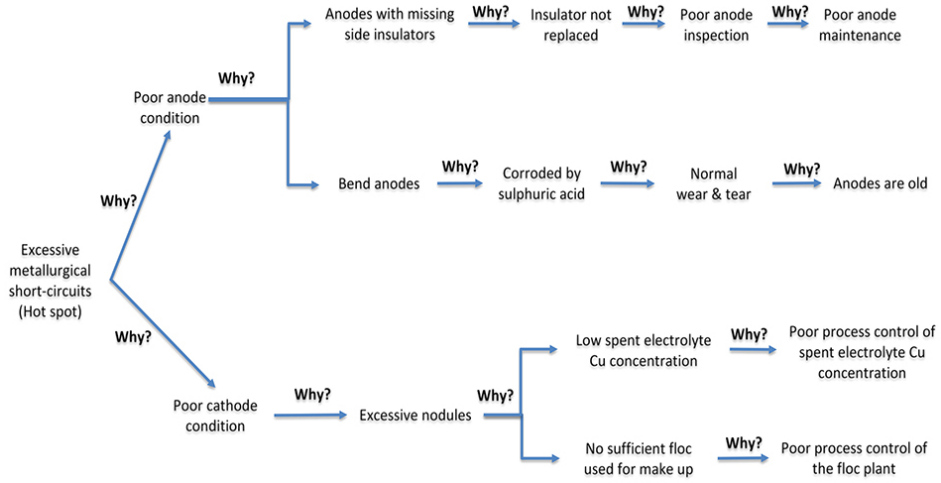

Figure 7—'Five why' root cause analysis for excessive hotspots

Figure 11—Replacing an anode with a missing side insulator

Figure 12—Cleaning anode contacts

Improvement in current efficiency

The individual moving range (I-MR) control chart for current efficiency (see Figure 13) shows that current efficiency improved as metallurgical short-circuits (hotspots) were brought under statistical control by applying the OCAP. The decrease in the number of hotspots can be seen on the proportion (P) control chart and units (U) control chart shown in Figures 14 and 15. Although hotspots have a 45.45% out-of-control points alignment, the percentage misalignment for the number of hotspots per cell and percent of cells with hotspots are 54.55% and 50.00% respectively (Moongo, 2020). These figures are the lowest compared to all other factors.

Furthermore, hotspots were found to have a higher Pearson correlation coefficient than all the other factors, at –0.361 for the number of hotspots per cell and –0.878 for the percentage of cells with hotspots. The negative sign signifies an inversely proportional relationship between metallurgical short-circuits and current efficiency (Moongo, 2020). Moreover, the questionnaire results regarding best practices for improving current efficiency also indicate that rectifying metallurgical short-circuits will most likely result in improved current efficiency (see Figure 16).

After implementing the developed OCAP, the current efficiency improved from 89.64% to 95.04%, an improvement of 5.40% (see Figure 17). This confirms that metallurgical short-circuits had the most significant effect on current efficiency. Metallurgical

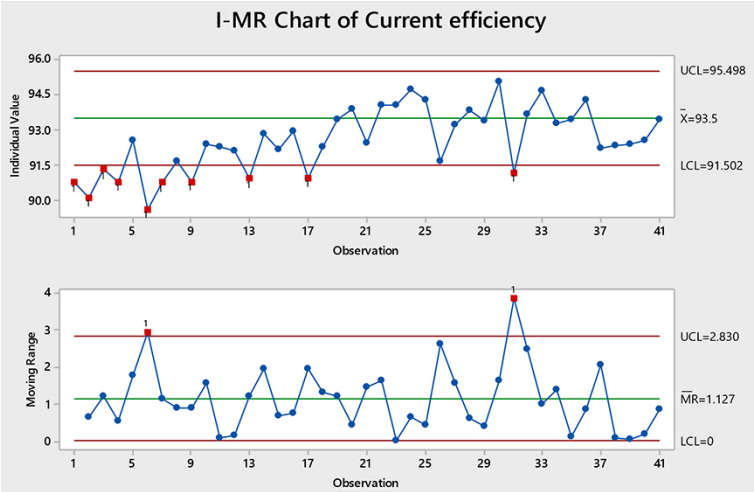

Figure 13—Individual moving range (I-MR) control chart for current efficiency

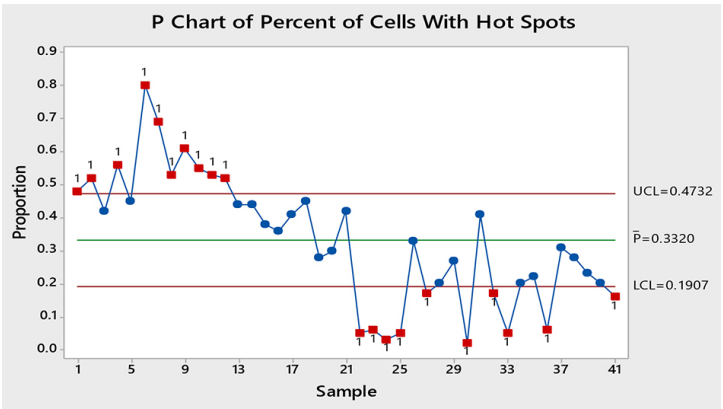

Figure 14—Proportion (P) control chart for the percentage of cells with hotspots

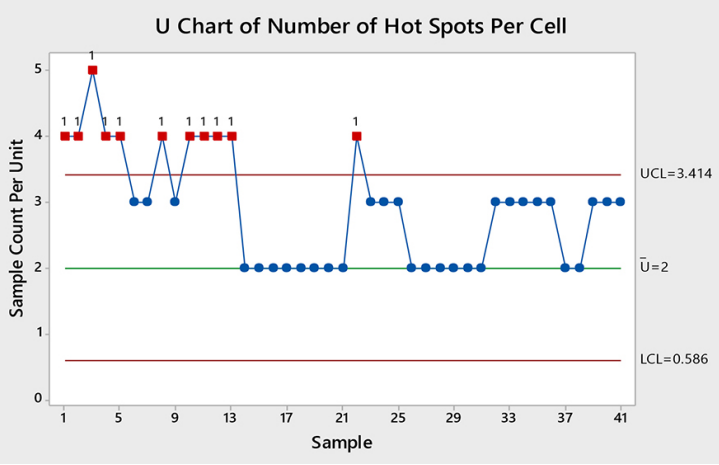

Figure 15—Units (U) control chart for the number of hotspots per cell

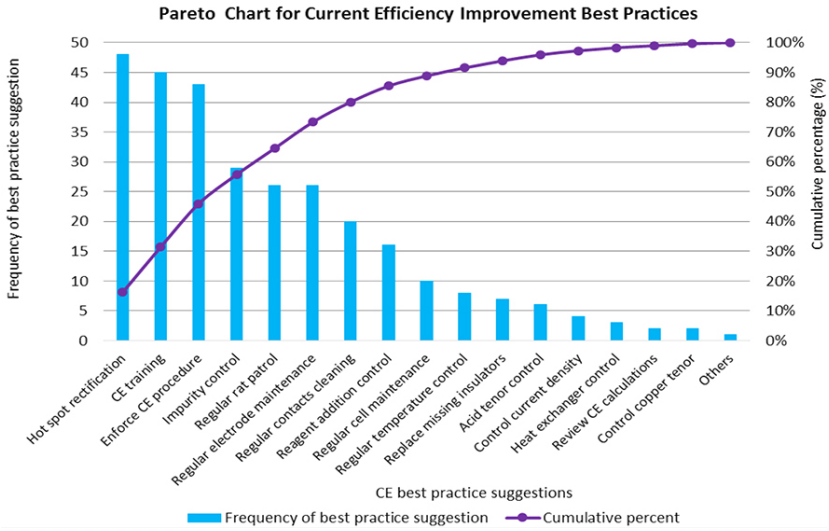

Figure 16—Current efficiency improvement best practices

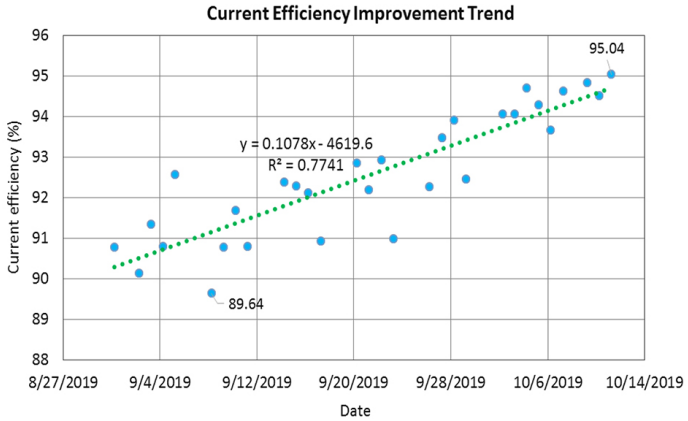

Figure 17—Actual improvement in current efficiency

short-circuits (hotspots) result in the conversion of direct current into heat energy, making less current available for electroplating copper onto the cathode blank sheets. The 5.40% improvement in current efficiency translates to approximately 74 t of 99.999% pure grade A copper cathode production over a period of 1.5 months (Moongo, 2020).

Designing a continuous quality improvement framework

The following factors were considered when designing a detailed continuous quality improvement framework for electrowinning current efficiency:

- Current efficiency factors

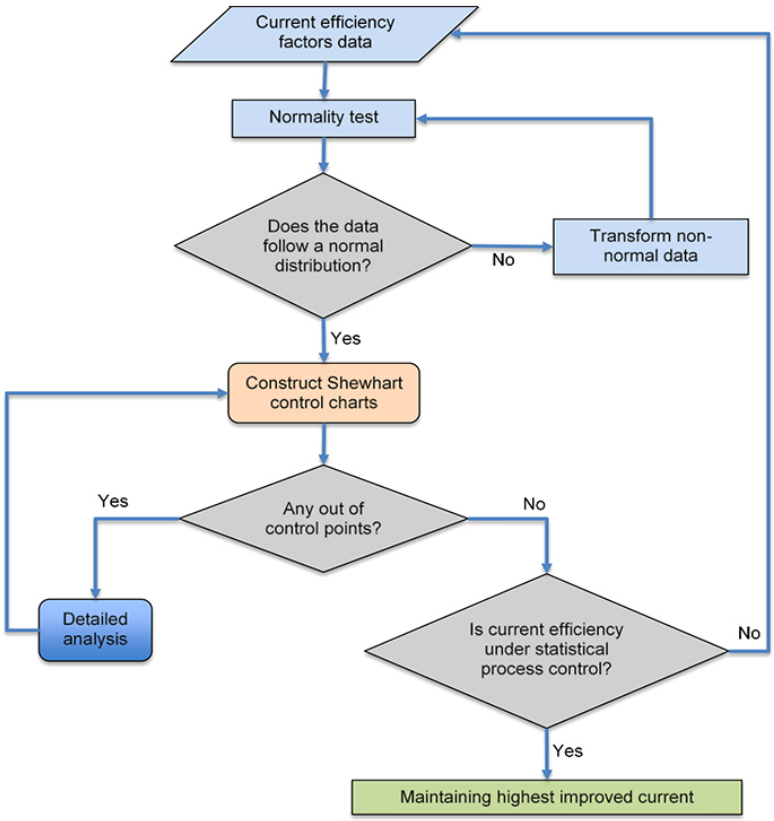

Figure 18—A simplified continuous quality improvement framework

- Anderson Darlington normality test
- Transforming non-normal data (using Box-Cox and Johnson transformation)
- Classifying data types
- Selecting suitable process control charts
- Pearson correlation analysis
- Out-of-control point alignment analysis
- Process capability analysis
- Root cause analysis
- Developing and implementing an OCAP
- Current efficiency training
- Developing a current efficiency improvement standard operating procedure (SOP).

A simplified version of the designed continuous quality improvement framework is depicted in Figure 18. The framework serves as a guide for improving current efficiency indirectly by applying statistical process control to current efficiency factors (Moongo, 2020).

Conclusions

The principal objective of the research was accomplished. It was found that metallurgical short-circuits (hotspots) contributed significantly to the reduction in electrowinning current efficiency. The root causes of hotspots were poor anode maintenance in terms of missing insulator replacement, old corroded anodes, poor spent electrolyte copper concentration control, and poor cathode smoothing agent (Magnafloc) control. These root causes were addressed by developing and implementing an out-of-control action plan (OCAP) which resulted in the improvement of current efficiency from 89.64% to 95.04%, an improvement of 5.40%. This translates to approximately 74 t of 99.999 % pure grade A copper cathode production over a period of 1.5 months.

A continuous quality improvement framework for improving electrowinning current efficiency from a quality perspective of the associated variables was designed by applying statistical process control. This was done by considering factors such as the Anderson Darlington normality test, non-normal data transformation (using Johnson and Box-Cox transformation), constructing process control charts, and analysing the process control charts in detail, which included Pearson correlation analysis, out-of-control points alignment analysis, root cause analysis, process capability analysis, and implementing an OCAP.

The main limitation of this research stems from the fact that the study was done in an industrial copper electrowinning plant while it was online, producing copper cathodes. The electrowinning process may not have been stable during the study. Future research is recommended to focus on improving current efficiency *via* the application of statistical process control by carrying out laboratory experiments, application of design of experiments (DOE), studying the effect of the interactions between current efficiency factors, application of other types of control charts such as multivariate control charts, cumulative sum (CUSUM) control charts, and exponentially weighted moving average (EWMA) control charts.

Acknowledgements

The authors would like to thank Mr Jomo Appolus (Processing Manager) for authorizing the study. The contributions by the copper refinery technical team, operations team, Mr Nobert Paradza, and Mr John Moody are highly appreciated.

References

Adcock, P. 2017. Zinc electrowinning in the presence of iron (II). PhD thesis, University of Western Sydney, NSW.

Amitava, M. 2016. Fundamentals of Quality Control and Improvement. 4th edn. Wiley, Hoboken, NJ.

Baradaran, V. and Dashtbani, H. 2014. A decision support system for monitoring traffic by statistical control charts. https://www.researchgate.net/publication/307671037_A_decision_support_system_for_monitoring_traffic_by_statistical_control_charts/download

Ben, M. and Jiju, A. 2000. Statistical process control: an essential ingredient for improving service and manufacturing quality. *Managing Service Quality*, vol. 10, no. 4. pp. 233–238.

Beukes, N. and Badenhorst, J. 2009. Copper electrowinning: theoretical and practical design. *Journal of the Southern African Institute of Mining and Metallurgy*, vol. 109. pp. 343–356.

Corby Anderson, C. 2017. Optimization of industrial copper electro winning solutions. *Journal of Advanced Chemical Engineering*, vol. II, no. 2. p. 156.

Debmarine Namibia. 2020. Debmarine Namibia. https://debmarinenamibia.com/main/whoweare [accessed 22 September 2020].

Ehsani, A., Yazici, E.Y., and Deveci, H. 2016. The effect of temperature on the electrowinning of copper. *Proceedings of the 18th International Metallurgy and Materials Congress*, Istanbul. http://www1.metalurji.org.tr/immc2016/654.pdf

Eskom. 2019. Tariffs and charges. http://www.eskom.co.za/CustomerCare/TariffsAndCharges/Pages/Tariffs_And_Charges.aspx

Fereshteh, S., Naison, M., and Felix, W. 2010. The dependence of current efficiency on factors affecting the recovery of copper from solutions. *Journal of Applied Sciences Research*, vol. 6, no. 11. pp. 1862–1870.

Godina, R., Pimentel, C., Silver, F., and Joao, M. 2018. Improvement of the statistical process control certainty in an automotive manufacturing unit. *Procedia Manufacturing*, vol. 7. pp. 729–736.

Gonzalez-Dominguez, J. and Dreisinger, D. 1997. Identifying research opportunities in zinc electrowinning. *Review of Extraction & Processing*. p. 38.

Helm. 2018. Quality Control. *Unspecified*, I(1), pp. 1–18. Note: Please add publication details as required by SAIMM reference style. If not available, reference should be removed. I cannot trace this on the internet.

Kafumbila, K. 2017. Design of copper electrowinning circuit using conventional cells. https://www.scribd.com/document/339612505/Design-of-Copper-Electrowinning-Circuit-using-Conventional-cells#

Leavengood, S. and Reeb, J.E. 2015. Variables control charts. *Statistical Process Control*. Oregon State University Extension Services. https://catalog.extension.oregonstate.edu/sites/catalog/files/project/pdf/em9109.pdf

Moats, M. and Free, M. 2007. A bright future for copper electrowinning. *JOM*, vol. 59. pp. 34–36.

Chamber of Mines of Namibia. 2018. Annual Review. Windhoek.

Minitab. 2019. The Anderson-Darling statistic. https://support.minitab.com/en-us/minitab/18/help-and-how-to/statistics/basic-statistics/supporting-topics/normality/the-anderson-darling-statistic/[accessed 1 May 2020].

Minitab. 2020. Box-Cox-transformation. https://support.minitab.com/en-us/minitab/19/help-and-how-to/quality-and-process-improvement/control-charts/how-to/box-cox-transformation/before-you-start/overview/[accessed 1 May 2020].

Minitab. 2020. Johnson transformation. https://support.minitab.com/en-us/minitab/19/help-and-how-to/quality-and-process-improvement/quality-tools/how-to/johnson-transformation/before-you-start/overview/[accessed 1 May 2020].

Montgomery, D. 2009. Introduction to Statistical Quality Control. 6th edn. Arizona State University.

Moongo, T. 2020. Designing a continuous quality improvement framework for improving electrowinning current efficiency. Namibia University of Science and Technology, Windhoek.

Nampower. 2019. Schedule of approved distribution tariffs for the financial year 2019/20. https://www.nampower.com.na/Page.aspx?p=172

Natarajan, S. 1985. Current efficiency and electrochemical equivalent in an electrolytic process. *Bulletin of Electrochemistry*, Mar-Apr, vol. 1, no. 2. pp. 215–216.

Ntengwe, F., Mazana, N., and Samadi, F. 2010. The dependence of current efficiency on factors affecting the recovery of copper from solutions. *Journal of Applied Sciences Research*. pp. 1862–1870.

Ozdag, H., Bozkurt, K., Ipek, H., and Bilir, K. 2012. The influence of impurity ions on the electrowinning of copper from waste PBCs leaching solutions. *Journal of the Southern African Institute of Mining and Metallurgy*, vol. 112. pp. 112–121.

Parada, T. and Asselin, E. 2009. Reducing power consumption in zinc electrowinning. *JOM*, vol. 51. https://doi.org/10.1007/s11837-009-0152-1.

Pavol, G. 2015. Continuous Quality Improvement by **Statistical Process Control.** Elsevier. pp. 565–572.

Robinson, T. 2011. Electrowinning. Extractive metallurgy of copper. Schlesinger, M.E., King, M.J., Sole, K.C., and Daveport, W.G. (eds). Elsevier. pp. 349-371.

SCME. 2017. Control chart basics: Primary knowledge unit participant guide. National Science Foundation's Advanced Technological Education, New York.

Tuaweri, T., Adigio, E., and Jombo, P. 2013. A study of process parameters for zinc electrodeposition from a sulphate bath. *International Journal of Engineering Science Invention*, vol. 2, no. 8. pp. 17–24.

Vay, L. 2011. Studies of micromorphology and current efficiency of zinc electrodeposited from flowing chloride electrolytes. *Lawrence Berkeley National Laboratory*. 139 pp.

Wang, H., Xia, W., Yang, W., and Ren, B. 2016. Improving current efficiency through optimizing electrolyte flow in zinc electrowinning cell. *Proceedings of CFD Modeling and Simulation in Materials Processing 2016*. Wiley. https://doi.org/10.1002/9781119274681.ch29

Wild, C. J. and Seber, GA.F. 2017. Control charts. *Chance Encounters: A First Course in Data Analysis and Inference*. Elsevier, New York. Chapter 13.

World Nuclear Association. 2020. World uranium mining production. https://www.world-nuclear.org/information-library/nuclear-fuel-cycle/mining-of-uranium/world-uranium-mining-production.aspx#:~:text=Kazakhstan%20produces%20the%20largest%20share,%25)%20and%20Australia%20(12%25).&text=Uzbekistan%20(est.)[accessed 22 September 2020]. ◆

Exploratory development of a rotary offset crusher

T. Nghipulile[1], M. Bwalya[1], M. Moys[1], and H. Simonsen[1]

Affiliation:
[1] School of Chemical and Metallurgical Engineering, University of the Witwatersrand, Johannesburg, South Africa.

Correspondence to:
T. Nghipulile

Email:
1871606@students.wits.ac.za
ngh.titus@gmail.com

Dates:
Received: 25 Aug. 2020
Accepted: 15 Dec. 2020
Published: January 2021

How to cite:
Nghipulile, T., Bwalya, M., Moys, M., and Simonsen, H. 2021 Exploratory development of a rotary offset crusher. Journal of the Southern African Institute of Mining and Metallurgy, vol. 121, no. 1, pp. 29–38.

DOI ID:
http://dx.doi.org/10.17159/2411-9717/1325/2021

ORCID
T. Nghipulile
https://orcid.org/0000-0003-4399-2620

M. Bwalya
https://orcid.org/0000-0002-2009-2913

M. Moys
https://orcid.org/0000-0003-1533-2668

H. Simonsen
https://orcid.org/0000-0001-5302-7280

Synopsis

The quest for efficiency in comminution is an ongoing concern as comminution usually constitutes a major cost component in the metal production industry. Such improvements can be made by circuit optimization or development of more efficient equipment. A novel crusher, known as the rotary offset crusher (ROC), promises to deliver in this space. The ROC was invented in 2002 by Michael Hunt, Henry Simonsen, and Ian Sinclair, but failed to garner enough support to progress to production. The original design concept was recently rekindled, and a laboratory version of the crusher has been built and commissioned at the University of the Witwatersrand. The crusher is simple in design, with two cylindrical discs that are parallel to each other, and, as the name implies, there is an offset between the vertical axes of the discs. The top disc has a conical section on its lower face, and this creates a crushing zone between the opposite faces of the two spinning discs. Centrifugal motion transports particles through the crushing zone. Batch experiments have been conducted with quartz at various crusher settings (discs offset, rotational speed, and vertical exit gap) for various feed size distributions. The indications so far suggest that the disc speed is a key factor affecting the performance. Size reduction ratios as high as 11 were recorded from experiments with quartz at a speed of 830 r/min.

Keywords
rotary offset crusher, comminution, throughput.

Introduction

The mining industry consumes about 7% of global energy (Manouchehri, 2015), of which about 30 to 70% is utilized in comminution circuits (Ballantyne and Powell, 2014; Curry, Ismay, and Jameson, 2014; Jeswiet and Szekeres, 2016; Nadolski *et al.*, 2014; Napier-Munn, 2015; Radziszewski, 2013; Tromans, 2008). Comminution is, at present, a relatively inefficient process with only a small fraction of the energy, meant for size reduction, being used to effect breakage, with the rest being lost in different forms of energy; such as heat, sound, mechanical losses, and others (Tavares and King, 1998; Radziszewski, 2013; Wills and Finch, 2006). Energy efficiency in comminution is therefore an issue that continues to receive much attention. In addition, conventional crushers are characterized by low reduction ratios in the range of 3:1 and 10:1 (Gupta and Yan, 2006). Thus innovation to lower comminution costs and effect improvement of the overall efficiency remains a goal for the sustainability of the mineral industry. The rotary offset crusher (ROC), under development at the University of the Witwatersrand, has the potential advantage of reducing equipment size as energy can be concentrated in a small space simply by increasing the rate of rotation of the discs, which aids both particle transportation and comminution frequency.

The ROC is a novel crushing device that exploits the centrifugal motion of particles between two off-centre, high-speed spinning discs and the consequential closure and opening of the hollow conical space in the upper disc due the discs being off-centre. The ROC is a new device with many of its aspects yet to be understood, and thus an experimental programme has been initiated to establish what drives the capacity of this machine. The crusher has been instrumented to provide information about the process.

Theoretical background

Breakage mechanisms in comminution machines

Size reduction concerns the fracture of brittle particles due to applied compressive stress (Tavares

and King, 1998). The degree of fracture (of rocks) depends on the mechanical properties of the individual minerals in the ore matrix and, more importantly, upon the presence of cracks in the matrix. Cracks act as sites for stress concentration (Griffith, 1920; Tavares and King, 1998). Crack propagation, on which primary and secondary crushing rely, begins where the stress is concentrated and, depending on the magnitude of the applied stress relative to the strength of the material, the crack may propagate, resulting in some degree of comminution.

Fragmentation of rocks in comminution equipment occurs due to three mechanisms – impact, compression, and abrasion. Impact breakage occurs when a large compressive stress is applied rapidly on the particles resulting in the production of daughter particles of a wider size distribution. In the ROC, the rapid variation of the gap between the crushing discs during each revolution as particles are transported away from the centre to the crusher periphery will subject particles to cyclic impulses of compressive forces. At this point it can only be hypothesised that both impact, due to rapid movement of the discs, and compressive loading are possible. Compression breakage, which dominates in the high pressure grinding roll (HPGR) and vertical roller mill (VRM), is said to be energy-efficient (Altun *et al.*, 2015; Genç and Benzer, 2016; Reichert *et al.*, 2015; Rosario and Hall, 2010; Saramak, Wasilewski, and Saramak, 2017; Wang and Shrive, 1995; Wang *et al.*, 2009; Schönert, 1996, 1988). This is due to the application of stress (pressure) on the feed particles, resulting in the production of daughter particles that are about the same size as their component grain size in the parent particle, as well as much finer progeny particles that originate at the points of stress application. It is also claimed that the progeny particles from the HPGR and VRM contain many residual micro-cracks (Ozcan and Benzer, 2013), which suggests that less comminution energy will be required and grinding kinetics improved in the subsequent grinding mills such as a ball mill (Barani and Balochi, 2016). With the particles in the ROC being forced between the fast-spinning discs, there is a degree of compression breakage. The last mode of breakage, abrasion, is a surface phenomenon which occurs when particles move parallel to their plane of contact (Napier-Munn *et al.*, 2005). In the ROC, abrasion is expected due to the comminuted particles sliding along the discs' surfaces.

Energy laws in comminution

The relationship between the input energy and the particle size of the feed that provides a particular product size from the comminution device can be mathematically described by Equation [1].

$$\frac{dE}{dL} = -kL^{-m} \quad [1]$$

where dE is an infinitesimal change in specific energy, dL is an infinitesimal size change, L is the particle size, k is a constant and m is a constant related to the material and the way it is broken.

The exponent m in Equation [1] was assigned three possible values by three researchers (2, 1, and 1.5 for Rittinger, Kick, and Bond's laws respectively). Rittinger's law, which relates energy to the change in surface area, provides a reasonable estimate for energy when the machine is handling finer particles while Kick's law, which postulates that the energy required to reduce a material in size is directly proportional to the percentage reduction, applies to particles with sizes greater than 1 cm (Wills and Finch, 2016). Bond's law, called a third theory in comminution, states that the energy required in comminution is proportional to the new crack length created. Bond's law is commonly used as it applies to a wider range of particle size handled in conventional mills. Integrating Equation [1] and assigning a value of 1.5 to the exponent m results in the Bond work index equation below.

$$W = 10W_i\left(\frac{1}{\sqrt{P_{80}}} - \frac{1}{\sqrt{F_{80}}}\right) \quad [2]$$

where W is the input energy (kWh/t), W_i is the work index (kWh/t), and F_{80} and P_{80} are the 80% passing sizes of the feed and product respectively.

The Bond equation can predict the specific energy with acceptable accuracy for ball and rod mills but, as pointed out by Morrell (2004), this law tends to either over-predict, or under-predict the specific comminution energy for autogenous (AG) or semi-autogenous (SAG) mills, HPGRs, and conventional crushers. In the quest to establish a more accurate estimation of the specific energy, not just for tumbling mills but for more general application to comminution equipment such as jaw, gyratory, and cone crushers as well as HPGRs, Morrell (2009) proposed the equation below:

$$W = 4M_i\left(x_2^{f(x_2)} - x_1^{f(x_1)}\right) \quad [3]$$

where W is the specific energy in kWh/t, M_i is the work index related to the breakage property of an ore and the comminution machine (in kWh/t), x_2 is the 80% passing size for the product (µm), and x_1 is the 80% passing size for the feed (µm).

The Morrell equation differs from the Bond equation as the exponent $f(x_j)$ in Equation [3] does not have a specific value, but it is rather a function of the 80% passing size and can be estimated using another equation Morrell has developed:

$$f(x_j) = -\left(0.295 + \frac{x_j}{10^6}\right) \quad [4]$$

where x_j is the 80% passing size.

We thus have some basis for comparing specific energy consumption between different comminution equipment.

Design features and operating principles of the rotary offset crusher

Design features of the ROC

The working diagram and a photograph depicting the main components are shown in Figure 1. The crusher's cylindrical discs both have a radius of 250 mm, with the bottom disc having a thickness of 50 mm while top disc has a thickness of 80 mm. The discs, which are made of mild steel, are not mechanically linked. The whole structure is 1.1 m high and 1 m wide. The legs of the equipment are bolted onto the floor to minimize mechanical vibrations. In this design, only the bottom disc is driven by the motor using the V-belt. The speed can be varied by changing the diameters of the pulleys. The top disc moves due to transmission of motion by the particles that get nipped between the discs. The crusher is powered using a 3 kW three-phase induction motor that has a full-load speed of 1420 r/min.

Effect of the horizontal offset on the geometry of crushing zone

As shown in Figure 1, there is an offset between the vertical axes of the crusher discs. This horizontal offset of the top disc relative to the bottom disc produces a change in the geometry of the crushing zone during rotation. The horizontal offset between the discs is adjusted by sliding the top disc support structure. From the top view of the discs in Figure 2, it can be observed that there is a volume contraction in 180° rotation of the crushing chamber, which suggests that comminution occurs predominantly in this half. On the other hand, there is volume expansion in the other 180°, implying that transportation is dominant here. Due to the offset, as shown in Figures 2 and 3, the exit gap is not constant during a rotation (it is minimum on the left side and maximum on the right side). This implies that the largest particle that can be discharged from the crusher depends rather on the exit gap shown on the right side. The maximum exit gap (denoted as $G_{e,max}$) increases with the offset and thus it can be hypothesised that increasing the offset ensures fast transportation of particles to some extent, *i.e.* changing the offset results in an increase in crusher throughput. The effect of offset on the throughput, size reduction, and power draw are discussed later.

With the current configuration of the crushing surfaces, there is a variation in the input and exit gaps only when the offset is greater than the interior flat edge of the top disc, which is 10 mm. With the offset equal to, or less than, this value there is no variation in the exit gap as shown in Figure 3, but the volume contraction and expansion of the crushing zone still occurs regardless of the whether the offset is less than, equal to, or greater than the interior flat edge of the top disc.

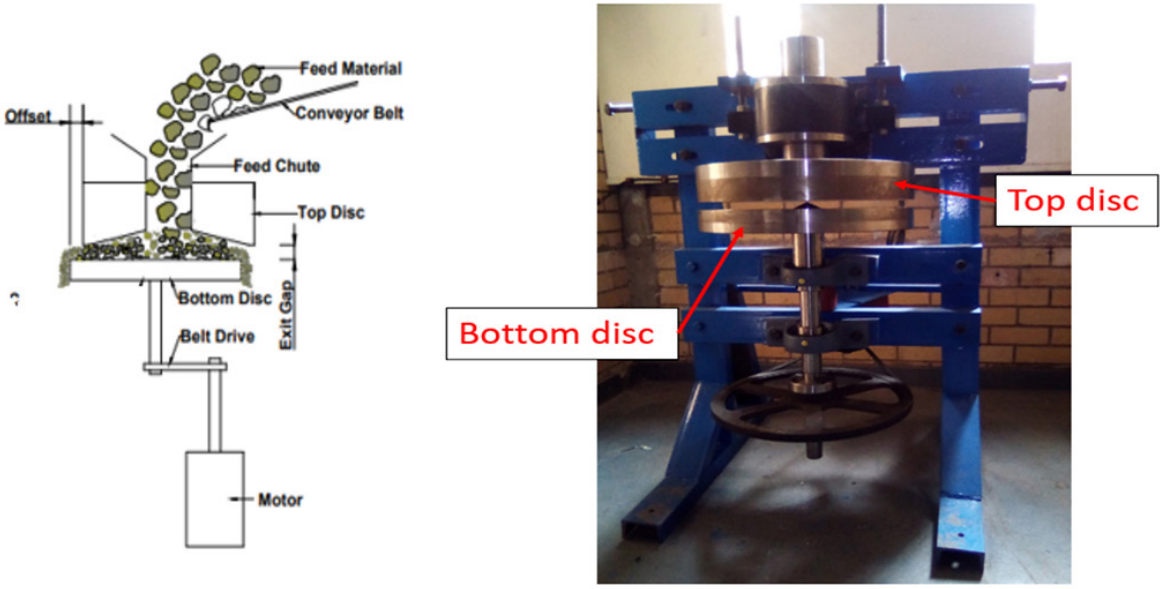

Figure 1—Working diagram for the rotary offset crusher (left) and photograph showing the discs (right)

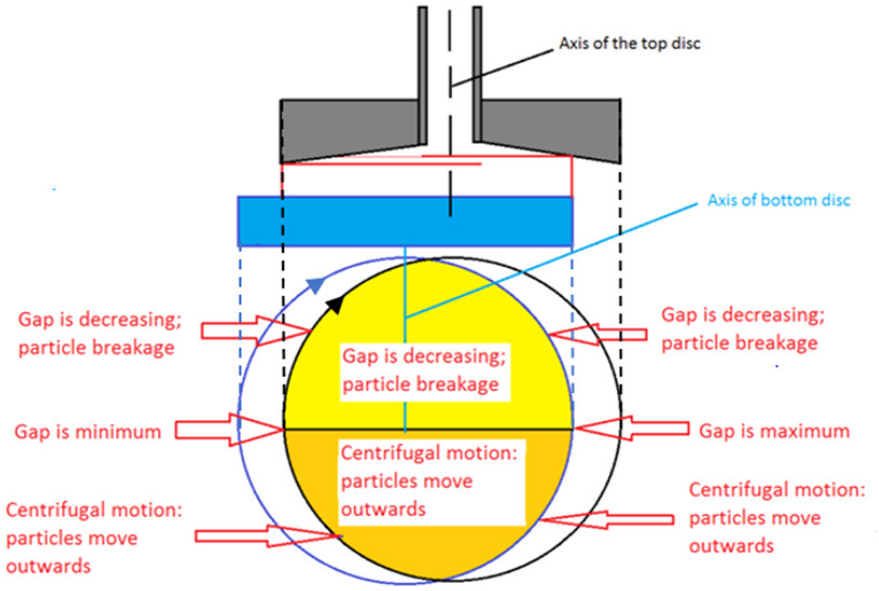

Figure 2—Influence of disc offset on the geometry of the crushing zone and exit gap

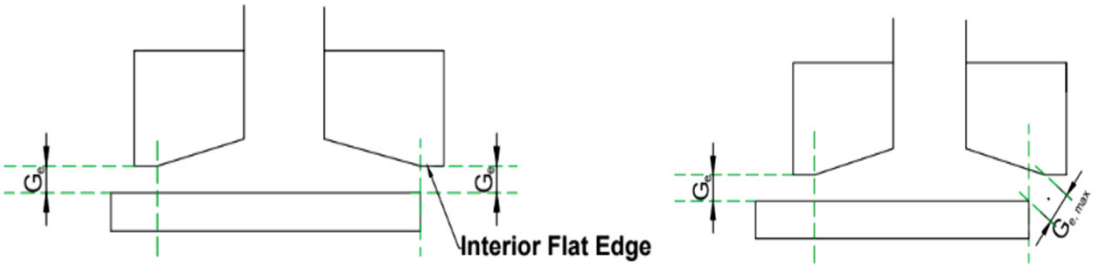

Figure 3—Side view of the discs when offset is equal to interior flat edge of the top disc (left), and with offset greater than the interior flat edge of the top disc (right)

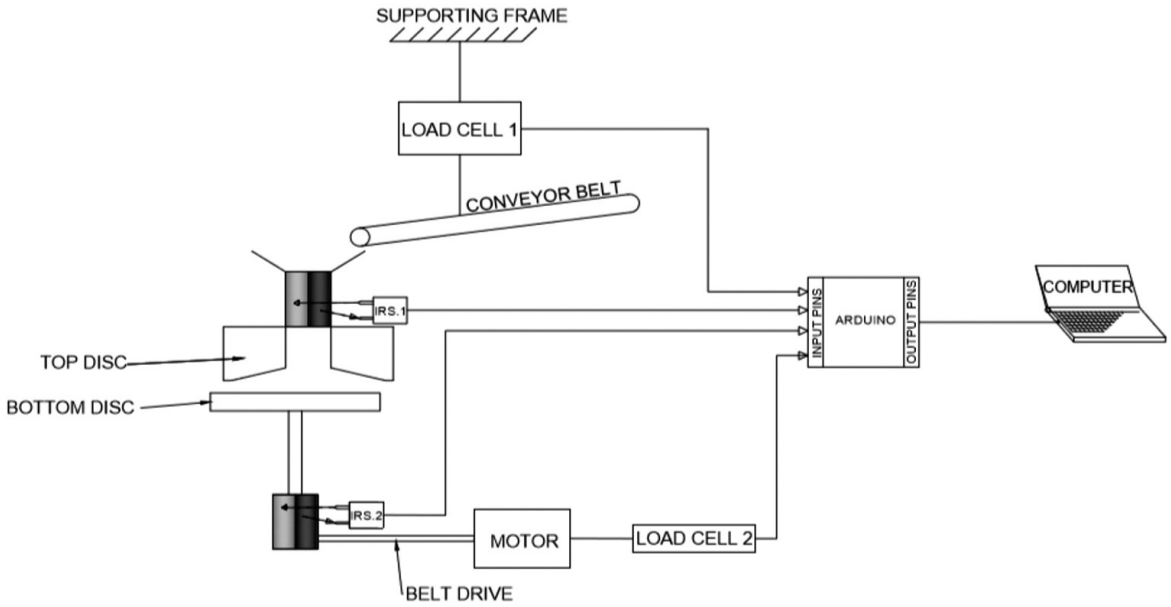

Figure 4—Overview of the crusher instrumentation

Crusher instrumentation

Figure 4 shows the positions of the four transducers installed on the crusher. These include two IR sensors (shown as IRS.1 and IRS.2) directed to the shafts for the two discs of the crusher to measure their rotational speeds and two strain gauge load cells for measuring the loads (weight of material fed to the crusher and force required to keep the torque arm of the motor stationary). The speeds of the discs and the motor drive torque are used to calculate the mechanical power of the system, while the change in the mass of the material on the conveyor belt gives the feed rate.

With the instrumentation circuit in Figure 4, various signals are captured. Figure 5 is a plot of some typical results obtained during batch operation. We observe the conveyor weight signals decreasing steadily between 89 600 µs and 92 000 µs, which can be converted to feed rate, using Equation [5], as 2220 kg/h.

$$F = \frac{M_{batch}}{t_f} \quad [5]$$

where F is the feed rate (kg/h or t/h), M_{batch} is the total mass fed to the crusher (in kg or tons), and t_f is the feeding time (in hours).

As soon as the particles get nipped between the discs, the upper disc is accelerated to the speed of the lower disc and its speed decrease only when there are no longer particles nipped between the discs. Thus, the signal of the top disc speed indicates the time when the particles are trapped between the discs.

The area under the power signal, for the time when the particles are being crushed, can be numerically integrated to provide the energy expended during crushing. The specific energy during crushing is calculated using Equation [6]. The power signal provides insight into mechanisms of crushing and transportation of particles in the crushing zone. For example, the first 'rise' in the power signal indicates the locking of particles between the discs and commencing of particle breakage. The subsequent 'rise' and 'drop' indicate the successive particle locking and releasing along the comminution cavity, respectively.

$$E_{cs} = \frac{E_i}{3.6\ x\ m_s} \quad [6]$$

where E_{cs} is the specific energy (in kWh/t), E_i is the input energy (in J) during crushing, m_s is the mass of the crushed rocks (in grams), and 3.6 is a factor for converting specific energy from J/g to kWh/t.

Particle transportation in the crusher

The centrifugal motion provides the means for transportation of particles from the centre of the crushing zone to the periphery, where they are discharged to the collection box, for as long as they are smaller than the spacing between the edges of the discs. The centrifugal acceleration is a function of the speeds and radii

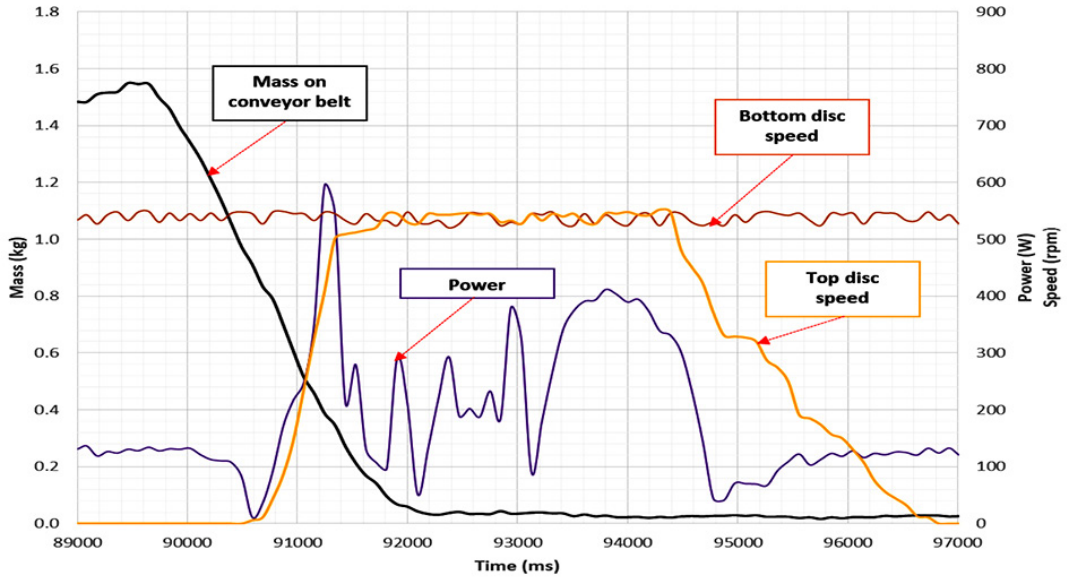

Figure 5—The performance curves during a ROC crushing test

of the two discs, as shown by Equation [7]. The higher the rotational speed, the higher the centrifugal acceleration which, in turn, implies high crusher throughput. Using Equation [7], the centrifugal accelerations in the crushing zone, as a function of the radius of the disc, were evaluated for speeds of 330, 550, and 830 r/min (the speeds that have been tested during the experiments). The results are plotted in Figure 6. It is observed that increasing the speed by a factor of 1.7 (*i.e.* from 330 to 550 r/min) results in the centrifugal acceleration increasing by a factor of 2.8 (obtained by dividing the slopes of the two graphs). Increasing the speed to 830 r/min would result in centrifugal acceleration increasing by a factor of 6.3 (with reference to a speed of 330 r/min).

$$a_c = \omega^2 r \quad [7]$$

where a_c is centrifugal acceleration, ω is angular velocity in rad/s, and r is the radius of the bottom disc.

The largest particle size in the feed material is dependent on the throat (internal diameter) of the chute and, most importantly, on input gap (G_{in}) of the crusher. This input gap is a function of the angle of the comminution cavity and the exit gap (G_e) as shown in Figure 7. A larger angle α suggests that coarser particles can be fed to the crusher. This angle greatly influences the geometry of the crushing chamber, and in turn, the capacity of the crusher. The angle of the comminution cavity for the current design used in this study is 6°.

The largest particle discharged from the crusher is dependent, to a degree, on the exit gap (G_e). The input and exit gaps are related by Equation [8]. Other factors that are expected to affect the product size distribution are feed material characteristics (hardness and size distribution), rotational speed, disc offset, and profile design. This exit gap is set before the experimental run and measured after every run to check if there is any change.

$$G_i = h_c + G_e \quad [8]$$

where h_c is the height of comminution cavity, G_e is the exit gap, and G_i is the input gap.

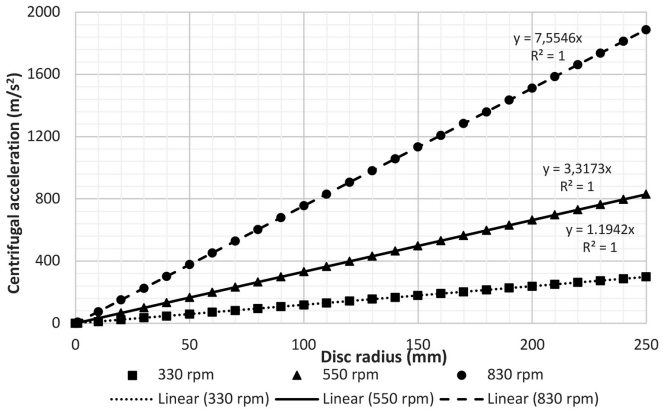

Figure 6—Relationship between the centrifugal acceleration acting on particles in the crushing chamber of the rotary offset crusher and the radius of the discs, for various speeds

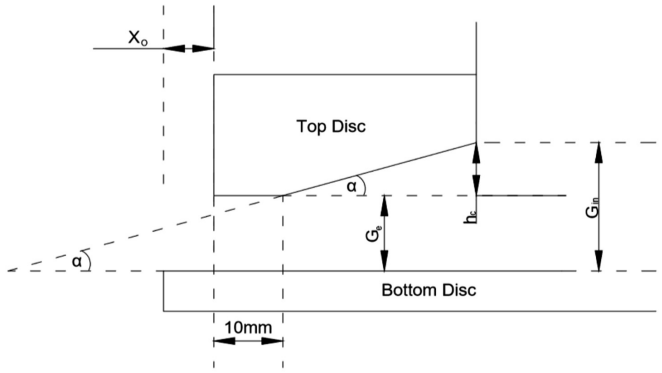

Figure 7—Relationship between input and output gaps, as well as the angle and the height of the comminution cavity. x_o is offset

Experimental work

Sample preparation

The quartz sample was dry-sieved to obtain the three narrow

size fractions, –6.7+4.75 mm, –13.2+9.5 mm, and –19+13.2 mm, in 1.5 kg sub-samples for the three size classes prepared using a rotary splitter. The prepared samples were used for the comminution tests discussed below.

ROC crushing tests

The effects of the operating variables (feed size distribution, rotational speed, horizontal offset between the vertical axes of the discs, and vertical exit gap) were investigated using the prepared single size fraction samples. The following crusher settings were considered: offset (10, 16, and 23 mm), rotational speed (330, 550, and 830 r/min), and vertical exit gap (1.5 and 3 mm). Firstly, the effect of rotational speed on crusher performance was investigated using the –13.2+9.5 and –19+13.2 mm size fractions and rotational speeds of 330, 550, and 830 r/min. The horizontal offset and vertical exit gap were fixed at 10 and 3 mm respectively. The effect of the horizontal offset on the performance of the ROC was then investigated using the –6.7+4.75 and –19+13.2 mm size fractions with offsets of 10, 16, and 23 mm. The speed was fixed at 830 r/min, while two vertical exit gaps (1.5 and 3 mm) were used. A typical test involves feeding the material using the conveyor and, after crushing is done (when the top disc has stopped), the machine is powered off before the crusher product in the collection box is collected for size analysis. The speeds of the two discs, weights of the material conveyed to the feed hopper, and the force required to keep the torque arm stationary are measured and recorded in real time during each test.

Results and discussion

Effect of rotational speed on crusher performance

The product size distributions for the two feed size classes (–13.2+9.5 and –19+13.2 mm) at various speeds are shown in Figure 8. The d80 sizes were interpolated from Figure 8 and are plotted, together with the crusher throughput, in Figure 9. It is observed that the higher the speed the finer the crusher product. As shown in Figure 9, the throughput increases with the rotational speed for both the –13.2+9.5 and –19+13.2 mm fractions.

Effect of horizontal disc offset and vertical exit gap

The product size distributions for the –19+13.2 and –6.7+4.75 mm size fractions of quartz that were used to investigate the effect of horizontal offset on crusher performance are listed in Appendix A. In Figure 10, the effects of varying the horizontal offset on the reduction ratio (based on product d_{80} size) and throughput are shown.

Relationship between energy and product size

The major types of energy in the ROC include (1) the rotational energy (stored in the discs) and (2) comminution energy (responsible for creating new surface areas). The balance is accounted for by the friction in the system. Figure 11 shows the specific energy calculated from the total energy utilized during crushing of the –19+13.2 mm particles. The methodology for calculating the specific energy was discussed earlier. The existing formulae (Bond's in Equation [2] and Morrell's in Equation [3]) for estimating the specific energy were assessed for the ROC application, and results are also plotted in Figure 11. In addition, the relationship between the product d_{80} sizes and specific energy from the drop weight tests (DWT) using single quartz particles was also used to estimate the energy input for the experimental d_{80} sizes obtained from the ROC, and the results included in Figure 11. As can be observed from the coefficient of correlation (R^2) values, there exist well-defined relationships (fitting the power function) between the product size and specific energy.

The relationship between the reduction ratio (calculated from the d_{80} in Figure 11) and specific energy is shown in Figure 12.

Discussion of results

From the trends in Figures 8 and 9, it is clear that the crusher product becomes finer with increasing speed. The frequency of crushing actions is the function of the rate of rotation of the discs. With a high rotational speed there is a corresponding increase in the frequency of comminution events, resulting in higher throughput as well as higher reduction ratios. Thus far the highest reduction ratio of 11 has been achieved with the highest speed attempted so far (830 r/min) and it is clear there is a need to attempt higher speeds in future to establish more optimal speeds related to both material and feed size distribution.

There is an indication that the horizontal offset affects the reduction ratio of the coarse feed (–19+13.2 mm) but has little effect with a finer feed (–6.7+4.75 mm), as seen in Figure 10. We also notice that the larger gap of 3 mm was optimal for the medium offset (16 mm) while the gap of 1.5 mm suggests otherwise for this offset. We do not have a complete explanation for this and this issue will probably become clearer when higher speeds are attempted in future. There is also technical challenge of structural flexure of the equipment to address, which we refer to later.

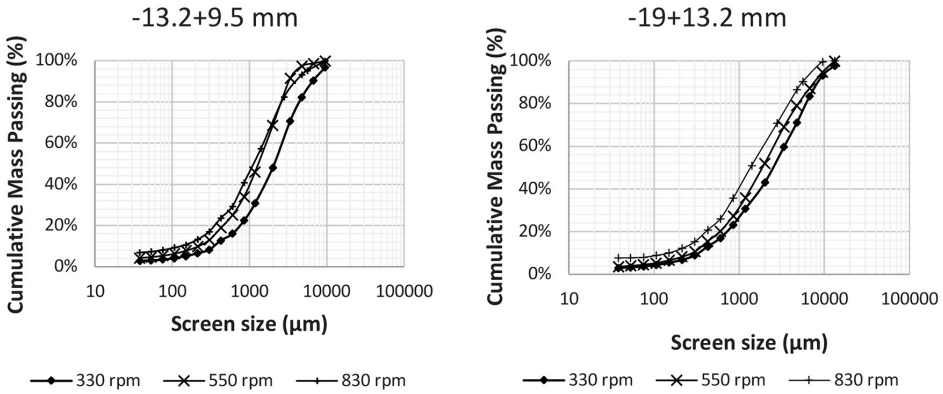

Figure 8—Size distributions of the crusher products from feed size classes of –13.2+9.5 and –19+13.2 mm for various disc rotational speeds (330, 550, and 830 r/min), offset of 10 mm and exit gap of 3 mm

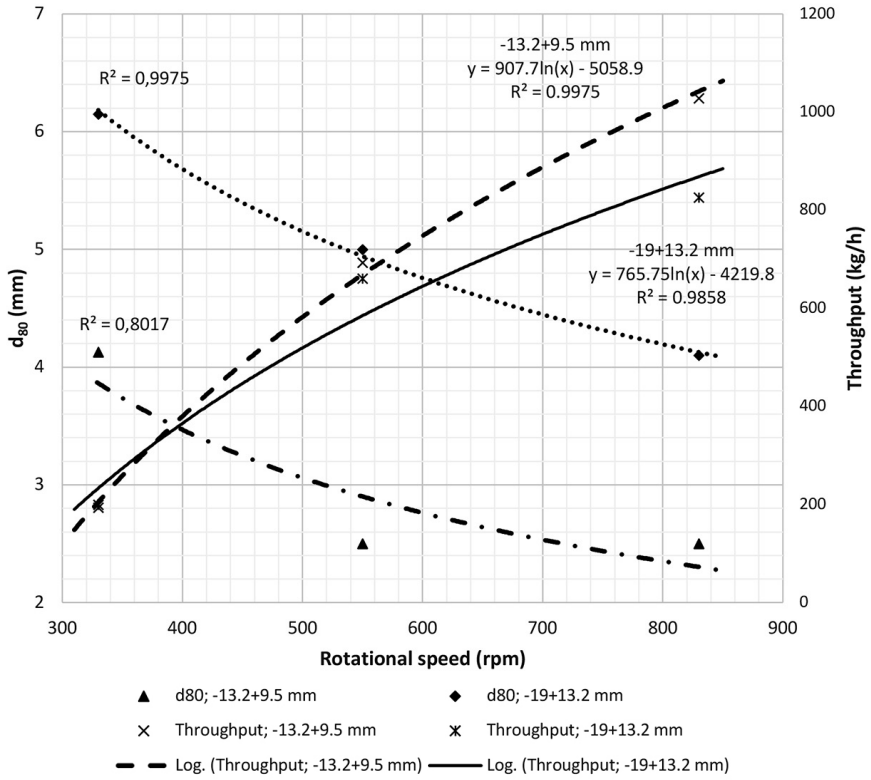

Figure 9—Product size and throughput as a function of rotational speed and feed size distribution

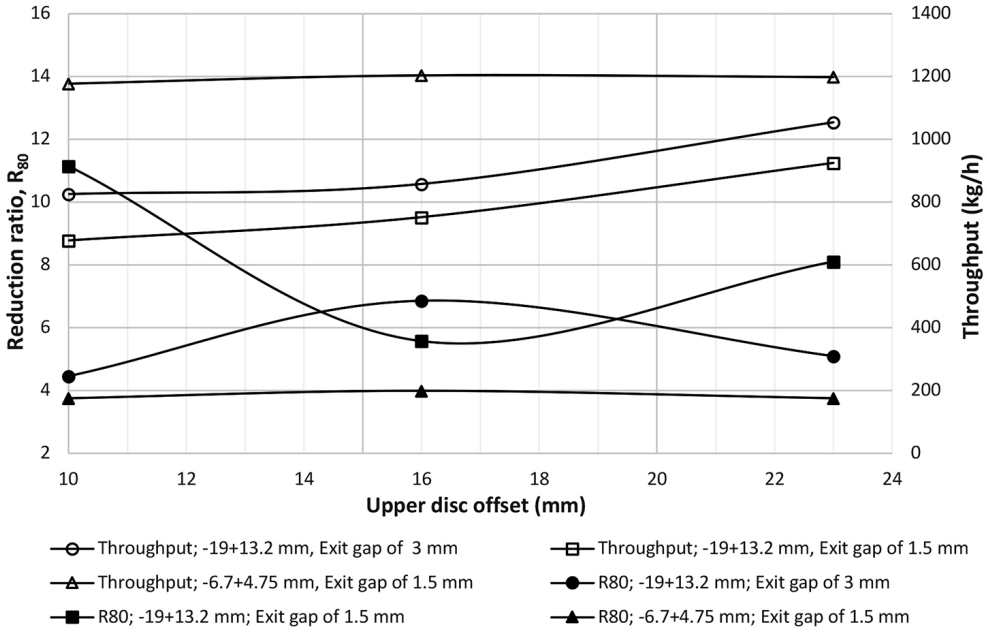

Figure 10—The relationship between reduction ratio (R_{80}), throughput, and offset for various feed size and exit gaps; speed 830 r/min

It can be seen from Figure 10 that feeding the crusher with fine particles (–6.7+4.75 mm) results in high throughputs (compare the throughputs for the –6.7+4.75 mm and –19+13.2 mm size classes. For the –6.7+4.75 mm feed particles, the throughput did not change with the increasing offset. This is contrary to the results for the –19+13.2 mm particles, where the throughput increased slightly with increasing offset, although the effect of offset on throughput is not as significant as that of speed (see Figure 9). The throughput dependence on the exit gap can be observed from the –19+13.2 mm size class plots for two exit gaps (1.5 and 3 mm). For each offset, a higher throughput was recorded for the larger exit gap (3 mm).

It is worth mentioning that 'slab' particles were produced by the ROC. We are considering using discrete element modelling (DEM) software to assess the crusher performance (breakage and transportation) for various shapes (profiles) of crushing surfaces to establish whether the production of slabs can be minimized. An apparent flexure in the structure was also observed, with the thickness of some of slab particles produced being greater than the exit gap. The present structure was designed primarily to

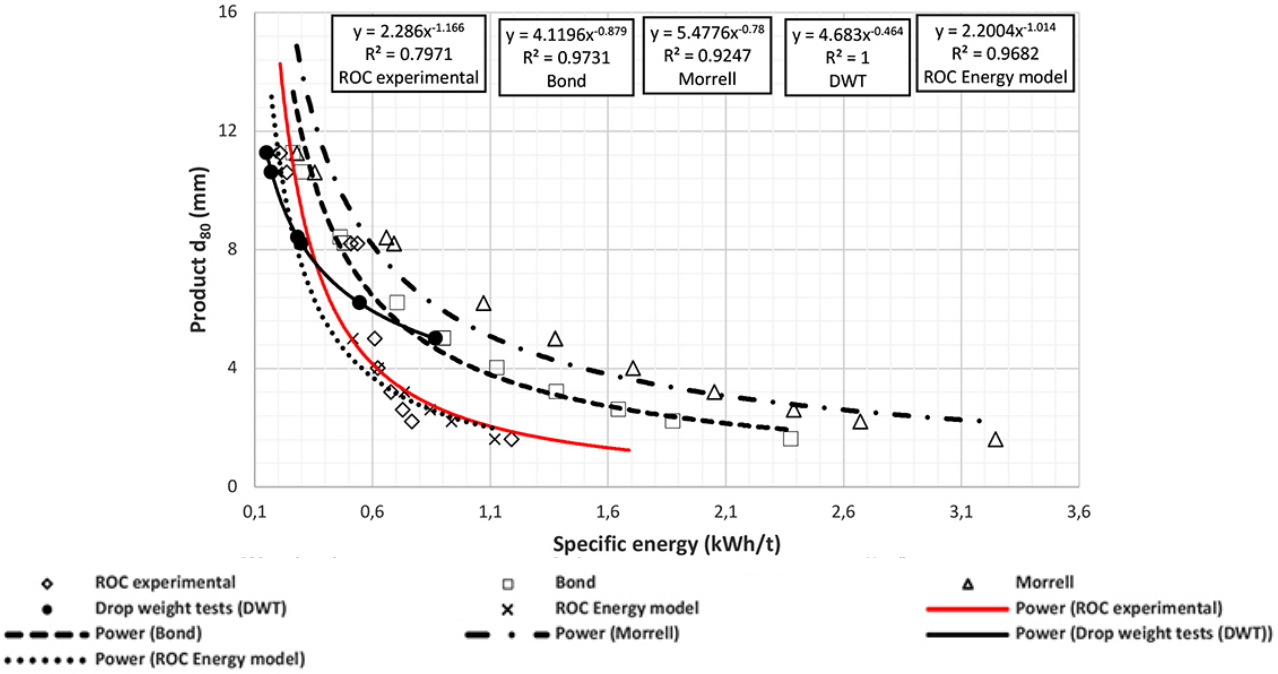

Figure 11—Relationships between the specific energy and d_{80} size for the crusher product estimated using various methods for the –19+13.2 mm feed size class

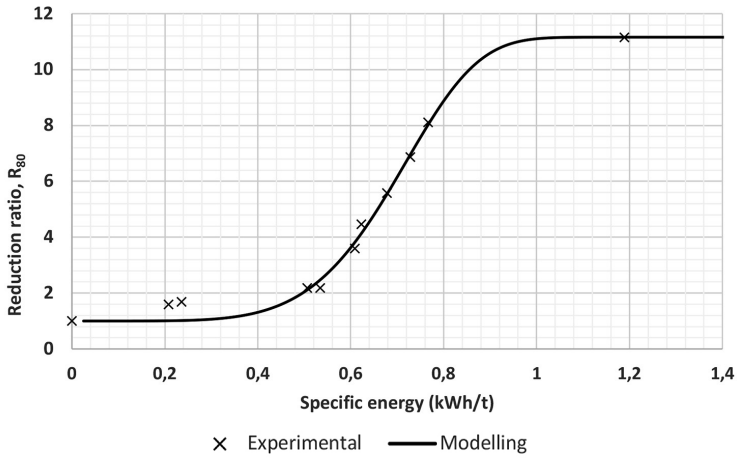

Figure 12—Relationship between the specific energy and reduction ratio

facilitate experimentation and thus its mechanical rigidity still needs to be reinforced to allow full transmission of energy to the particles.

In Figure 11, the energy efficiency of the ROC is analysed by applying the Bond and Morrell formulae and compared with drop weight test (DWT) data that was obtained for this quartz sample. It is seen that the experimental data (shown as the red curve) lies between the relationships for the DWT and Bond data for product specific energies less than 0.35 kWh/t. For specific energies greater than 0.35 kWh/t, the experimental specific energies are below what is predicted by Bond's and Morell's equations as well as the relationship from the single particle DWTs. The specific energies predicted using the relationship established from the DWT experiments, are smaller than those predicted by Bond's and Morrell's equations. Single particle breakage is the most efficient breakage mechanism in terms of energy utilization (Tavares, 2004). The estimated values using the Bond equation are lower than those indicated by Equation [3] (Morrell, 2004).

It is important to note that for both Equations [2] and [3], the Bond work index of 13.57 kWh/t for quartz (as reported in Wills and Finch, 2016) was used. The most reliable work index for the rocks crushed in the ROC could perhaps be obtained from the SCM test® (Morrell, 2009) and this is likely to be smaller than 13.57 kWh/t. It should be noted that the ROC is classed as a secondary or tertiary crusher.

A more reliable relationship between ROC specific energy and the feed and product size distributions was found to take the form of Equation [9] with exponent m equal to 0.216 (obtained using the iteration method with the objective function set to measure the minimum root mean square error). The specific energies computed using Equation [9] for the experimental d_{80} sizes are also plotted in Figure 11, where they are labelled 'ROC energy model'. This relationship gives a better estimate for the ROC specific energy, especially for specific energies above 0.6 kWh/t, as compared to Bond's and Morrell's equations. It should, however, be noted that this is from the small amount

of experimental data generated thus far. A more reliable model would have to be formulated as the experimental programme progresses.

$$W = W_i(P_{80}^{-m} - F_{80}^{-m}) \quad [9]$$

where W is the specific energy in kWh/t, W_i is the Bond work index in kWh/t, P_{80} is the 80% passing size of the product in µm, F_{80} is the 80% passing size in µm, and m is the exponent with an estimated value of 0.216187582.

It can be seen from Figure 12 that the reduction ratio generally increases with specific energy. The experimental data was fitted to Equation [10]. For energies below 0.4 kWh/t there is no significant size reduction, as it can be seen that the reduction ratios are very similar and equal to unity. The size reduction ratio increases steadily with input energy for specific energies between 0.4 and 1 kWh/t. When further experiments are conducted in future at higher speeds, this model needs to be revisited.

$$R_{80} = A\left(1 - e^{-mE_{cs}{}^{n}}\right) + 1 \quad [10]$$

where A, m, and n are constants and 1 is the reduction ratio at zero input energy.

Conclusions

- A working prototype of the laboratory ROC has been built and an experimental programme has been commissioned.
- The work so far has revealed that the disc speed is a key factor affecting the performance. Size reduction ratios as high as 11 were recorded for experiments with quartz at a speed of 830 r/min.
- From the experimental results there are no clear trends between the horizontal offset of the upper disc and product size distribution. However, there is a noticeable increase in crusher throughput with the offset.
- Slab particles were produced from the ROC. This is could be attributed to insufficient crushing energy (suggesting a need to attempt higher speeds to increase the energy intensity in the crusher) and the shape of the profiles on the crushing surfaces. Consideration is being given to using the discrete element method (DEM) for various design configurations to study the flow and breakage behaviours of the particles in the crusher.
- There is also a need to strengthen the structure to ensure that there is no significant flexure, thereby ensuring that the energy meant for breaking the particles is efficiently utilized and thus allowing the full potential of the crusher to be established.
- Further experimental work will be conducted on more materials, including some common ores, under a variety of operating conditions to establish sufficient data on which to base comparison with other comminution equipment such as the HPGR, cone crusher, and Loesche mill.
- Measurement of the wear rate on the crushing surfaces will also need to be considered in future.

Acknowledgement

We acknowledge the financial support in the form of grant from South African Minerals to Metals Research Institute (SAMMRI). The workshop team in the School of Chemical and Metallurgical Engineering at University of the Witwatersrand is acknowledged for their technical support.

References

Altun, D., Gerold, C., Benzer, H., Altun, O., and Aydogan, N. 2015. Copper ore grinding in a mobile vertical roller mill pilot plant. *International Journal of Mineral Processing*, vol. 136. pp. 32–36. https://doi.org/10.1016/j.minpro.2014.10.002

Ballantyne, G.R. and Powell, M.S. 2014. Benchmarking comminution energy consumption for the processing of copper and gold ores. *Minerals Engineering*, vol. 65. pp. 109–114. https://doi.org/10.1016/j.mineng.2014.05.017

Barani, K., and Balochi, H. 2016. A comparative study on the effect of using conventional and high pressure grinding rolls crushing on the ball mill grinding kinetics of an iron ore. *Physicochemical Problems of Mineral Processing*, vol. 52, no. 2. pp. 920–931. https://doi.org/10.5277/ppmp160231

Curry, J.A., Ismay, M.J.L., and Jameson, G.J. 2014. Mine operating costs and the potential impacts of energy and grinding. *Minerals Engineering*, vol. 56. pp. 70–80. https://doi.org/10.1016/j.mineng.2013.10.020

Genç, and Benzer, A.H. 2016. Effect of High Pressure Grinding Rolls (HPGR) pre-grinding and ball mill intermediate diaphragm grate design on grinding capacity of an industrial scale two-compartment cement ball mill classification circuit. *Minerals Engineering*, vol. 92. pp. 47–56. https://doi.org/10.1016/j.mineng.2016.02.009

Griffith, A.A. 1920. The phenomena of rupture and flow in solid. https://royalsocietypublishing.org/doi/pdf/10.1098/rsta.1921.0006

Gupta, A. and Yan, D.S. 2006. Mineral Process Design and Operations: An Introduction (1st edn). Elsevier, Amsterdam.

Jeswiet, J., and Szekeres, A. 2016. Energy consumption in mining comminution. *Procedia CIRP*, vol. 48. pp. 140–145. https://doi.org/10.1016/j.procir.2016.03.250

Manouchehri, H.R. 2015. Towards sustainability by bridging the gap in comminution - from finely crushed ore to stirred media milling. *Proceesings of the 6th International Semi-Autogenous Grinding and High Pressure Grinding Roll Technology Conference*, Vancouver, September 2015. pp. 1–16. https://www.ceecthefuture.org/wp-content/uploads/2015/11/55-Hamid-Reza-Manouchehri-Towards-Sustainability-by-Bridging-the-Gap-in-Comminution-%E2%80%93-From-Finely-Crushed-Ore-to-Stirred-Media-Milling.pdf

Morrell, S. 2004. Predicting the specific energy of autogenous and semi-autogenous mills from small diameter drill core samples. *Minerals Engineering*, vol. 17, no. 3. pp. 447–451. https://doi.org/10.1016/j.mineng.2003.10.019

Morrell, S. 2009. Predicting the overall specific energy requirement of crushing, high pressure grinding roll and tumbling mill circuits. *Minerals Engineering,* vol. 22, no. 6. pp. 544–549. https://doi.org/10.1016/j.mineng.2009.01.005

Nadolski, S., Klein, B., Kumar, A., and Davaanyam, Z. 2014. An energy benchmarking model for mineral comminution. *Minerals Engineering*, vol. 65. pp. 178–186. https://doi.org/10.1016/j.mineng.2014.05.026

Napier-Munn, T. 2015. Is progress in energy-efficient comminution doomed? *Minerals Engineering*, vol. 73. pp. 1–6. https://doi.org/10.1016/j.mineng.2014.06.009

Napier-Munn, T. J., Morrell, S., Morrison, R. D., and Kojovic, T. 2005. Mineral Comminution Circuits: Their Operation and Optimisation (3rd edn). Julius Kruttschnitt Mineral Research Centre, University of Queensland, Australia.

Ozcan, O. AND Benzer, H. 2013. Comparison of different breakage mechanisms in terms of product particle size distribution and mineral liberation. *Minerals Engineering*, vol. 49. pp. 103–108. https://doi.org/10.1016/j.mineng.2013.05.006

Radziszewski, P. 2013. Energy recovery potential in comminution processes. *Minerals Engineering*, vol. 46–47. pp. 83–88. https://doi.org/10.1016/j.mineng.2012.12.002

Reichert, M., Gerold, C., Fredriksson, A., Adolfsson, G., and Lieberwirth, H. 2015. Research of iron ore grinding in a vertical-roller-mill. *Minerals Engineering*, vol. 73. pp. 109–115. https://doi.org/10.1016/j.mineng.2014.07.021

Rosario, P. and Hall, R. 2010. A structured approach to the evaluation of the energy requirements of HPGR and SAG mill circuits in hard ore applications. *Journal of the Southern African Institute of Mining and Metallurgy*, vol. 110, no. 3. pp. 117–123.

Saramak, D., Wasilewski, S., and Saramak, A. 2017. Influence of copper ore comminution in HPGR on downstream minerallurgical processes. *Archives of Metallurgy and Materials*, vol. 62, no. 3. pp. 1689–1694. https://doi.org/10.1515/amm-2017-0258

Tavares, L. 2004. Optimum routes for particle breakage by impact. *Powder Technology*, vol. 142, no. 2–3. pp. 81–91.

Tavares, L. and King, R. 1998. Single-particle fracture under impact loading. *International Journal of Mineral Processing*, vol. 54, no. 1. pp. 1–28. https://doi.org/10.1016/s0301-7516(98)00005-2

Tromans, D. 2008. Mineral comminution: Energy efficiency considerations. *Minerals Engineering*, vol. 21, no. 8. pp. 613–620. https://doi.org/10.1016/j.mineng.2007.12.003

Wang, E.Z. and Shrive, N.G. 1995. Brittle fracture in compression: Mechanisms, models and criteria. *Engineering Fracture Mechanics*, vol. 52. pp. 1107–1126. https://doi.org/10.1016/0013-7944(95)00069-8

Wang, J.H., Chen, Q.R., Kuang, Y.L., Lynch, A.J., and Zhuo, J.W. 2009. Grinding process within vertical roller mills: experiment and simulation. *Mining Science and Technology*, vol. 19, no. 1. pp. 97–101. https://doi.org/10.1016/S1674-5264(09)60018-1

Wills, B.A. and Finch, J. 2016. Wills' Mineral Processing Technology: An Introduction to the Practical Aspects of Ore Treatment and Mineral Recovery. 8th edn. Elsevier Butterworth-Heinemann. ◆

Appendix A

Size distributions for the effect of offset

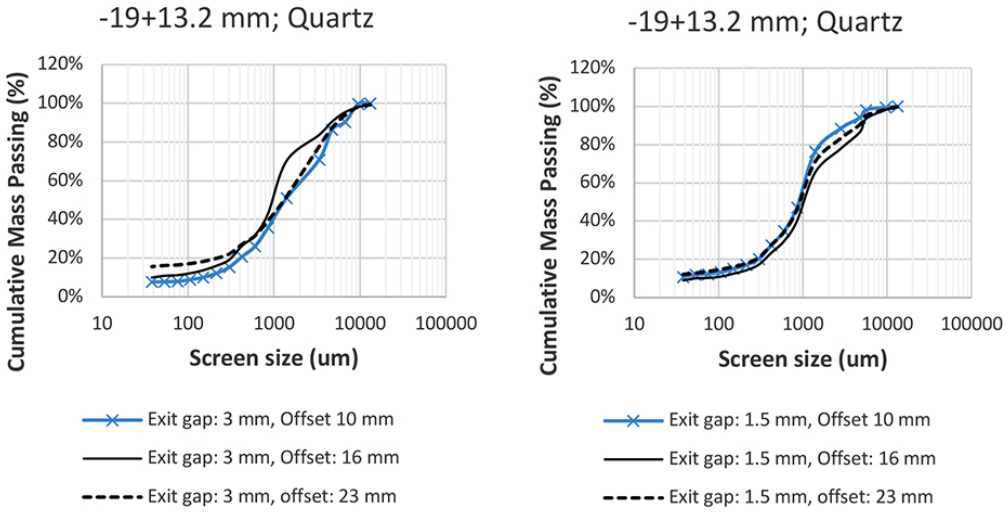

Figure A1— Size distributions for the –19+13.2 mm quartz crushed in the ROC as a function of offse

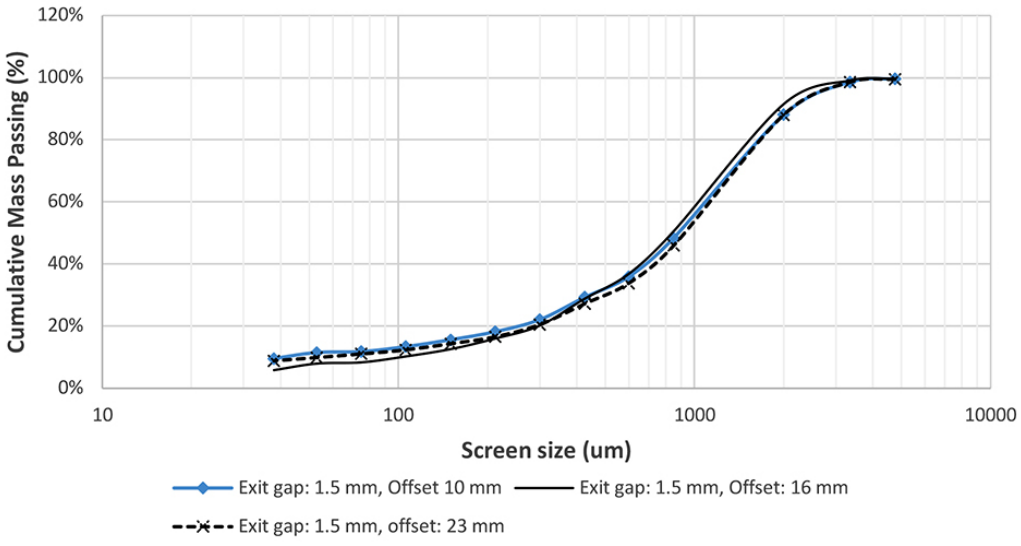

Figure A2—Size distributions for the –6.7+4.75 mm quartz crushed in the ROC as a function of offset

Identification of cost factors relating to mining incidents

E.P. Preis[1] and R.C.W.Webber-Youngman[1]

Affiliation:
[1] Mining Engineering Department, University of Pretoria.

Correspondence to:
E.P. Preis
R.C.W. Webber-Youngman

Email:
eugenepreis@gmail.com
ronny.webber@up.ac.za

Dates:
Received: 10 Sep. 2018
Accepted: 13 Jan. 2021
Published: January 2021

How to cite:
Preis, E.P. and Webber-Youngman, R.C.W. 2021 Identification of cost factors relating to mining incidents. Journal of the Southern African Institute of Mining and Metallurgy, vol. 121, no. 1, pp. 39–46.

DOI ID:
http://dx.doi.org/10.17159/2411-9717/16/484/2021

Synopsis

The real cost of any mining incident has, empirically, proven to be estimation-driven, rather than fact-driven. One of the main reasons for this lies with the complexity of the cost composition of any given mining incident. Incident costs comprise both direct and indirect cost factors, and in many cases the costs associated with these factors are incurred during different time periods following the incident. In this paper we aim to identify the various cost factors arising from mining incidents, provide a thorough understanding of all the potential cost factors identified, and draw general conclusions on the knowledge obtained.

Furthermore, recommendations are made on how mining companies could use the results, in order to assist them in calculating the costs of mining incidents. The paper also provides suggestions for further research, with the emphasis on the most significant immeasurable cost factors, namely the costs of implementing job accommodations following an incident, the harm to company reputation, and the decreased productivity due to low worker morale/psychological factors following an incident.

If mining companies are aware of and understand which factors could contribute to the cost of any given incident, future planning and incident cost estimations could be easier. It should, however, be noted that although this study provides a comprehensive list of cost factors (and detailed explanations), other unknown cost factors relating to mine incidents could prevail in extreme cases.

Keywords
direct costs, indirect costs, mining incidents.

Introduction

Zero harm is a vision that is fully subscribed to by all South African mines. The main objective of the vision is to eliminate injuries and fatalities. Apart from the effects related to injuries and fatalities, mining incidents involve considerable costs for mines. The various factors that influence the costs of an incident are not always that obvious, and this can have major downstream implications (*e.g.* an incident may result in future opportunity losses due to the harm caused to a company's reputation). The purpose of this investigation was to identify all the potential cost factors associated with mine incidents and quantify the understanding and significance related to incidents. The difference between, and impact of, quantifiable and non-quantifiable factors was also addressed.

Background

To ensure a clear understanding of the cost of incidents and related factors, it is necessary to firstly provide definitions for the primary components of incident costs. These terms/phrases are used throughout this study. The total cost associated with an incident can be broadly classed into three main categories: costs to employees, costs to society as a whole, and costs to the employer (Table I).

The objective of this study was to focus solely on identifying the cost factors relating to mine incidents, from a 'cost to employer' perspective. It was, however, necessary to provide definitions for the other incident cost categories to prevent any misunderstanding or confusion.

The actual cost of an incident is a concept that seems simple to calculate and understand. Incident costs are split into direct (visible) costs and indirect (hidden) costs. The relationship between direct and indirect costs of an incident can be compared to an iceberg. The entirety of the iceberg represents all incident costs – with the submerged part representing the indirect costs and the visible part representing the direct costs (Figure 1).

The iceberg analogy suggests that the indirect costs of an incident are much more substantial than the direct costs. To quantify the relationship between direct and indirect costs, a ratio of direct to indirect costs can be expressed. However, whether this ratio is in fact something that can or should be quantified and benchmarked is unclear. The literature suggests that ratios vary greatly, from 1:1 to 1:36 (Table II).

Identification of cost factors relating to mining incidents

Table I

Broad incident cost categories

Category	Definition
Costs to employees	All incident-related costs for which the affected employee is responsible for (or in the case of a deceased employee, their family will assume this r esponsibility). The costs to employee includes the loss of future earnings, the cost of human suffering, as well as other miscellaneous expenses (*e.g.* an injured employee not at work has a higher cost of living than if at work). Costs to Employee do not affect the cost to employer, although the burden of some costs due to an incident is shared between the two parties.
Costs to society	All incident-related costs for which society as a whole is responsible for, whether directly or indirectly. An example of this is the worker's compensation fund, the burden of which falls upon the widespread economy of South Africa. In the case of an injured/deceased working individual, the economic impact of this individual not being able to contribute towards the country's economy falls upon the country as a whole (society).
Costs to employer	All incident-related costs for which the employer is responsible. These can be costs that are direct or indirect, costs which are only felt some time after incident occurrence, and costs that take on the form of losses relating to the company (real losses or opportunity losses). The approach to determining which costs fall within this category is to ask the question – 'Would this cost/loss have been incurred if the incident had not happened?' If the answer is no, then it is a cost to the employer due to incident occurrence.

Table II

Different ratios of direct *vs.* indirect costs of incidents

	Ratio	Comments	Source
Average	1:4	Based on historical cost data of incidents.	Manuele, 2011
Range	1:2–1:20		
Average	1:2.12	As perceived by 231 financial decision-makers.	Huang *et al.*, 2009
Range	1:0–1:11		
Average	1:4.5	For incidents with a direct cost of up to US$2 999.	United States Department of Labour, 2011
	1:1	For incidents with a direct cost of more than US$10 000.	
Average	1:10	Average ratio of insured to uninsured costs, perceived by the British Health & Safety Executive (HSE) as direct and indirect costs.	British Health & Safety Executive, 1998
Range	1:2–1:36	Range of historical insured to uninsured cost ratios (direct *vs.* indirect).	

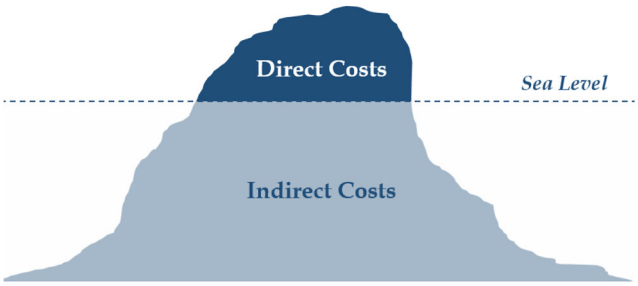

Figure 1—Incident cost iceberg analogy

The great variance in ratios shows that estimating the costs of incidents involves a large degree of uncertainty. In terms of this study, this variance showed that further investigation was required into the actual factors that contribute to the total cost of an incident. The identification and understanding of all cost factors relating to mine incidents acts as the starting point in understanding (and more accurately quantifying) the cost of mining incidents. This could assist in classifying incidents by type, and estimating direct *vs.* indirect ratios for each class of incident much more accurately.

By identifying and understanding the potential cost contributing factors, it would be possible to highlight the most significant financial consequences of mine incidents. This, in turn, would enable the separation or highlighting of specific individual factors, and then determining their effect on the total cost of incidents, which in turn will quantify their significance.

Cost factors relating to mining incidents

Cost factors relating to mining incidents were identified through a literature search. The approach focused firstly on any previous work done on incident cost factors in the workplace, irrespective of the type of workplace, and then narrowing down to work on the cost factors of mining incidents. The cost factors identified were all found to be potentially applicable to the mining industry, albeit with varying probabilities of occurrence.

A total of 34 main cost factors relating to mine incidents were identified, along with numerous sub-factors. Out of the 34 factors identified, eight were classified as direct cost factors and 26 as indirect factors.

Direct cost factors

The eight direct cost factors relating to mining incidents, as well as any relevant sub-factors, are explained under their respective headings.

Lost planned reserves

Blumenstein *et al.* (2011) identified lost reserves as a potential cost-contributing factor in mining incidents. However, their description was found to be broad, and thus the cost item was adopted rather as 'Lost planned reserves'. A lost planned reserve refers to the loss of future planned reserves due to an incident, resulting in mineable future reserves being rendered unmineable. This only applies to non-active work sites – if production is lost from an active workplace, the cost item 'Lost planned production and recovery thereof' applies.

Identification of cost factors relating to mining incidents

The loss of reserves should be seen as a lost asset, the amount of loss depending on the size of the lost reserve and the specific reserve quality (*e.g.* in the case of coal, calorific value, ash content, volatiles content, *etc.*).

Lost sales

Lost sales refers to the value of sales lost due to an accident (Blumenstein *et al.*, 2011). Lost sales will be applicable only when a mine is unable to deliver product to a customer, both on the contractually agreed-upon date and the agreed amount. Lost sales will apply only if the mine in question does not stockpile, else this item should be seen as a loss of asset. The assumption is that if the mine stockpiles, there is no chance of lost sales being incurred. There will, however, be a loss of asset due to the stockpile size decreasing.

Property damage, repair and replacement

Lebeau, Duguay, and Boucher (2013) identified property damage as a common contributor to incident costs. Property damage, repair and replacement refers to the cost of replacing or repairing any type of equipment damaged due to an incident. This item also includes all costs pertaining to temporary measures put in place, such as hiring equipment until permanent equipment has been purchased.

It must be noted that property damage requiring repairs or replacement should be analysed carefully, as numerous indirect costs can be overlooked. Any wages associated with property damage, repair and replacement should fall under the cost item 'All lost-time salaries', unless the salaries are for external contractors. The potential sub-factors that may arise through damage to property are shown in Table III.

All lost-time salaries

All lost-time salaries can be defined as the full salary (plus benefits) cost of non-performance of work due to (Lebeau, Duguay, and Boucher, 2013; Blumenstein *et al.*, 2011; Workers Compensation Board of British Columbia, n.d.):

- Injury to employee(s)
- Permanently disabled employee(s)
- Non-productive employees due to incidents prohibiting work from commencing.

The salary cost of a permanently disabled employee due to an incident will be incurred until workers compensation comes into effect. The full cost should be measured from the time of the incident until employer salary responsibilities are relieved by the worker's compensation fund. The salary cost of an employee who suffers a non-disabling injury will be incurred until the employee is declared fit to return to work. This cost should be measured from the time of the incident until the injured employee returns to work. It should be noted that upon returning to work, the employee could temporarily be less productive and incur further costs related to decreased productivity.

The cost of long-term absenteeism includes one component that short-term absenteeism does not incur, and that is the loss of productivity/momentum of the employee. An employee returning to work from an extended leave of absence has to readjust to work conditions. This means that for a certain time period after returning to work, the employee will be less productive than he/she is normally. The cost of this temporary loss in productivity is included under the cost item 'Lost productivity'. The salary cost of an employee rendered inactive due to an incident will be incurred until work can resume.

Lost planned production and recovery thereof

This item refers to the loss of production from an active work site due to an incident. It must be noted that the cost of lost planned production will be incurred only if the lost product can never be retrieved. The loss of planned production should be seen as a lost revenue-generating opportunity, and not necessarily a cost. The only real cost for this item is the additional operating expense incurred during recovery efforts. Nevertheless, both the opportunity loss and recovery cost should be included as a cost due to the incident.

Work site recovery

Work site recovery includes the costs incurred due to recovery efforts in an affected work site. If the recovery of the work site is performed by idle workers, then it should not be seen as a cost item, unless the idle workers incur overtime (the assumption being that the idle workers would have been paid regardless). Work site recovery may include reconstruction of access or moving of material or equipment (Blumenstein *et a*l., 2011).

If the work is performed by a contractor, then the contractor wages will be accounted for. Additional consumables due to recovery efforts also need to be accounted for (such as fuel, explosives, *etc.*). This item excludes the clean-up of a work site due to property damage, which is included under Equipment repair and replacement.

Penalties and SIMRAC levies

This cost item refers to the penalties/levies payable to the South African Safety in Mines Research Advisory Committee (SIMRAC). The South African Mines Reportable Accidents Statistical System (SAMRASS) codebook provides further information on the lost-days penalties payable for specific injuries. As an example, the safety levy component of a fatality on a mine will result in a

Table III

Potential sub-factors: Property damage, repair and replacement

Sub-factor	Definition/example
Removal of damaged/written-off equipment from work site	The cost of towing services to remove the equipment from the site, whether it is taken to a scrapyard, or to the on-site workshops.
Clean-up of spillage caused by damaged equipment	The cost of clean-up of the site following the property damage incident (*eg.* oil spillage from hydraulics of equipment).
Cost of repair work and parts (Workers Compensation Board of British Columbia, n.d.)	The cost of repairing the damaged equipment, as well as the cost of ordering, receiving, and installing new parts.
Cost of replacement equipment (LaBelle, 2000)	The cost of replacement equipment if equipment repair is not financially viable. The depreciated book-value of the written-off equipment should be used.
Cost of renting interim equipment	The cost of renting equipment while the damaged equipment is being repaired, or for the waiting period associated with the ordering of new equipment.

total of 6 000 lost days' penalty. Using the 2009-2012 levy cycle rate of R9.77 per lost day, the safety levy component per fatality would be R58 620 (during 2009–2012).

Incident response operations

An incident response operation includes all expenses related to direct incident response. This can include items such as mine rescue, fire-fighting, ambulance services, first aid, *etc.* (Blumenstein *et al.*, 2011). The items comprising the incident response operations include materials consumed as well as services costs (measure with time lapsed).

If the mine made use of internal mine rescue/incident response which did not result in overtime, the cost should not be added. The assumption is that if an incident-related task falls under the specific person's job description and does not result in overtime, the task should not be seen as a cost contributor. Whether or not the incident occurred, the task performer would have been remunerated by the same amount. The potential sub-factors that may arise through incident response operations can be seen in Table IV.

Indirect cost factors

The 26 indirect cost factors relating to mining incidents, as well as any relevant sub-factors, are explained under their respective headings.

Harm to company reputation

Harm to company reputation, or reputational loss (Gagne, 2011), refers to the cost of harm caused to a company's reputation following an incident. This can be incurred in several forms, such as:

- **Cancelled/lost orders** (Royal Borough of Kensington and Chelsea, 2002): Cancelled/lost orders can be seen as future orders lost from an existing customer, or as lost opportunities. An incident may lead to a potential customer deciding to not make use of the company services in the future. The company may also never know that they lost business opportunities due to the incident. Damage to a company's reputation might result in customers turning to competitor suppliers (Malaysian Department of Occupational Health and Safety, n.d.).
- **Possible tensions in labour relations:** Employees may decide to strike due to their feeling unsafe in the workplace following an incident. In this case, harm will be caused to the company reputation, as well as production losses.
- **Recruitment problems** (Lebeau, Duguay, and Boucher, 2013): A company with a damaged reputation could struggle to recruit new employees (people do not want to work for a company with a poor reputations). If the company is unable to employ new workers, productivity levels will drop.
- **Department of Mineral Resources (DMR) impact**: Harm caused to a mining company's reputation could lead to the withholding of rights from the DMR for future/expansion projects.

There are numerous factors involved in harm to company reputation. The company's market capitalization could be affected; and potential future investment from external investors might not be realized. These factors will manifest over time, and their financial effects might be realized only long after the incident has occurred.

The ACE Group (2013) conducted a study on risk management for European companies. The study focused on the potential financial impact felt due to a tainted company reputation.A questionnaire was sent to more than 100 medium to large-sized companies. One of the questions was aimed at sdetermining which potential impacts of reputational risk would cause the greatest concern to a business (Figure 2).

Figure 2 shows that damage to existing customer relationships, followed by a loss of earnings and fall in company share price, were the three biggest concerns in terms of the impacts of harm to a company's reputation. These concerns all apply to the mining industry, albeit in derivative forms.

Decreased productivity

Blumenstein *et al.* (2011) define the cost of decreased productivity as the cost of lower productivity due to using inexperienced replacement workers. An employee returning to work after recovering from an injury could be less efficient and/or less productive than before the injury. This could last for a finite time period, or until the employee reaches retirement. Assuming that the employee returns to the same specific job, a reduced efficiency will have a considerable cost impact on the company. This could be due to physical constraints (recovering from the injury) or to psychological aspects (*e.g.* increased risk averseness, anxiety, and stress).

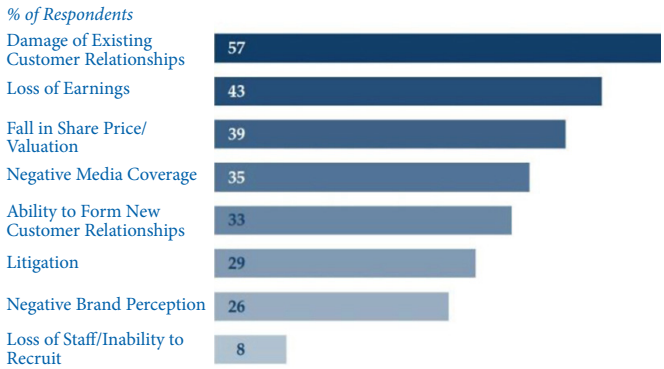

Figure 2—Potential impacts of reputational risk that cause the greatest concern to a business (ACE Group, 2013)

Table IV

Potential sub-factors: Incident response operations

Sub-factor	Definition/example
Ambulance services (LaBelle, 2000; Lebeau, Duguay, and Boucher, 2013)	Costs as per service provider. For transport (if required) from incident site to treatment facility/hospital.
Time to provide first-aid (Avma Plit, 2008; Gagne, 2011)	Salary cost of first-aid worker attending to injured employee and of persons arranging ambulance services and transportation.
Time for transportation following incident (Workers Compensation Board of British Columbia, n.d.)	Salary cost of person taking injured employee to hospital (if not ambulance services); salary cost of waiting for transportation; salary cost of person remaining with injured employee in hospital.
Police/firefighting services (Blumenstein *et al.*, 2011)	The cost incurred due to the call-out of police or fire-fighting services

In this case the company will have to spend the same amount on the employee's wages (input) for a reduced output. To maintain the same level of productivity as before the incident, the company will have to spend more money elsewhere to compensate for the lost efficiency of the temporarily 'handicapped' employee. In mining, this potential reduction in efficiency will most likely apply to physical labourers.

The removal of a worker from a familiar workplace will decrease in productivity in the area the employee was removed from as well as in the relocation area. However, this will not always be the case – the effect may be the opposite in some cases (Workers Compensation Board of British Columbia, n.d.).

Impact of decreased worker morale

An incident could lead to a decrease in worker morale (AVMA PLIT, 2008; Gagne, 2011), and the potential impacts on productivity following an incident can be numerous. Lower motivation to work, workforce morale decreasing, and an increased rate of absenteeism by fellow workers may be felt following an incident (Malaysian Department of Occupational Safety and Health, n.d.). In theory, all these factors can be measured by comparing historical production rates and rates of absenteeism before and after the incident. This would, however, be possible only if all other factors remained equal (*ceteris paribus*), which in practice is impossible. Studies have been conducted in order to understand the link between the level of safety in the workplace and employee morale (Figure 3).

A low level of employee morale could lead to a decrease in productivity, which will inevitably result in financial loss. A workplace that does not comply with safety standards could cause poor morale due to the psychological impact on employees (employees working in an unsafe environment are more likely to be demoralized and less productive).

Processing plant stoppage costs

Processing plant stoppage costs refers to the cost/loss incurred due to any form of plant stoppage caused by an incident, including both mining incidents and processing plant incidents. It must, however, be noted that this cost factor is unlikely to be incurred unless an incident causes damage to plant-related equipment, or it is deemed unsafe to continue running the plant after an incident.

Job accommodations

Job accommodation refers to the long-term cost of a loss in production time due to an adjustment to or implementation of new safety procedures/practices. This cost item comprises two components, namely the cost of implementing modifications to equipment, procedures, or standards and the long-term cost impact of the modifications.

If an incident necessitates the redesign of a piece of equipment, methodology, or standard operating procedure, the direct cost of the redesign must be included. The after-effects of the redesign must also be considered (indirect cost of job accommodations). This will most likely take the form of a decrease in productivity, which could last for a finite or indefinite time period. This being said, a job accommodation will not always result in decreased productivity, and could potentially have a positive impact in the long run (by improving efficiencies). The redesign could in actual fact lead to an improvement to the system and a consequent improvement in productivity. Thus, job accommodations could be either positive or negative in terms of the total cost estimation.

Consider a scenario where an incident occurs on a mine. This type of incident has never occurred before, and exposes a flaw in one of the company's safety procedures. This flaw is corrected by adapting the specific safety procedure in question, which leads to an extra 15 minutes in the pre-shift safety meeting. This results in a shift losing 15 minutes of production time. The adjusted safety procedure is implemented for the rest of the life of mine. Thus, the mine is now losing production time every day. The cost of this continuous lost production time will not be minimal – however, quantifying this cost is nigh-on impossible. The potential sub-factors that may arise through employee replacement and training can be seen in Table V.

Damage to the environment

This cost item refers to penalties payable due to environmental contamination following an incident. It also includes the cost of restoring the environment to its natural, pre-incident state. It must be noted that this cost item can comprise of several sub-factors, depending on the nature of the mine and the incident.

Product replacement

An incident could lead to product needing to be replaced in order to meet contractual obligations. Product replacement refers to the cost incurred if an incident results in a client not receiving product that has been paid for, and which has to be replaced by the mine at their own cost (Blumenstein *et al.*, 2011). This item

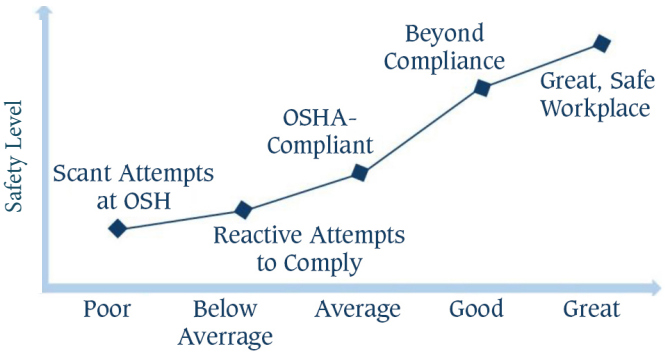

Figure 3—Hypothetical relationship between safety level and employee morale (Behm, 2009)

Table V

Potential sub-factors: Job accommodations

Sub-factor	Definition/example
Equipment/tool/personal protective equipment (PPE) redesign (LaBelle, 2000)	The cost/gain from redesigning a specific tool or piece of equipment, following an incident. For example, installation of hand-guard on the conveyor belt operating switch.
Process redesign	Redesign/redirection of process flow.
Standard operating procedure redesign (methodology redesign)	Cost of changes to COP/SOP. Essentially changes to the standard methodology used to complete a specific task.

will be incurred only if the mine does not stockpile and cannot deliver its own product to a specific client. It will be very rare for this cost item to arise due to an incident, but nevertheless it can occur.

Workers compensation premium adjustment

This refers to the cost of an increased compensation premium, measured over a certain time period. The premiums that mining company has to pay towards the National Workers Compensation Fund, can increase or decrease according to safety performance.

Workers compensation payments are not regarded as a cost-contributing factor for the company. The reason for this is the way that the fund is structured. Each mine pays a time-based premium towards the fund, and this premium is adjusted according to the safety records for that year. Thus, where the workers compensation fund will impact on the cost of incidents is the rise in yearly/monthly premiums payable. This value will be time-sensitive.

Liability paid

This cost factor refers to the uninsured amount paid in third-party claims or non-mine liability claims. Specific insurance agreements with the mine's insurance provider can be consulted, if the company is not self-insured.

Legal fees

Incidents involving lawsuits and/or liability claims need to account for the fees paid for legal assistance due to the incident. This item will include all legal fees incurred due to an incident, as well as employee lost time. The time that an employee has to sit with a legal team and testify must be accounted for. If, for example, the CEO has to sit with a legal team (and this does not result in overtime) the lost time must not be accounted for as it falls within the CEO's job description.

Insurance premium increase

An incident that results in an insurance claim could lead to a company's premiums increasing, and this cost needs to be accounted for. The annual premium that a company pays is determined according to an estimate of leave of absence, number of hospitalization days, the severity of the accident, potential lawsuits, and the financial cost of damage to equipment, commodities, and facilities. The premium varies from year to year according to events that occurred in the previous year.

Insurance deductible

Insurance deductible refers to the amount of a claim payable by the company before compensation takes effect. If the company is not self-insured, the insurance agreement with the insurance provider should be consulted.

Excess claim payments

An excess claim payment on insurance refers to the amount payable by a company over and above insurance coverage. Specific insurance agreements with the mine's selected insurance provider can be consulted if the company is not self-insured.

Incident investigation time

Incident investigation time includes the costs associated with the investigation of the incident by inspectors as well as SHEQ mine employees. If mine employees perform investigations, the cost should be included only if it falls outside of their job description or results in overtime. Investigation of incidents is what SHEQ does; their salaries would have been paid regardless of whether or not sthe incident occurred. The potential sub-factors that may arise through uncompensated medical expenses can be seen in Table VI.

Incident-related interviews

The cost of time spent interviewing employees and witnesses is categorized as the cost of incident-related interviews. The interviewer time should be considered as a cost only if the interview falls outside their job description, results in overtime, or if the interviewer is a contractor. The interviewee cost component should be included only if the interview prevents the employee from performing work. If the interview is performed during idle time, it should not be accounted for (as it has already been accounted for in lost-time salaries). If the interview results in the interviewee incurring overtime, it should be accounted for.

Incident-related meetings and report preparation

Any incident has to be investigated and a report written up. All meetings pertaining to the incident, as well as report preparation, fall under this cost item. The time spent in meetings and preparing the report should be accounted for only if it resulted in overtime, fell outside the job description of those involved, or if a contractor was brought in.

Employee replacement and training

This item refers to the cost of hiring and training replacement employees following an incident. This applies to both temporary employees and new full-time employees. The costs in this item would include the time spent interviewing potential replacements, but only if the interview time falls outside the job description of the interviewer or if overtime is incurred. The wages paid to the hired employee during the training period have to be accounted for.

There will be a substantial difference in the total cost incurred for this item if the replacement is an existing employee. The potential sub-factors that may arise through employee replacement and training can be seen in Table VII.

Product damage

The Malaysian Department of Occupational Safety and Health (n.d.), amongst other types of damage, identified product damage as a potential cost factor. In mining, the product is essentially ore,

Table VI

Potential sub-factors: Incident investigation time

Sub-factor	Definition/example
Ambulance services	Costs as per service provider for transport (if required) from incident site to treatment facility/hospital.
Time to provide first-aid	Salary cost of first-aid worker attending to injured employee; salary cost of persons to arrange for ambulance services and transportation.
Time for transportation following incident	Salary cost of person taking injured employee to hospital (if not ambulance services); salary cost of waiting for transportation; salary cost of person remaining with injured employee in hospital.

and it seems almost impossible for ore to be 'damaged' (although it can occur in extreme cases). Consider an example where a gold processing plant experiences a drop in recovery due to contaminated ore as a result of a hydraulic oil spill from damaged equipment. The reduction in plant recovery is an indirect cost of product damage.

Claims paperwork time

If an incident results in insurance claims being filed, the cost of time spent preparing and filing claims paperwork needs to be accounted for. This cost should be included only if it falls outside the job description, results in overtime, or is performed by a third party.

Interest paid on delayed insurance claims compensation

Interest paid on delayed insurance claims compensation refers to the interest lost due to expenditure incurred by the company for which it will be remunerated later. (Blumenstein *et al.*, 2011).

Security

This item refers to the cost of additional security required due to an incident. Security costs should be included only if the incident required an increased level of security for a certain time period (*e.g.* the company needed 10 more security guards for a week while the incident was being investigated). If, however, security staff assist with an incident that leads to a security breach such as theft, this could result in an additional cost. If this temporary breach does lead to some form of criminal activity, the cost can also be indirectly attributed to the incident, since if the incident had not occurred, the theft would not have taken place.

Work in progress

This cost item refers to the cost incurred due to work-in-progress (WIP) products being halted along the production line. It is not as applicable to the mining industry as it would be to other industries. However, this could become a cost factor when an incident leads to a stoppage, where ore flow is stopped while undergoing a process (or where ore/waste needs to be re-handled due to an incident).

Demurrage

Demurrage refers to the penalties payable for not receiving delivery of consumables on contract (Blumenstein et al., 2011). Supplier contracts will provide the ruling on demurrage. It should, however, be noted that this is not a common occurrence in the mining industry, as the contracts are set up in such a way as to avoid these penalties.

Uncompensated medical expenses

An uncompensated medical expense refers to the cost of medical expenses other than those included in insurance. Examples would be mine dispensary costs (lump sum costs) and non-emergency transportation to a medical provider (time- and unit-related costs). Which medical expenses are covered by worker's compensation, and those that are the responsibility of the company, needs to be investigated. The potential sub-factors that may arise through uncompensated medical expenses can be seen in Table VIII.

Additional consultant fees

Additional consultant fees refers to any additional work performed relating to an incident. This item should, however, be added only if it was not accounted for under any of the other cost items.

Fluctuating operating expenses

Fluctuating operating expenses refers to a change in the average operating expenses due to an incident. The terms 'cost' or 'loss' are avoided as this item will in most cases lead to the mine expending less than it would have at steady-state production. Thus this item applies only if there is a mine stoppage. The assumption is that, for the duration of the stoppage no employee can work overtime, bonuses for the month fall away (depending on bonus structure), and employees who fall ill and are unable to work during that time will not have a financial impact (will not be double-accounted for with a replacement worker). The calculation of this item should focus on all expenses not incurred due to the incident, and it should reflect as a positive value.

Table VII

Potential sub-factors: Employee replacement and training

Sub-factor	Definition/example
Costs to attracting candidates (advertisements, agencies, *etc.*)	The cost of a recruiting agency to place advertisements and attract potential candidates.
Costs to select candidates	The cost of a recruiting agency conducting preliminary interviews for potential candidates.
Costs for interviews	The time cost for company human resources (HR) to conduct final interviews.
Costs for psychometric assessments	The cost of an external contractor providing these tests, as well as interpreting the results and writing up individual reports.
Administrative, accounting, and legal costs	The time cost of company HR, as well as the costs associated with signing new contracts (if the time falls outside of normal duties).
Travel and lodging expenses	The cost to company of providing allowance for travel and lodging while the candidate is going through the selection process.
Costs for medical examinations	The cost of necessary medical examinations in order for the candidate to be declared medically fit to perform the specific job.
Training costs	The additional costs associated with training a new employee (mostly time-based costs).
Other employees' time for on-the-job training	The additional cost incurred in training more employees than is the norm.
Pay during training	The cost associated with the company paying salary in full, even when the employee is not working and busy with training.
Training of temporary and replacement personnel	Costs associated with training an existing employee to do other work until a new employee has been assigned and trained.
Costs for the team of integrating a new member	The loss in productivity when introducing a new member to a team (mostly due to on-the-job training).

Table VIII

Potential sub-factors: Uncompensated medical expenses

Sub-factor	Definition/example
Medical bills/health care professional	Additional treatment required for an injured employee, outside of the scope of normal, on-site treatment (physician, specialist doctor, *etc.*). This can also include follow-up consultations with specialists.
Medical treatment supplies	Consumption of medical supplies not provided on-site.
Drug testing	Additional fees for drug testing due to incident (special tests) or fees for off-site testing.
Medical equipment that is unusable after treatment	If an injured employee needs immediate medical treatment which requires equipment and the equipment cannot be used again (due to health and safety reasons).

This item is not really a cost item at all. The approach is to look at what the mine would have spent if no stoppage had occurred. Consumables are not consumed, electricity consumption goes down, *etc*. Thus this means that the mine is spending less during the stoppage than it would have while producing.

Conclusions

The identification and understanding of all cost factors relating to mine incidents proved to be more complex than expected. A number of objectives were reached through this study, and the following lessons learnt.

- In general, cost factors relating to workplace incidents can vary greatly. This is due to the difference in workplace environments across different industries. Another factor that plays a role in the cost factors relating to workplace incidents is the specific country where the incident occurred. Different policies around the world lead to different employer responsibilities in terms of the financial impact of incidents.
- The same can be concluded when narrowing down 'workplace incidents' to 'mining incidents'. Nevertheless, this study focused on identifying and understanding any potential cost factors relating to mine incidents, and these factors remained constant (regardless of the country of occurrence). Although the eventual financial impact felt by the employer would be country-specific, the potential factors remained the same.
- A list of 34 main factors relating to mine incidents, as well as numerous sub-factors, was compiled. From this list of potential factors it can be concluded that mine incidents can comprise a vast number of cost-contributing factors.
- These factors can also be very different in nature. Some may be incurred instantaneously, and others may only be realized long after the incident occurred.

In conclusion, the identification of any cost factors relating to mine incidents can be valuable to mining companies. If companies are aware of and understand which factors could contribute to the cost of any given incident, future planning and incident cost estimations will be easier. It should, however, be noted that although this study provides a comprehensive list of cost factors (and detailed explanations), other unknown cost factors relating to mine incidents could prevail in extreme case.

Recommendations and suggestions for future work

It is recommended that the work done in this specific study be used by mining companies to enhance understanding in the field of incident costs. Mine management and safety officers can benefit from the information presented, as it can provide a sound base for the on-site estimation of the cost of mining incidents.

It is further recommended that if the work in this study is to be used, the cost factors identified should be reviewed for the intended application, and sound judgment should be applied when assessing the applicability of factors to specific incidents.

It is suggested that further investigations be conducted into three of the identified cost factors. These three factors are:

- The financial impact of implementing job accommodations and/or work process modifications following an incident
- The financial impact of harm caused to a company's reputation following an incident
- The financial impact of decreased worker productivity caused by decreased morale, as well as the relationships between productivity, safety, and worker morale.

The abovementioned factors each lend themselves to highly detailed investigations, and it is suggested that each of these immeasurable factors be investigated in isolation.

References

ACE Group. 2013. Reputation at Risk: ACE European risk briefing 2013. http://www.acegroup.com/global-assets/documents/Europe-Corporate/Thought-Leadership/ace_reputation_at_risk_july_2013.pdf [accessed 12 September 2014].

AVMA PLIT. 2008. Direct *versus* indirect costs of injuries on the job at your practice. http://www.avmaplit.com/uploadedFiles/AVMAPLIT/Publications/Safety_and_Loss_Control/664-Direct%2520and%2520Indirect%2520Costs%2520of%2520Injuries.pdf [accessed 15 April 2014].

Behm, M. 2009. Employee morale – Examining the link to occupational safety and health. *Journal of the American Society of Safety Engineers*, October 2009. pp. 42–49.

Blumenstein, D.. Ferriter, R., Powers, J., and Reiher, M. 2011. Accidents – The total cost: A guide for estimating the total cost of accidents. Colorado School of Mines.

British Health and Safety Executive. 1998. Managing health and safety: Five steps to success. http://www.citb.co.uk/documents/awards [accessed 18 February 2014].

Gagne, R. 2011. What does a workplace injury cost? Direct versus indirect costs and their affect to the bottom line. Fit2Work, Melbourne.

Huang, Y., Leamon, T.B., Courtney, T.K., DeArmond, S., Chen, P.Y., and Blair, M.F. 2009. Financial decision makers' views on safety. *Journal of the American Society of Safety Engineers*, April 2011, pp. 36–42.

LaBelle, J. 2000. What do accidents truly cost? - Determining total incident costs. *Journal of the American Society of Safety Engineers*, April 2000. pp. 38-42.

Lebeau, M., Duguay, P., and Boucher, A. 2013. Estimating the costs of occupational injuries: A feasibility study in the mining industry. Institut de Recherche Robert-Sauvé en Santé et en Sécurité du Travail (IRSST), Montreal, Quebec.

Malaysian Department of Occupational Health and Safety. Not dated. Occupational safety & health accident cost calculator (OSHACC). http://www.dosh.gov.my/e_apps/oshacc/oshacc_model_acc_cost.pdf [accessed 20 March 2014].

Manuele, F. 2011. Accident costs: Rethinking ratios of indirect to direct costs. *Journal of the American Society of Safety Engineers*, January 2011. pp. 39-47.

Royal Borough of Kensington and Chelsea. 2002. Reduce risks – Cut costs: The real cost of accidents and ill health at work. http://www.rbkc.gov.uk/pdf/Reduce%20risks%20and%20cut%20costs%20in%20the%20workplace.pdf [accessed 20 February 2014].

US Department of Labor. 2011. Background of cost estimates. http://www.osha.gov/dcsp/smallbusiness/safetypays/background.html [accessed 18 April 2014].

Workers Compensation Board of British Columbia. Not dated. Small business safety calculator. http://www2.worksafebc.com/calculator/Calculator_worksheet.pdf [accessed 21 March 2014]. ◆

Investigation of stress in a pothole in the Bushveld Complex: A case study

B.P. Watson[1], D. Hoffmann[2], and D.P. Roberts[3]

Affiliation:
[1] Associate Professor - School of Mining Engineering, University of the Witwatersrand, Johannesburg.
[2] Group Mineral Resources Manager - Northam Platinum.
[3] Principal Researcher - CSIR.

Correspondence to:
B. Watson

Email:
Bryan.Watson@wits.ac.za

Dates:
Received: 9 Mar. 2020
Revised: 21 Dec. 2020
Accepted: 18 Jan. 2021
Published: January 2021

How to cite:
Watson, B.P., Hoffmann, D., and Roberts, D.P. 2021
Investigation of stress in potholes in the Bushveld Complex: A case study.
Journal of the Southern African Institute of Mining and Metallurgy, vol. 121, no. 1, pp. 47–56.

DOI ID:
http://dx.doi.org/10.17159/2411-9717/1152/2021

ORCID
B.P. Watson
https://orcid.org/0000-0003-0787-8767

D. Hoffmann
https://orcid.org/0000-0003-4660-2018

Synopsis

Potholes on the Merensky and UG2 reefs in the Bushveld Complex occur as near-circular to elliptical depressions or slumps on the reef horizon, normally presenting as severe disruptions which prevent economic extraction. Within the pothole, the reef and other strata may either be attenuated, absent, or highly deformed, this being the result of the overlying hangingwall strata having slumped down. The hypotheses for pothole formation involve several mechanisms, including downward erosion, upward fluid movement, or synmagmatic deformation.

When potholes are exposed in mine workings, significant fracturing is often observed. This fracturing is particularly evident in anorthosite rock types. Stress measurements were conducted in a pothole on the Merensky Reef to determine if the fracturing was due to high stress conditions. The paper describes the measurement results and numerical modelling that was done to determine the influence of depth and mining on the stress condition at the site. The results show that high stresses do exist in at least some potholes, and that current formation theories do not adequately explain the measured stresses. In support of understanding the high local stress associated with the pothole, the study explored several rock engineering modelling processes to validate the conditions of the study site and enclosing excavations. A better understanding of the stress conditions in potholes with additional data could lead to more appropriate support design and avoidance of potential rockbursts in these structures.

Keywords
potholes, stress, fracturing, discontinuities, jointing, Merensky, UG2.

Introduction

Potholes are widely developed on the Merensky and UG2 reefs in the Bushveld Complex, typically having circular-to-elliptical shapes in plan, and surface areas ranging from 2% to as much as 35% of the reef area for shaft blocks. Usually one or several of the lithological layers are missing where material from the hangingwall strata appears to have slumped or scoured down and filled the underlying depression during or soon after formation (Figure 1). In a pothole, the reef may be developed, but often with irregular morphology and at a lower elevation. Some potholes are large enough to be mined, but generally they are left as stability pillars, and may form part of the regional support. Anorthositic rocks that are exposed in an excavation as a result of a pothole often display a significant amount of fracturing (Urcan *et al.*, 2003). In some instances the fracturing is severe and the rock difficult to support, and falls of ground (FOGs) have occurred. This investigation was designed to determine whether the fracturing is due to high stress. A pothole at shallow depth below surface on the eastern limb of the Bushveld Complex was instrumented. This pothole bottomed out on the base of the Merensky Reef, *i.e.*, the Merensky Reef was missing in the area of the pothole as shown by the schematic in Figure 1.

Usually the bases of potholes are U-shaped, but V-shaped potholes have also been recorded. The up-dip contacts of potholes are steeper, whereas the contacts in the down-dip sections tend to flatten out. The strata thicknesses within the potholes are often variable, but locally they may be similar to those of the undisturbed strata. On the mining horizon, stoping often stops short of the pothole edge where the transgressive hangingwall lithologies are found. At these locations, the attenuation of the reef may be accompanied by deteriorating ground conditions, often associated with increased jointing (Urcan *et al.*, 2003).

In this paper we describe a case study of stress measurements that were performed from a raise line (approx. 1.8 m × 1.8 m tunnel cut on the reef elevation and following the dip of the strata) cut through the centre of a pothole at a depth of 250 m below surface. The objective was to determine stress levels within the pothole. The cover stress was calculated to be 8 MPa (virgin stress). The induced vertical field stress according to 3D elastic modelling, which included mining at the time of the investigation, was

Investigation of stress in a pothole in the Bushveld Complex: A case study

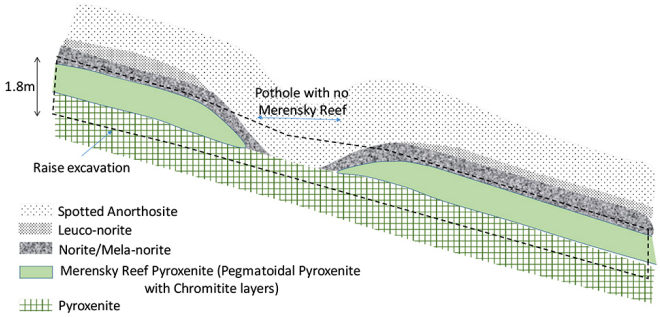

Figure 1—Schematic cross-section through the pothole and raise excavation in the study area. Note the local absence of the reef. The dashed line represents a raise tunnel

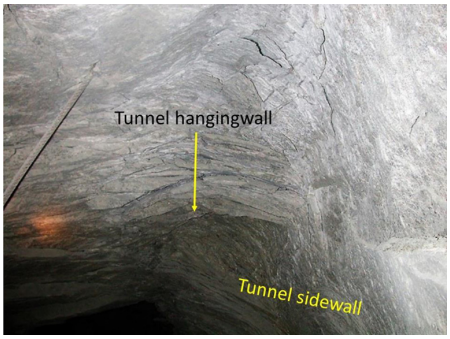

Figure 2—A view looking up the raise excavation (approx. square 1.8 m x 1.8 m tunnel) on the Merensky horizon, showing stress fracturing observed in the centre of the pothole

10 MPa. At such shallow levels, stress fracturing is not normally observed on the Merensky Reef because of the relatively high strength of the rocks. Figure 2 shows the fracturing observed at the instrumented site. The measurements described in the paper were performed as part of a PlatMine project (Watson *et al.*, 2005). Significantly, more work has been added to the original PlatMine investigations in terms of a pothole formation theory review, baseline stress measurements, and numerical modelling. The final part of the study was to determine if current pothole formation theories could explain the measured stresses.

Site description

A site plan of the pothole is shown in Figure 3. Two distinct rock types, norite and anorthosite, were identified in the exposed section of the pothole, as shown in the figure. The stress condition was determined for each of the two rock types, and in the reef beyond the pothole from two separate boreholes. The positions and orientations of these boreholes are shown in plan and section in Figure 3 and Figure 4, respectively. The section shown in Figure 4 was estimated from borehole intersections. Figure 5 shows the collars of the boreholes in the sidewall of the approximately 1 m deep and 1 m high ledge (siding) located in the lower section of the pothole (southwest side in Figure 3). The average dip of the strata at the site was 17° (outside the pothole).

A generalized stratigraphic column for the rock sequences normally surrounding the Merensky Reef, *i.e.*, outside of a pothole area, is shown in Figure 6. In this area the Merensky Reef is typically a 1 m thick poikilitic feldspathic pyroxenite. The immediate hangingwall is a 0.4 m thick norite, overlain by a 0.4 m thick leuconorite which grades upwards into an approximately 3.5 m thick spotted anorthosite and subsequently a 7 m thick mottled anorthosite. No definite parting planes exist between lithologies up to the base of the Bastard Reef.

Strain measurement technique

CSIR triaxial strain cells were oriented and glued in a small diameter borehole at the desired positions for the strain measurements, and subsequently the rock surrounding the gauges was strain-relieved by overcoring with a much larger

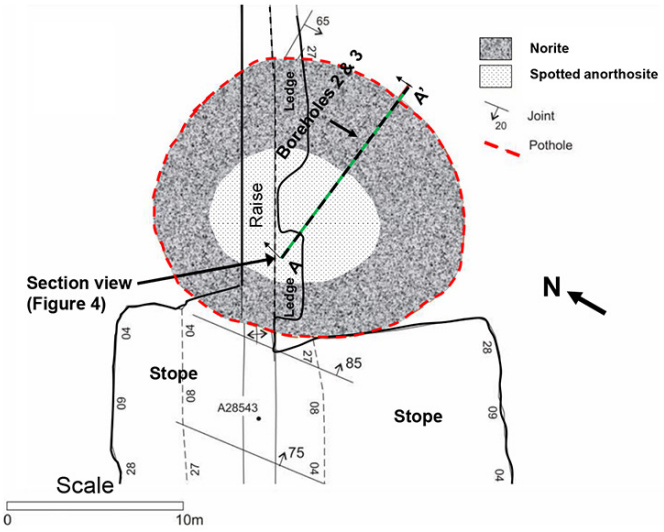

Figure 3—Plan showing the pothole in the raise and the boreholes used for the stress measurements. Note the stoped-out area below the pothole (1 m stope height), and the ledge (siding), at the same height, on the right side of the centre raise in the pothole

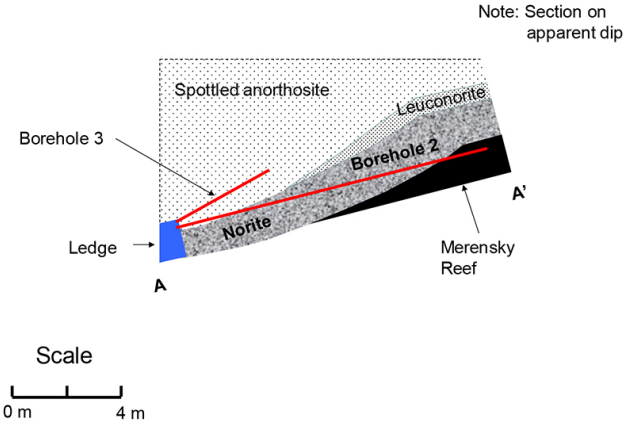

Figure 4—West-east section of the pothole through A-A' in Figure 3 (looking north) - conceptualized from observations made in the boreholes

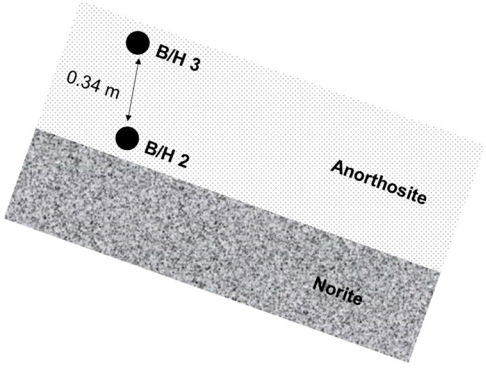

Figure 5—Front view' section, looking east as shown in Figure 3, indicating the borehole collar positions in the face of the 1 m deep centre-raise-ledge The 0.34 m gap refers to the distance between the boreholes, sidewall to sidewall

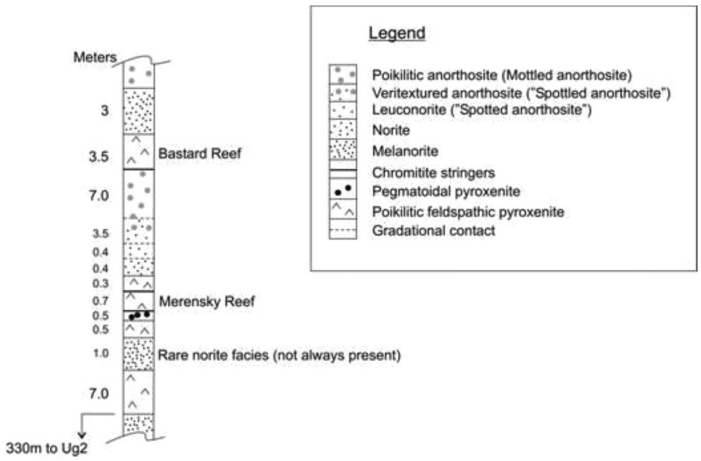

Figure 6—Generalized stratigraphic column for the normal rock sequences surrounding the Merensky Reef in the area of the measurements (represents the geology outside the pothole)

diameter bit (van Heerden, 1983). The strain gauges within the unit recorded the strain relief and the stresses were determined using standard analytical solutions (Leeman and Hayes, 1966).

Stress measurement results

The strains measured by the cells were converted to stress using the elastic constants of rock specimens that were retrieved from the same borehole, immediately adjacent to the measurement sites. Uniaxial compressive tests were performed under laboratory conditions on the two rock types. The results provided Young's moduli and Poisson's ratio values of: 67 GPa and 0.26, respectively, for the anorthosite; 89 GPa and 0.18 for the norite; and 73 GPa and 0.28, for the pyroxenite. The stress-strain results of the tests are shown in Figure 7.

The results of the field stress measurements are provided in Table I, and shown in Figures 8 to 10. Triax2 and triax3 were installed in borehole 2, and triax 4 was installed in borehole 3 (Figures 8 and 9). A reliability index of less than 13 is considered acceptable (Coetzer, 2005). (The reliability index is the average percentage deviation of all the strains from the ideal strains used to calculate the stress.) Stress measurements were conducted in the anorthosite, norite, and pyroxenite, but the measurements in the norite were not considered reliable. The norite measurements were therefore not used in the analyses. The measurement in the pyroxenite was made outside, but near the edge of the pothole. The orientations of the major principal stress changed in the two rock types, from approximately WNW-ESE in the anorthosite to N-S in the pyroxenite (Figure 8). Interestingly, the ratio between σ_1 and σ_3 in both rock types was about two.

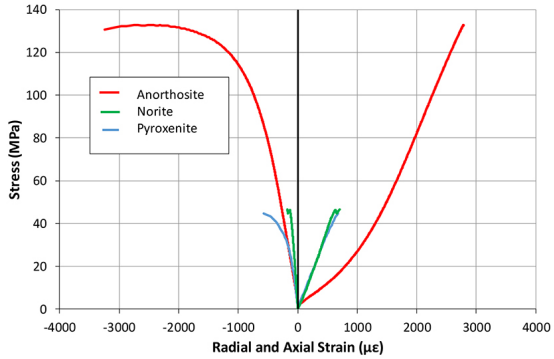

Figure 7—Uniaxial strength test results for the anorthosite, norite, and pyroxenite rock types

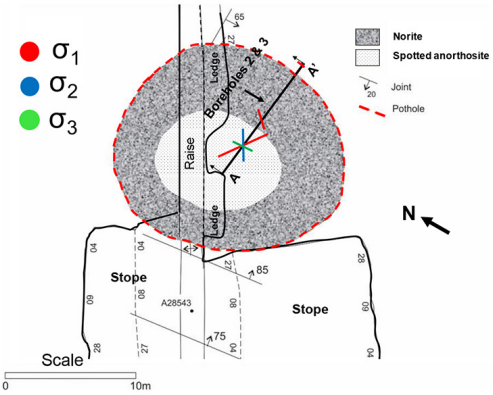

Figure 8—Plan showing the pothole and the stress measurement positions, and the orientations and magnitudes of the principal stress components

Table I

Results of the stress measurements performed in a pothole 250 m below surface

Instrument no.	Rock type	σ_1 (MPa)	Direction of σ_1 (deg. from north)	Dip of σ_1 (deg. from horiz.)	σ_2 (MPa)	Direction of σ_2 (deg. from north)	Dip of σ_2 (deg. from horiz.)	σ_2 (MPa)	Direction of σ_3 (deg. from north)	Dip of σ_3 (deg. from horiz.)	Vert. stress (MPa)	Reliability index (%)	Young's modulus (GPa) (at 50% of UCS)	Poisson's ratio (at 50% of UCS)
Triax 4	Spottled anorthosite	107	119	37	62	233	28	48	170	40	72	5.0	67	0.26
Triax 2	Norite	35	36	4	7	282	79	3	126	10	7	67.8	89	0.18
Triax 3	Pyroxenite (Merensky Reef)	16	180	37	11	286	19	8	37	47	11	8.3	73	0.28

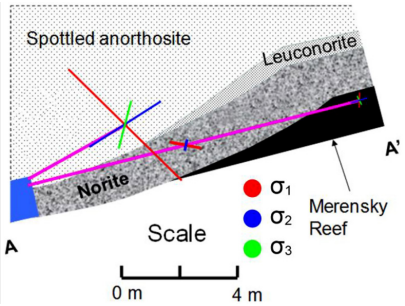

Figure 9—West-east section of the pothole through A-A' in Figure 8 (looking north) showing the stress measurement positions, and orientations and magnitudes of the principal stress components

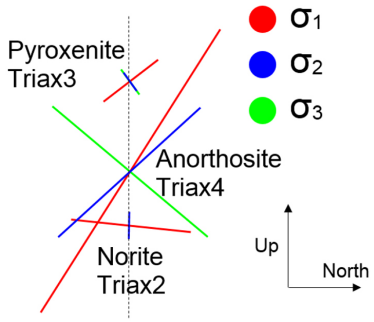

Figure 10—North-south section looking west, showing the orientations and magnitudes of the principal stress components

Stresses in anorthosite elsewhere on the mine

Coetzer (1999) conducted virgin stress measurements at the same mine, but in anorthosites that were located outside of potholes and a stratigraphic unit below the Merensky Reef. One measurement, was made at a similar depth below surface to the study site pothole, and about 500 m from the site horizontally. The results showed a near-horizontal major principal stress of 14 MPa and a vertical stress of 7 MPa, which was close to the cover load (Table II). Other measurements in the same anorthosite layer, but at a depth of 470 m below surface (220 m deeper than the study site), showed a near-horizontal average major principal stress of 30 MPa. For most of these measurements, the vertical stress component was equivalent to the cover load (assuming a density of 3 000 kg/m^3). In addition, the average k-ratio (horizontal to vertical stress) was about 1.9.

A comparison between Coetzer's (1999) stress results and those measured in the pothole suggests that the stresses in the pothole anorthosite were abnormally high (Table III). Importantly, the Coetzer (1999) measurements were conducted in virgin stress conditions, *i.e.*, there being no mining influences on the stress state. This was not the case in the pothole measurements and therefore it was necessary to do some modelling to determine the stress state expected at the elevation of the pothole due to the cover load and surrounding mining. Since the depth below surface was shallow and the mining spans around the pothole were relatively small, it was appropriate to use an elastic model.

Elastic boundary element model

A pseudo-3D, linear elastic, boundary element code, named MinSim (COMRO, 1981) was used to estimate the field stresses expected in the pothole as a result of depth below surface and the surrounding mining. The model included a sufficient area of mining around the site to reliably determine its influence on the pothole. The stress measurements done by Coetzer (1999) had a horizontal stress/vertical stress (k-ratio) variation of between 1.4 and 2.4. In addition, the vertical component of stress in these measurements generally showed a stress similar to the cover load if the average density of the overlying rock was assumed to be 3 000 kg/m^3. Ryder, Watson, and Kataka (2005) also found that elastic models provided reasonable results if the density of the rock and virgin k-ratio of 3 000 kg/m^3 and 2, respectively, were assumed as input parameters. The model assumed uniform material throughout, and was used to determine the field stresses resulting from the mining geometry (the pothole was assumed to have the same elastic properties as the surrounding rock mass for the purposes of this analysis). Stresses were calculated at even intervals along a line representing borehole 2. The model results are shown together with the stress measurements in Figure 11.

Table II

Results of the stress measurements performed outside a pothole 297 m below surface

Instrument no.	Rock type	σ_1 (MPa)	Direction of σ_1 (deg. from north)	Dip of σ_1 (deg. from horiz.)	σ_2 (MPa)	Direction of σ_2 (deg. from north)	Dip of σ_2 (deg. from horiz.)	σ_2 (MPa)	Direction of σ_3 (deg. from north)	Dip of σ_3 (deg. from horiz.)	Vert. stress (MPa)	Reliability index (%)	Young's modulus (GPa) (at 50% of UCS)	Poisson's ratio (at 50% of UCS)
B6-3	Spottled anorfhosite	14.1	26.4	16.0	10.1	282.6	39.6	4.0	133.6	46.0	7.3	6.7	76	0.2

Table III

Results of the stress measurements performed in a pothole 250 m below surface

Instrument no.	Rock type	σ_1 (MPa)	Direction of σ_1 (deg. from north)	Dip of σ_1 (Ddeg. from horiz.)	σ_2 (MPa)	Direction of σ_2 (deg. from north)	Dip of σ_2 (deg. from horiz.)	σ_2 (MPa)	Direction of σ_3 (deg. from north)	Dip of σ_3 (deg. from horiz.)	Vert. stress (MPa)	Reliability index (%)	Young's modulus (GPa) (at 50% of UCS)	Poisson's ratio (at 50% of UCS)
Triax 4	Spottled anorfhosite	107	119	37	62	233	28	48	170	40	72	5.0	67	0.26

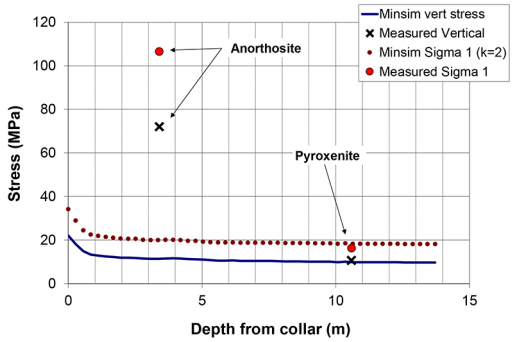

Figure 11—Major principal- and vertical- stress measurements compared to elastic results calculated by MinSim

The magnitudes of both the major principal and vertical stresses measured in the pyroxenite lithology were similar to the elastic model. These results suggest that the stresses outside of the pothole (near the edge of the pothole) were not disturbed by the pothole, and furthermore, were aligned with the range of k-ratios measured by Coetzer (1999). The vertical stress component in the pothole anorthosite, however, was significantly larger at 72 MPa.

Verification of the model was done using a similar elastic model (MAP3D, 2013) with the same input parameters, and was found to provide similar results (Figure 12). Importantly, the stress profiles along boreholes 2 and 3 in Figure 12, were shown to be similar in the region where the measurements were made.

Analysis of stress measurements

A back-analysis of the stress results was done to determine the influence of mining on the measured stress. MAP3D (2013) was used for this analysis because MinSim was not available to the authors at the time this work was done. The assumptions were that the k-ratio was maintained, and the cover load in the model was increased until the principal stress profiles at the study site coincided with the measured stresses in the spotted anorthosite. The depth of cover required to produce the measured principal stresses was about 1 400 m, which provided virgin principal stresses of 41 MPa and 82 MPa in the vertical and horizontal directions, respectively. Figure 13 shows the influence of mining on the virgin stress magnitudes at the positions of the measured stresses in the anorthosite. Importantly, the orientations of the field principal stresses in the model are not the same as those that were measured. The modelling implies that the mining influenced the dip of the major principal stress by only 4° from horizontal. The measurements revealed that the dip was about 37° (Table I). Examine2D (Curran and Corkum, 1988), which is a 2D elastic model, was used to determine the possible influence of the surrounding excavations if the orientation of the major principal stress was at 37° (Figure 14). The results show that the magnitude of the stresses could have been influenced by a further 6% (Figure 15), *i.e.* the virgin major principal stress in the pothole would have been about 77 MPa.

It could be argued that the dissimilar moduli of the material in the pothole may have affected the stress, *i.e.* a zone with a different modulus would have been affected differently by the mining. However, the modulus of the anorthosite was lower than the values for both the surrounding norite and pyroxenite

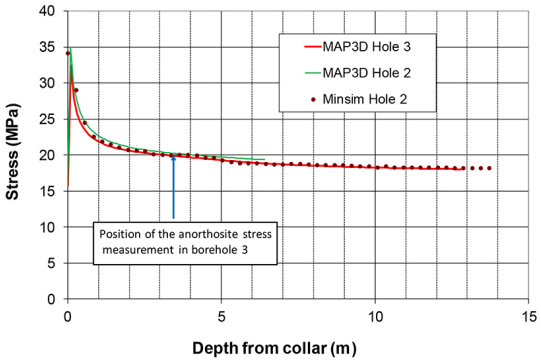

Figure 12—MAP3D/MinSim comparison for boreholes 2 and 3

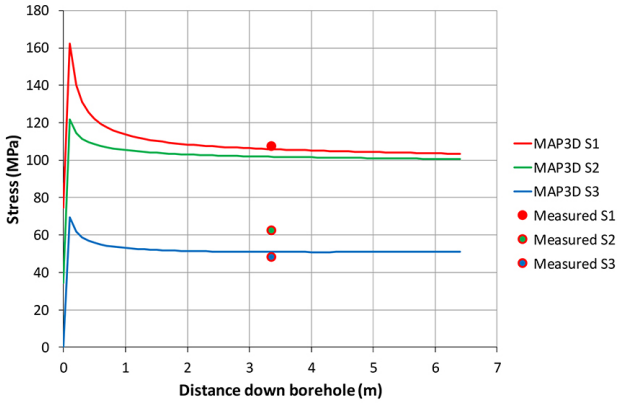

Figure 13—Stress profile with an increased cover load to coincide with the measured major principal stress in the anorthosite. S1, S2, and S3 refer to the principal stresses

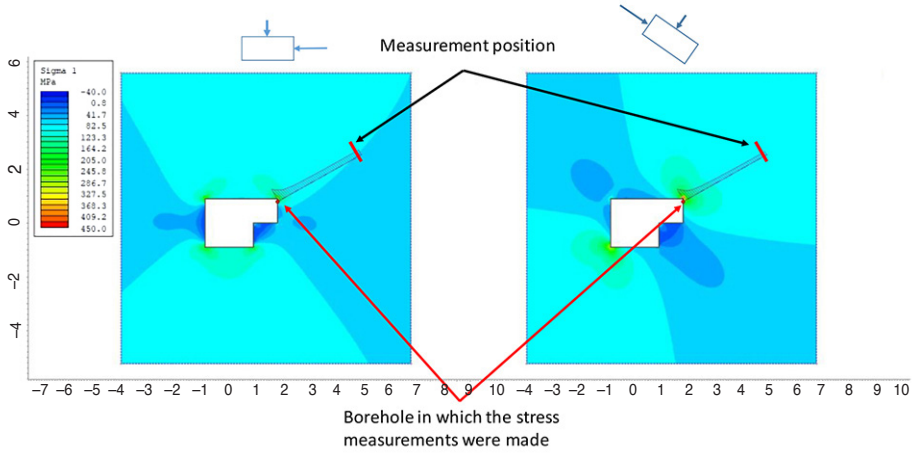

Figure 14—Influence of stress orientation on the stress measurements, Sigma 1 horizontal (left) and 37° (right)

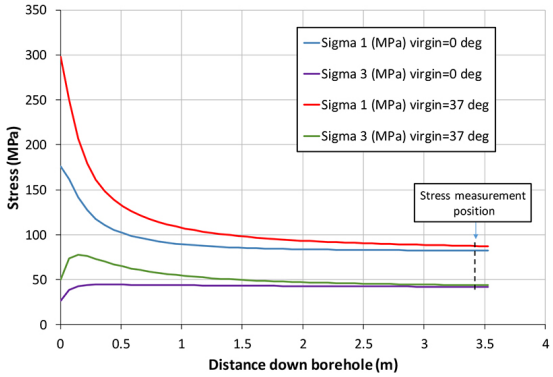

Figure 15—Results of the Examine2D modelling. The influence of the stress orientation is shown by the difference in the zero and 37° lines

and therefore should have had the opposite effect (*i.e.* lower stresses would be expected in the lower modulus anorthosite). The FLAC3D (Itasca Consulting Group, Inc., 2017) modelling, described below, suggests that the difference in measured modulus had a minimal effect.

Visual evidence of high stress in the pothole

Confirmation of the stress and its orientations was evident in the field observations made in the raise. On the southwest side of the pothole, a blast-hole socket was observed near the collar of the boreholes used for the stress measurements. This socket was left during the original mining of the raise, and was therefore not influenced by subsequent stoping. Blast-hole sockets can be used to estimate stress ratios (Watson *et al.*, 2006). Blast gases follow the line of least resistance, and in the absence of joint-related influences will force the rock to open parallel to the minor principal stress. Sockets will thus elongate in the direction of the major principal stress, and the ratio of largest and smallest dimensions of the oval shape will be similar to the ratio of the major to minor principal stresses. The socket in Figure 16 showed a stress ratio of about 2:1, and suggested a near-horizontal direction of the major principal stress in the plane of the raise.

Gothic arching or dog-earing (borehole breakout) occurs when tunnels or boreholes are created/drilled in high stress conditions (Jager and Ryder, 1999). The orientation of the major principal stress will, in this instance, be perpendicular to the elongation, and the severity of the condition is dependent on the magnitude of the principal stresses in the plane of the tunnel or borehole (Jager and Ryder, 1999). Gothic arching can be clearly observed in Figure 17, again suggesting a near-horizontal major principal stress direction in the plane of the raise. The photograph was taken in the centre of the pothole, looking up-dip, *i.e.*, towards the northeast. The orientation of the breakout correlates with that of the measurements, and the severity once more suggests high stress conditions. Figure 18 shows extensive fracturing that was observed in the raise hangingwall, in the anorthosite around the centre of the pothole. The authors have observed such intense fracturing elsewhere in high stress environments, particularly in anorthositic and quartzitic rock types.

Towards the top and bottom of the pothole in the norite rock type, the intensity of the fracturing reduced. In addition, evidence at the upper (northeast) side of the pothole suggested that the orientation of the breakout, and thus the principal stresses, may have changed in the norite (Figure 19).

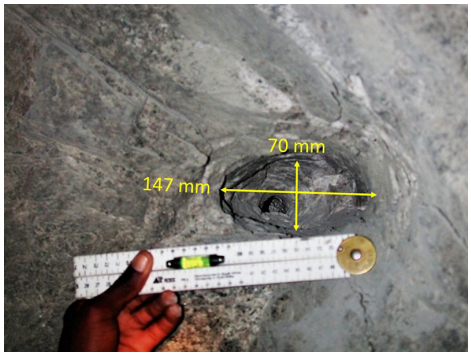

Figure 16—Blast-hole socket in the ledge at the stress measurement site

Figure 17—Looking northeast up the raise in the centre of the pothole

Figure 18—Extensive fracturing in the anorthosite, in the hangingwall of the raise

The orientation of the breakout in the raise tunnel, where it was located in the anorthosite, suggested a near-horizontal major principal stress, dipping towards the southeast, which was similar to the orientation of the measured principal stresses in the same rock type. The blast-hole socket dimensions implied a ratio between the major and minor principal stresses of about 2:1, in the plane of the raise tunnel, which was also similar to the measured stress in the anorthosite. The intensity of the fracturing agrees with the high stresses measured in the anorthosite. Although the stress measurements made in the norite are not considered reliable, there does appear to be some agreement between the observations and the measurements regarding a much lower magnitude of stress in the norite compared to stress in the anorthosite.

Laboratory rock tests

Geomechanical tests were conducted on the two rock types in the pothole and the Merensky Reef pyroxenite taken near the edge of the pothole (Figure 7). All the materials were weaker than elsewhere on the mine, as shown in Table IV.

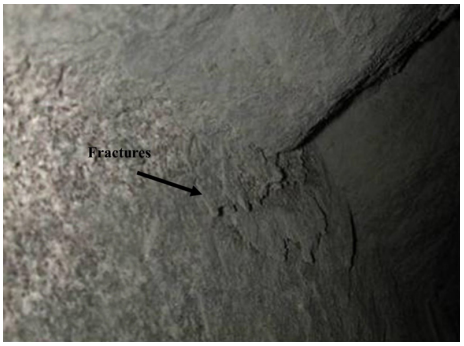

Figure 19—Fracturing in the sidewall looking northeast up the raise

The geomechanical behaviour of the anorthosite sample was compared to a more typical sample of the same rock type elsewhere on the mine (Figure 20). The significant nonlinear behaviour shown by the sample from the pothole is typical of a deeper mine with high virgin stress conditions, or a borehole being drilled into relatively high stress conditions. Similar conditions were recorded by Watson *et al.* (2009) in areas of high stress on other Bushveld platinum mines. The nonlinear behaviour is caused by micro-cracks that develop between different minerals in a polycrystalline material during unloading. The micro-cracks would also explain the relative weakness of the rocks in the pothole.

Pothole formation theory

Key to the formation of potholes is an earlier defect in the cumulate pile (underlying crystallized material) that led to development of the cavity. Earlier research, summarized by Ballhaus (1988) reveals a variety of processes that have been interpreted to serve as a mechanism for pothole formation. These include scouring of the cumulate pile by magmatic currents, resorption (re-melting of the cumulate pile) to form cavities related to the influx of new superheated magma, and suppressed development of the cumulate pile due to volatiles from localized fumaroles in the footwall, or subsequent collapse of the underlying cumulate pile due to localized overpressure from the volatiles. These synmagmatic mechanisms are plausible explanations for the development of the cavities, which were subsequently filled by replenishing magma. An alternative and generally preferred model is the 'pull-apart' mechanism of Carr Groves, and Cawthorne (1994) where tensional conditions in the underlying cumulate pile promote separation (pull-apart) within the footwall due to the effect of 'cumulate sagging and layer-parallel slip', a result from loading by the replenishing magma. These sites of extension promote the development of cavities, and were likely the preferred sites for later magmatic erosion or de-volatilization processes.

In this study, the high compressive stress values measured in the hangingwall strata are notably higher within the pothole footprint, and also higher than that predicted from the numerical modelling. According to the model of Carr, Groves, and Cawthorne (1994), an extensional environment together with its lower stress regime along the perimeter of the Bushveld Complex would be associated with the formation of cavities. However, this theory does not support the higher measured stress for the pothole in the study area. A higher compressive stress environment would be located towards the deeper central part of the Bushveld Complex where the effect of the depositional loading would be the greatest. The instrumented site is proximal to the edge of the present erosional limit, being about 800 m from the suboutcrop position.

Table IV

Comparison of the uniaxial compressive strength (UCS) between the pothole and normal environments at the mine

Rock type	Pothole environment (MPa)	Normal environment (MPa)
Spotted anorthosite	132	179
Norite	50	118
Pyroxenite	45	100

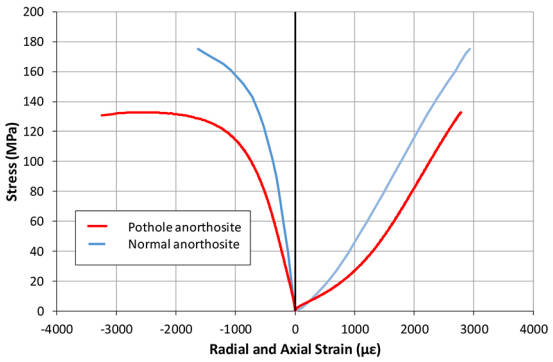

Figure 20—Comparison between the geomechanical behaviour of the pothole anorthosite and the same rock type elsewhere on the same mine

Possible explanation for the high stress condition in the pothole

While none of the explored theories of magmatic processes for pothole formation adequately explain the measured stress, the higher compressive stress measured in the spotted anorthosite may be related to the behaviour of the strata in response to de-stressing from erosion of the land surface. This may have been aided by the concentration of stress in local nodes related to defects associated with the irregular geometry of the strata in the proximity of potholes.

It appears that the Bushveld magma was injected as a large sill approximately 3 km to 7 km below surface (Watson, 2004), constrained by the underlying sediments of the Transvaal Supergroup and an overlying shell of the Rooiberg lavas (Kruger, 2005). The extent of the magma intrusion was wide and shallow, exhibiting a lobate shape, interconnected between east and west and having upturned margins (Kruger, 2005) analogous to a 'flat-bottom soup dish'. The molten rock would have been subjected to a hydrostatic stress of between 80 MPa and 190 MPa in its fluid state, because of its depth below surface. Once solidified, the horizontal stress in the rock mass would have been controlled by the Poisson effect when subjected to further loading and unloading. Consequently, significant horizontal stress could have been locked in when geological erosional processes brought the rock to the current depth below surface. The concept is illustrated by use of Equation [1] to determine the horizontal stress drop due to erosional process, shown in Figure 21. The Poisson's ratio for the materials appears to be similar at 0.3 (Sellers, Coetzwe, and Kamstra, 2002).

$$q_h = \frac{\nu}{(1-\nu)} q_v \quad [1]$$

where

q_h = horizontal stress
q_v = vertical stress,
v = Poisson's ratio (assumed to be 0.3) (Sellers, Coetzer, and Kamstra, 2002).

Figure 21 suggests that for the erosional theory to be the sole reason for the high stresses measured in the pothole, solidification of the rock would need to have taken place at a depth of 6.2 km below surface. However, the theory does not explain why such stress levels were locked into the pothole, rather than being pervasive throughout the orebody. It should be noted that Equation [1] assumes the rock mass is elastic and therefore does not account for other geological processes, such as creep, faulting, *etc*. An elastic model was set up using the elastic moduli of the anorthosite and surrounding norite and pyroxenite to determine whether a rock enclosed on all sides by materials with different Young's moduli could cause stress to be locked into a pothole.

Elastic continuum model

An elastic continuum (FLAC3D) model (Itasca Consulting Group, Inc., 2017) of the pothole was generated to explore possible origins of the high stresses recorded in the anorthosite, as described above. The configurations described in Figures 3 and 4 were used to generate the geometry of the pothole. The leuconorite layer was not included in the model geometry. No interfaces were specified between the strata. Figure 22 shows the strata boundaries. The model itself is provided in Figure 23. All boundaries were constrained by rollers.

Initial stresses corresponding to 4 000 m of cover were applied. If it is assumed that the rock mass was molten at that time, the stress state would be hydrostatic. The vertical stress was then reduced by moving the uppermost boundary of the model upwards. This simulates removal of the cover load through erosion. It was expected that the lateral stresses would be proportionately reduced in accordance with the 'Poisson effect'. The stress field would be further modified by the geometry of the pothole and the different stiffness of each stratum.

An initial hydrostatic stress of 120 MPa was applied throughout the model. The resulting σ_1 distribution after boundary displacement of 60 m is shown in Figure 24. The range of values is only 11 MPa, though it is evident that the stress in the stiffer norite layer is higher than in the surrounding strata. The lowest stresses are indicated below the centre of the pothole. The minor principal stress distribution shows the same trend. Stresses at the measurement positions are provided in Table V. The results do not correspond with the measured values. The orientations of the pyroxenite and norite measurements are not significantly altered, while the anorthosite major principal stress is rotated towards the normal of the surface defining the norite stratum within the pothole.

The model did not replicate the measured stresses, indicating that the origin and evolution of the measured stresses are more complex than the mechanism suggested in the previous section. High stresses could have been induced during the formation of the pothole, but the presence of such high stresses now, in concert with relatively low stresses around the pothole, suggests that some other mechanism (fracturing, slip along discontinuities, *etc*.) has 'trapped' these high stresses in a region above the pothole.

Discussion of the stress results

As far as the authors are aware, the stresses described in this paper are the only such measurements that have been made in a pothole of the Bushveld Complex. The extensive fracturing often observed in potholes suggests that high stresses may be a common feature of potholes. Should the stress levels in some potholes increase with depth below surface, there is a possibility that bursting may occur when such features are uncovered in deeper mines. The current pothole formation theories do not adequately describe the high stress conditions that were measured or observed and therefore cannot be used to predict how potholes will behave at depth. The extensive fracturing, as shown in Figure 18, constitutes a rockfall safety hazard which is difficult to support and may also interrupt mine production.

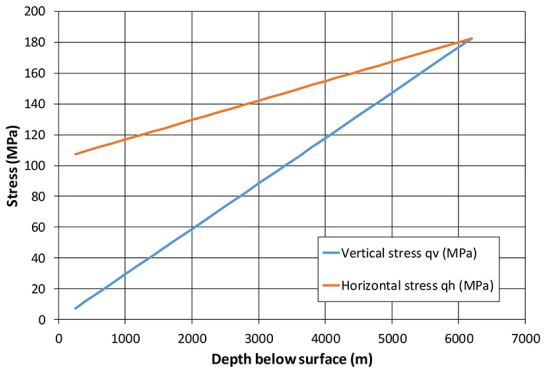

Figure 21—Change in vertical and horizontal stress with erosional processes

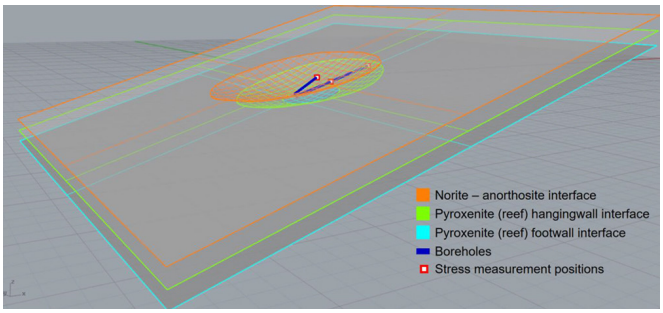

Figure 22—Interfaces used to define a continuum model of the pothole

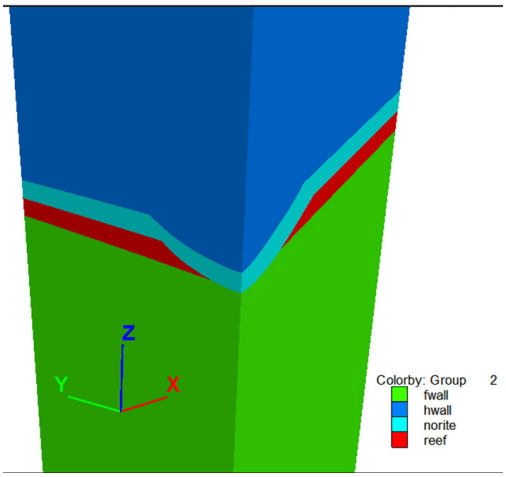

Figure 23—Model of the pothole, cut by vertical planes through the centre of the pothole

Conclusions and recommendations

Stress fracturing is often observed in areas on the Merensky Reef

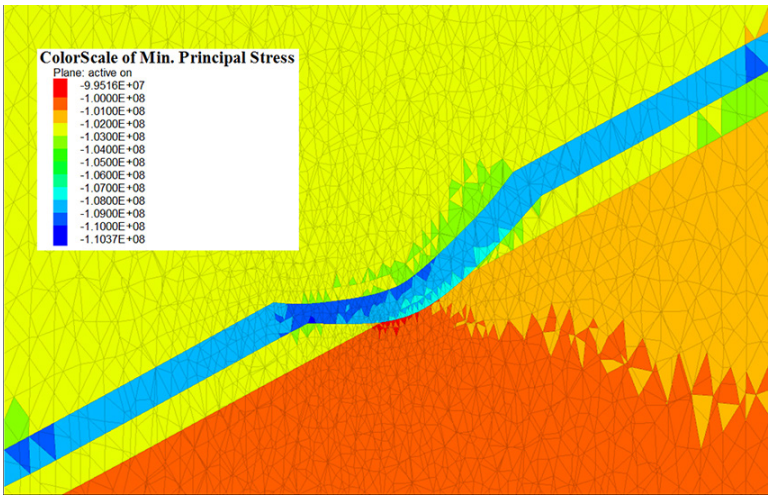

Figure 24—Modelled σ_1 distribution in a vertical section corresponding with the plane of the measurement boreholes

Table V

Modelled principal stress vectors at the measurement positions

Measurement	σ_1	σ_2	σ_3	Bearing 1	Bearing 2	Bearing 3	Dip 1	Dip 2	Dip 3
Norite (Triax2)	108.4	105.1	71.3	0.3	90.3	91.2	0.1	–3.4	86.6
Pyroxenite (Triax3)	102.8	102.4	69.9	86.2	–3.8	–94.3	–0.8	0.0	–89.2
Anorthosite (Triax4)	103.0	102.8	70.3	64.1	–25.9	–91.7	–1.2	0.6	–88.7

where potholes have been exposed during mining, particularly in anorthosite rocks. Stress measurements conducted in a pothole on the Merensky Reef showed that the stresses were unusually high, yet with a similar σ_1 to σ_3 ratio to the Merensky pyroxenite outside the pothole. In addition, none of the measurements conducted in anorthosite outside of a pothole showed such high stresses. Observations of fracturing and blast-hole sockets near the high stress measurement confirmed that high stresses were present in that area.

None of the explored theories of pothole formation adequately explain the measured stress. Modelling indicated that the difference in Young's modulus between the different strata in juxtaposition during unloading cannot, on its own, explain the higher stresses in the anorthosite.

It is recommended that further stress measurements be made in potholes at a variety of depths below surface and across the Bushveld Complex. A better understanding of the stress conditions in potholes could lead to more appropriate support design and avoidance of potential rockbursts in these structures. The reason for the existence of characteristic geological discontinuities around the periphery of potholes should also be investigated.

Acknowledgements

The CSIR and PlatMine are acknowledged for facilitating the success of the original research work described in this paper.

References

Ballhaus, C.G. 1988. Potholes of the Merensky Reef at Brakspruit Shaft, Rustenburg Platinum Mines: Primary disturbances in the magmatic stratigraphy. *Economic Geology*, vol. 83. p. 1140–1158.

Carr, H.W., Groves, D.I., and Cawthorne, R.G. 1994. The Importance of synmagmatic deformation in the formation of Merensky Reef potholes in the Bushveld Complex. *Economic Geology*, vol. 89. p. 1398–1410.

Coetzer, S.J. 1999. Measurement of rock stress at a mine. Consultancy report no. 99-0299.

Coetzer, S.J. 2005. Personal communication.

Curran, J.H. and Corkum, B.T. 1988. EXAMINE 2D Version 3.1 Users Manual: a 2D boundary element program for calculating stresses around underground excavation in rock, Data Visualization Laboratory, Department of Civil Engineering, University of Toronto.

COMRO. 1981. MINSIM-D user's manual. Chamber of Mines of South Africa, Johannesburg.

Itasca Consulting Group, Inc. 2017. FLAC3D — Fast Lagrangian Analysis of Continua in Three-Dimensions, Ver. 6.0. Minneapolis: MN.

Jager, A.J. and Ryder, J.A. 1999. A Handbook on Rock Engineering Practice for Tabular Hard Rock Mines, Safety in Mines Research Advisory Committee (SIMRAC), Braamfontein, South Africa. 19 pp.

Kruger, F.J. 2005. Filling the Bushveld Complex magma chamber: Llateral expansion, roof and floor interaction, magmatic unconformities, and the formation of giant chromitite, PGE and Ti-V-magnetitite deposits. *Mineralium Deposita*, vol. 40, no. 5. pp.451–472.

Leeman, E.R. and Hayes, D.J. 1966. A technique for determining the complete state of stress in rock using a single borehole. *Proceedings of the. 1st Congress.of the International Society of Rock Mechanics*, Lisbon. vol. 2. pp. 17–24.

MAP3D. 2013. www.map3D.com.

Ryder, J.A., Watson, B.P., and Kataka, M.O. 2005. Estimation of UG2 and Merensky Reef pillar strengths through back-analyses. PlatMine project report, CSIR, Division of Miningtek, Johannesburg.

Sellers, E.J., Coetzer, S.J., and Kamstra, R. 2002. Understanding and determining the variability of the primitive stress environment Appendix A. https://www.mhsc.org.za/ [accessed: 27 September 2018].

Urcan, H., Grodner, M., Watson, B., Lamos, R.A., Roberts, M.K.C., Stewart, R., Squelch, A.P., le Grange, R., and Xaba, D. 2003. Investigate the rock mechanics aspects of potholes in the platinum mines, their contribution to poor ground conditions, and if proactive identification is possible, SIMRAC project GAP 846. Safety in Mines Research Advisory Committee (SIMRAC), Braamfontein, South Africa.

Van Heerden W.L. 1983. Stress-strain relations applicable to overcoring techniques in transversely isotropic rocks. *International Journal of Rock Mechanics and Mining Sciences & Geomechanical Abstracts*, vol. 20, no. 6. pp 277–282.

Watson, B.P. 2004. Report on the workshop examining the loading and unloading history of the Bushveld. *Internal report*, CSIR, Division of Miningtek, Johannesburg.

Watson, B.P., Kuijpers, J.S., Henry, G., Palmer, C.E., and Ryder, J.A. 2009. Nonlinear rock behaviour and its implications on deeper level platinum mining. *Journal of the Southern African Institute of Mining and Metallurgy*, vol. 108, no. 1. pp 5–13.

Watson, B.P., Roberts, M.K.C., Jager, A.J., Naidoo, K., Handley, R., Milev, A.M., Roberts, D.P., Sellers, E.J., and Kanagalingam, Y. 2005. Understanding the mechanical properties of the anorthosite suite of rocks. PlatMine project report, CSIR, Division of Miningtek, Johannesburg.

Watson, B.P., Sellers, E.J., Kuijpers, J.S., Grave, D.M.H., Roberts, M.K.C., and Coetzer S.J. 2006. Alternative cost effective ways of determining the state of stress in mines. PlatMine project report, CSIR, Division of Miningtek, Johannesburg. ◆

dimi
COMMITTEE
DIVERSITY AND INCLUSION
IN THE MINERALS INDUSTRY

SAIMM
THE SOUTHERN AFRICAN INSTITUTE
OF MINING AND METALLURGY

IN COLABBORATION WITH
wimsa
WOMEN IN MINING SA

SAIMM DIMI CONFERENCE 2021

Empowering the African minerals industry through diversity and inclusion

3-4 AUGUST 2021
RIVERSANDS CANVAS,
FOURWAYS, GAUTENG

BACKGROUND

The SAIMM through its committee for Diversity and Inclusion in the Minerals Industry (DIMI) and in collaboration with Women in Mining South Africa (WiMSA) is excited to announce its first ever conference focusing on the issues of diversity and inclusion in the mining and minerals industry.

The Southern African Mining sector, just like the global mining industry, still faces huge challenges when it comes to diversity and inclusivity in the workplace. While the landscape might be changing due to a lot of companies becoming more aware of the need for a more representative and diverse workforce, there is still a lot to be done. Beside issues of gender disparity in the industry, safe spaces in the workplace, protective equipment, sanitation facilities, pregnancy and childcare facilities for women are some of the challenges that continue to plague the sector. The industry also needs to go beyond workforce diversity to inclusion. Identifying individuals from different geographic, gender, economic and cultural groups, creating safe spaces for them, providing support for them to grow into their roles and creating conditions that promote inclusion on a daily basis can go a long way in retaining and advancing the careers of these individuals and hence contribute to the long term growth of the mining sector. There is thus, a need for platforms that allow for discussions that can lead to the development of strategies for advancing and encouraging decisions that are in the best interest of a diverse workforce.

Conference Coordinator:
Camielah Jardine, Head of Conferencing
E-mail: camielah@saimm.co.za
Tel: +27 11 834-1273/7

NATIONAL & INTERNATIONAL ACTIVITIES

2021

1–5 March 2021 — **MINEXCHANGE 2021 SME Annual Conference & Expo and the CMA 123rd National Western Mining Conference**
Virtual Conference Platform
Contact: knasinski@smenet.org

18–22 April 2021 — **IMPC2020**
XXX International Mineral Processing Congress
Cape Town, South Africa
Contact: Camielah Jardine
Tel: +27 11 834-1273/7, Fax: +27 11 838-5923/833-8156
E-mail: camielah@saimm.co.za, Website: http://www.saimm.co.za

9–10 June 2021 — **Diamonds – Source To Use — 2021 Hybrid Conference**
'Innovation And Technology'
The Canvas, Riversands, Fourways, South Africa
Contact: Camielah Jardine
Tel: +27 11 834-1273/7, Fax: +27 11 838-5923/833-8156
E-mail: camielah@saimm.co.za, Website: http://www.saimm.co.za

23–25 June 2021 — **ROLLS6 2021**
London, UK
Contact: Chelsea Wallis, Tel: +44 (0)207 451 7302

24–26 June 2021 — **AGROMIN II AGRO-Mining Convention - Agriculture and Mining joined by Nature**
Trujillo
Contact: (51-1) 989-590-328
E-mail: informes@agrominperu.com, peru.agromin@gmail.com

27–30 June 2021 — **European Metallurgical Conference, EMC 2021**
Salzburg, Austria
Tel: +49 (5323) 93 79-0
E-Mail: verein@gdmb.de, Website: https://emc.gdmb.de/contact/

28–30 June 2021 — **Renewable Solutions for an Energy Intensive Industry Hybrid Conference 2021**
Mintek, Randburg, South Africa
Contact: Camielah Jardine
Tel: +27 11 834-1273/7, Fax: +27 11 838-5923/833-8156
E-mail: camielah@saimm.co.za, Website: http://www.saimm.co.za

1–2 July 2021 — **The Mine Waste & Tailings Stewardship Conference 2021**
Brisbane
Website: https://www.ausimm.com/conferences-and-events/mine-waste-and-tailings/

13–16 July 2021 — **Copper Cobalt Africa**
Incorporating
The 10th Southern African Base Metals Conference
Avani Victoria Falls Resort, Livingstone, Zambia
Contact: Camielah Jardine
Tel: +27 11 834-1273/7, Fax: +27 11 838-5923/833-8156
E-mail: camielah@saimm.co.za, Website: http://www.saimm.co.za

28–29 July 2021 — **5th Mineral Project Valuation Hybrid Colloquium**
The Canvas Riversands, Fourways, Johannesburg
Contact: Gugu Charlie
Tel: +27 11 834-1273/7, Fax: +27 11 838-5923/833-8156
E-mail: gugu@saimm.co.za, Website: http://www.saimm.co.za

16–17 August 2021 — **Worldgold Hybrid Conference 2021**
Misty Hills Conference Centre, Muldersdrift,
Johannesburg, South Africa
Contact: Camielah Jardine
Tel: +27 11 834-1273/7, Fax: +27 11 838-5923/833-8156
E-mail: camielah@saimm.co.za, Website: http://www.saimm.co.za

29 August–2 September 2021 — **APCOM 2021**
Minerals Industry Hybrid Conference
'The next digital transformation in mining'
Misty Hills Conference Centre, Muldersdrift,
Johannesburg, South Africa
Contact: Camielah Jardine
Tel: +27 11 834-1273/7, Fax: +27 11 838-5923/833-8156
E-mail: camielah@saimm.co.za, Website: http://www.saimm.co.za

21–22 September 2021 — **5th Young Professionals Hybrid Conference 2021**
'A Showcase of Emerging Research and Innovation in the Minerals Industry'
The Canvas, Riversands, Fourways, South Africa
Contact: Gugu Charlie
Tel: +27 11 834-1273/7, Fax: +27 11 838-5923/833-8156
E-mail: gugu@saimm.co.za, Website: http://www.saimm.co.za

26–29 September 2021 — **The 16th International Ferroalloys Congress (INFACON XVI)**
Clarion Hotel & Congress Trondheim
infacon2021@videre.ntnu.no

4–6 October 2021 — **PGM The 8th International Conference 2021**
Sun City, Rustenburg, South Africa
Contact: Camielah Jardine
Tel: +27 11 834-1273/7, Fax: +27 11 838-5923/833-8156
E-mail: camielah@saimm.co.za, Website: http://www.saimm.co.za

18–20 October 2021 — **Southern African Rare Earths International Conference 2021**
Swakopmund Hotel and Entertainment Centre,
Swakopmund, Namibia
Contact: Camielah Jardine
Tel: +27 11 834-1273/7, Fax: +27 11 838-5923/833-8156
E-mail: camielah@saimm.co.za, Website: http://www.saimm.co.za

26–27 October 2021 — **SAMCODES Conference 2021**
The Canvas Riversands, Fourways, South Africa
Contact: Gugu Charlie
Tel: +27 11 834-1273/7, Fax: +27 11 838-5923/833-8156
E-mail: gugu@saimm.co.za, Website: http://www.saimm.co.za

8–10 November 2021 — **Global Tailings Standards and Opportuniries Hybrid Conference 2021**
'For the Mine of the Future'
Sun City, Rustenburg, South Africa
Contact: Gugu Charlie
Tel: +27 11 834-1273/7, Fax: +27 11 838-5923/833-8156
E-mail: gugu@saimm.co.za, Website: http://www.saimm.co.za

Company affiliates

The following organizations have been admitted to the Institute as Company Affiliates

3M South Africa (Pty) Limited
AECOM SA (Pty) Ltd
AEL Mining Services Limited
African Pegmatite (Pty) Ltd
Air Liquide (Pty) Ltd
Alexander Proudfoot Africa (Pty) Ltd
AMEC Foster Wheeler
AMIRA International Africa (Pty) Ltd
ANDRITZ Delkor(Pty) Ltd
Anglo Operations Proprietary Limited
Anglogold Ashanti Ltd
Arcus Gibb (Pty) Ltd
ASPASA
Atlas Copco Holdings South Africa (Pty) Limited
Aurecon South Africa (Pty) Ltd
Aveng Engineering
Aveng Mining Shafts and Underground
Axiom Chemlab Supplies (Pty) Ltd
Axis House Pty Ltd
Bafokeng Rasimone Platinum Mine
Barloworld Equipment -Mining
BASF Holdings SA (Pty) Ltd
BCL Limited
Becker Mining (Pty) Ltd
BedRock Mining Support Pty Ltd
BHP Billiton Energy Coal SA Ltd
Blue Cube Systems (Pty) Ltd
Bluhm Burton Engineering Pty Ltd
Bond Equipment (Pty) Ltd
Bouygues Travaux Publics
Castle Lead Works
CDM Group
CGG Services SA
Coalmin Process Technologies CC
Concor Opencast Mining
Concor Technicrete
Council for Geoscience Library
CRONIMET Mining Processing SA Pty Ltd
CSIR Natural Resources and the Environment
Data Mine SA
Digby Wells and Associates
DRA Mineral Projects (Pty) Ltd
DTP Mining - Bouygues Construction
Duraset
Elbroc Mining Products (Pty) Ltd
eThekwini Municipality
Ex Mente Technologies (Pty) Ltd
Expectra 2004 (Pty) Ltd
Exxaro Coal (Pty) Ltd
Exxaro Resources Limited
Filtaquip (Pty) Ltd
FLSmidth Minerals (Pty) Ltd
Fluor Daniel SA (Pty) Ltd
Franki Africa (Pty) Ltd-JHB
Fraser Alexander (Pty) Ltd
G H H Mining Machines (Pty) Ltd
Geobrugg Southern Africa (Pty) Ltd
Glencore
Hall Core Drilling (Pty) Ltd
Hatch (Pty) Ltd
Herrenknecht AG
HPE Hydro Power Equipment (Pty) Ltd
Immersive Technologies
IMS Engineering (Pty) Ltd
Ingwenya Mineral Processing (Pty) Ltd
Ivanhoe Mines SA
Joy Global Inc. (Africa)
Kudumane Manganese Resources
Leica Geosystems (Pty) Ltd
Longyear South Africa (Pty) Ltd
Lull Storm Trading (Pty) Ltd
Maccaferri SA (Pty) Ltd
Magnetech (Pty) Ltd
Magotteaux (Pty) Ltd
Malvern Panalytical (Pty) Ltd
Maptek (Pty) Ltd
Maxam Dantex (Pty) Ltd
MBE Minerals SA Pty Ltd
MCC Contracts (Pty) Ltd
MD Mineral Technologies SA (Pty) Ltd
MDM Technical Africa (Pty) Ltd
Metalock Engineering RSA (Pty)Ltd
Metorex Limited
Metso Minerals (South Africa) Pty Ltd
Micromine Africa (Pty) Ltd
MineARC South Africa (Pty) Ltd
Minerals Council of South Africa
Minerals Operations Executive (Pty) Ltd
MineRP Holding (Pty) Ltd
Mining Projections Concepts
Mintek
MIP Process Technologies (Pty) Limited
MLB Investment CC
Modular Mining Systems Africa (Pty) Ltd
MSA Group (Pty) Ltd
Multotec (Pty) Ltd
Murray and Roberts Cementation
Nalco Africa (Pty) Ltd
Namakwa Sands(Pty) Ltd
Ncamiso Trading (Pty) Ltd
New Concept Mining (Pty) Limited
Northam Platinum Ltd - Zondereinde
Opermin Operational Excellence
Optron (Pty) Ltd
Paterson & Cooke Consulting Engineers (Pty) Ltd
Perkinelmer
Polysius A Division Of Thyssenkrupp Industrial Sol
Precious Metals Refiners
Ramika Projects (Pty) Ltd
Rams Mining Technologies
Rand Refinery Limited
Redpath Mining (South Africa) (Pty) Ltd
Rocbolt Technologies
Rosond (Pty) Ltd
Royal Bafokeng Platinum
Roytec Global (Pty) Ltd
RungePincockMinarco Limited
Rustenburg Platinum Mines Limited
Salene Mining (Pty) Ltd
Sandvik Mining and Construction Delmas (Pty) Ltd
Sandvik Mining and Construction RSA(Pty) Ltd
SANIRE
Schauenburg (Pty) Ltd
Sebilo Resources (Pty) Ltd
SENET (Pty) Ltd
Senmin International (Pty) Ltd
SISA Inspection (Pty) Ltd
Smec South Africa
Sound Mining Solution (Pty) Ltd
SRK Consulting SA (Pty) Ltd
Time Mining and Processing (Pty) Ltd
Timrite Pty Ltd
Tomra (Pty) Ltd
Ukwazi Mining Solutions (Pty) Ltd
Umgeni Water
Webber Wentzel
Weir Minerals Africa
Welding Alloys South Africa
Worley

PGM THE 8TH INTERNATIONAL CONFERENCE

4-5 OCTOBER 2021 - CONFERENCE
6 OCTOBER 2021 - TECHNICAL VISIT

VENUE - SUN CITY, RUSTENBURG, SOUTH AFRICA

PGMs - Enabling a cleaner world

The Platinum conference series has covered a range of themes since inception in 2004, and traditionally addresses the opportunities and challenges facing the platinum Industry.

This prestigious event attracts key role players and industry leaders through:

- High quality technical papers and presentations
- Facilitating industry networking
- Having large, knowledgeable audiences
- Global participation, and
- Comprehensive support from industry role players.

The 8th International PGM Conference will, under the guidance of the organising committee, structure a programme which covers critical aspects of this continually evolving and exciting industry.

The success and relevance of this event to the industry really depends on your participation and support.

You can participate in this event as an organising committee member, author/ presenter, delegate or sponsor.

FORMAT OF THE EVENT

At this point in time, the event is planned as a full contact conference with international participation through web links. It is also planned to hold technical visits to nearby facilities.

However, as we are still in Stage 2 Lock down as a result of COVID-19, this will be constantly reviewed, and if it appears that the effects of the pandemic are still such as to pose a threat to the health and safety of delegates, this will be changed to a digital event.

WHO SHOULD ATTEND

- Academics
- Business development managers
- Concentrator managers
- Consultants
- Engineers
- Exploration managers
- Explosives engineers
- Fund managers
- Geologists
- Hydrogeologists
- Innovation managers
- Investment managers
- Market researchers and surveyors
- Marketing managers
- Mechanical engineers
- Metallurgical managers
- Metallurgical consultants
- Metallurgists
- Mine managers
- Mining engineers
- New business development managers
- Planning managers
- Process engineers
- Product developers
- Production managers
- Project managers
- Pyrometallurgists
- Researchers
- Rock engineers
- Scientists
- Strategy analysts
- Ventilation managers

ABOUT THE VENUE

The Sun City resort lies in a tranquil basin of an extinct volcano in the Pilanesberg adjacent to South Africa's rich platinum belt. It boasts four hotels, an award-winning golf course and many other attractions.

Nestled in the rolling hills of the Pilanesberg, one of South Africa's most scenic locations, Sun City is a world unto itself and has earned its reputation as Africa's Kingdom of Pleasure.

Finally re-discovered and now part of Sun City, the Lost City and the Valley of Waves, fabled to be the Ruins of a glorious ancient civilisation,celebrate and bring to life the legends of this mystical city.

FOR FURTHER INFORMATION, CONTACT:

Camielah Jardine,
Head of Conferencing

E-mail: camielah@saimm.co.za
Web: www.saimm.co.za

SAIMM
THE SOUTHERN AFRICAN INSTITUTE OF MINING AND METALLURGY

SAIMM HYBRID CONFERENCE

SOUTHERN AFRICAN RARE EARTHS

INTERNATIONAL CONFERENCE 2021

18-20 OCTOBER 2021

SWAKOPMUND HOTEL AND ENTERTAINMENT CENTRE, SWAKOPMUND, NAMIBIA

cerium (Ce), dysprosium (Dy), erbium (Er), europium (Eu), gadolinium (Gd), holmium (Ho), lanthanum (La), lutetium (Lu), neodymium (Nd), praseodymium (Pr), promethium (Pm), samarium (Sm), scandium (Sc), terbium (Tb), thulium (Tm), ytterbium (Yb), and yttrium (Y)

Driving the future of high-tech industries

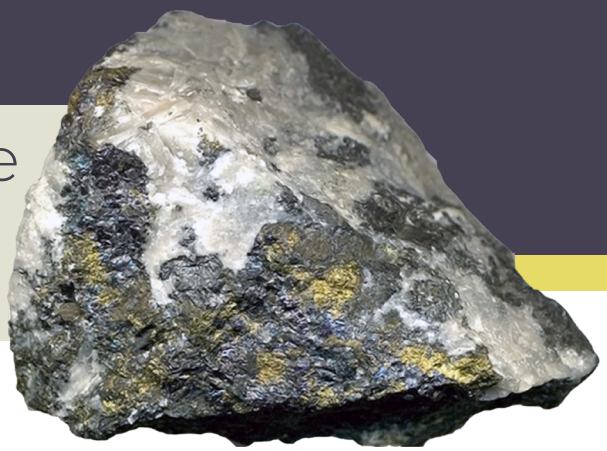

ABOUT THE CONFERENCE

The global demand for rare earth elements (REEs) and their alloys has increased enormously in the last few decades. REEs are critical materials in high-technology applications due to their unique chemical, catalytic, electrical, magnetic, and optical properties. In particular, REEs are used in emerging and niche technologies such as medical devices, electric vehicles, energy-efficient lighting, wind turbines, rechargeable batteries, catalytic converters, flat screen televisions, mobile phones. and disk drives. In fact, the 4IR-driven digital revolution will not be possible without the critical rare REEs.

The supply security of rare earth metals is of global concern. The need to diversify the supply of REEs thus creates significant opportunities for southern Africa to contribute to the global supply. In fact, as one of the regions with large REE resources, southern Africa can exploit this window of opportunity and significantly contribute to the sustainable supply of these high-tech materials.

PLEASE NOTE THAT SPONSORSHIP OPPORTUNITIES AND EXHIBITION SPACE IS AVAILABLE.

The need to fully participate along the REE value chain has also inspired interest in developing downstream capacity for refining, through the Southern African Centralized Rare Earth Refinery (SACREF). Thus, in order to maximize value from the REEs industry in the region, further discussions on optimizing the REE value chain are needed. This conference, focusing on the optimization of the primary production and refining of rare earth metals, is designed to stimulate debate on growth, creating opportunities for the southern African rare earths industry.

FOR FURTHER INFORMATION, CONTACT:

Camielah Jardine,
Head of Conferencing

E-mail: camielah@saimm.co.za
Web: www.saimm.co.za

SAIMM
THE SOUTHERN AFRICAN INSTITUTE OF MINING AND METALLURGY